UNIVERSITÀ DEGLI STUDI DI MILANO

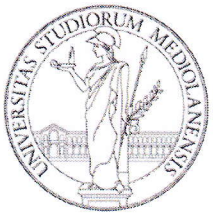

SCUOLA DI DOTTORATO IN SCIENZE E TECNOLOGIE CHIMICHE
DIPARTIMENTO DI SCIENZE FARMACEUTICHE
CORSO DI DOTTORATO IN CHIMICA DEL FARMACO
CICLO XXVII

THE PERMEATION OF BIOMACROMOLECULES THROUGH HUMAN SKIN: AN INSIGHT INTO THE FAMILY OF GLYCOSAMINOGLYCANS

SETTORE CHIM/09 FARMACEUTICO TECNOLOGICO APPLICATIVO

Dott.ssa SILVIA FRANZÉ

Matricola: R09584

Tutor: Prof. FRANCESCO CILURZO

Coordinatore del dottorato: Prof. ERMANNO VALOTI

ANNO ACCADEMICO
2013/2014

A mio nonno

Table of contents

Introduction

Glycosaminoglycans (GAGs) are natural polysaccharides ubiquitously distributed on cell membranes and in the extracellular matrix (ECM) of all animal organisms. Owing to their peculiar chemical structure, GAGs bind to several proteins and cell signaling factors in cell environment, thus being involved in many physiological and pathological processes [1, 2]. As result, they find application in pharmaceutical field as both therapeutic agents and targeting molecules in drug delivery.

According to the type of the constituent monosaccharides and the substitution degree, GAGs are classified into four broad groups [2]. They are acidic linear polymers composed of many repeating disaccharide units of hexosamine and uronic acid, with the exception of keratan sulfate which contains galactose instead of uronic acid [3]. Keratan sulfate (KS) has less variable primary structure compared to other sulfated GAGs. Its basic repeating unit is made of N-acetyl-glucosamine linked (β 1→3) to a galactose residue. Sulfation may occur in position 6 of both moieties and non-sulfated, mono-sulfated and di-sulfated disaccharides alternate along KS chain [4].

KS is a component of ECM of cartilages, bone and cornea, where it acts as signaling and hydrating agent. Like other GAGs, it is involved in several physiopathological conditions and its possible use as therapeutic or target agent is gaining interest in pharmaceutical field [4]. As an example, since it was found that KS-deficiency makes the mice cartilage more fragile, the administration of hexogen KS was suggested as a novel strategy for the treatment of human inflammatory diseases, such as rheumatoid arthritis and osteoarthritis [5].

Chondroitin sulfate (CS) and dermatan sulfate (DS) (also known as chondroitin sulfate B) have a common chemical precursor, the chondroitin, which consists of uronic acid linked (β 1→3) to N-acetyl-galactosamine. For this feature, they are more properly defined as “galactosaminoglycans” [6]. The disaccharide unit can be un-, mono- or di-sulfated. DS contains uronic acid in two epimeric forms, namely glucuronic and iduronic acids, whereas the uronic acid residues of chondroitin sulfate are all glucuronic acids [7]. CS and DS have numerous potential therapeutic applications but, as matter of fact, their clinical administration is limited [8]. DS preparations have been used for the prophylaxis and treatment of venous thromboembolism, disseminated intravascular coagulation

syndrome and for the prevention of deep vein thrombosis in patients with hip fracture. CS is indicated for the treatment of osteoarthritis [9].

Heparin (UFH) and heparan sulfate (HS) are the sulfated GAGs that present the most complex structure. They are a mixture of polysaccharide chains of different length and degree of substitution having as monomeric unit a glucosamine linked through 1,4 glycosidic linkage to an iduronic or glucuronic acid [10]. The glucosamine may be either sulfated or acetylated and each disaccharide may have up to three functional groups sulfated, thus resulting in a huge number of possible combinations, among which the most frequent is the trisulfated disaccharide having the glucosamine sulfated at the amino group and at the carbon in position 6, and the iduronic acid sulfated in position 2. With respect to UFH, HS exhibits a lower content of iduronic acid, lower degree of sulfation and an increased percentage of N-acetyl glucosamine (up to 10%) [6, 11]. The presence of heterogeneous regions on UFH/HS chains is the basis of their therapeutic value, which relies on the ability to bind to a variety of proteins (chemokines, growth and coagulation factors, metalloproteinase, low-density lipoproteins, adhesion proteins and many others, up to 100 different proteins), modulating their biological activity [2, 12]. Despite of the wide range of effects, UFH/HS are mainly known for their widespread use as anticoagulant and antithrombotic agents. Nowadays, the use of UFH is restricted to the hospital and low molecular weight heparins (LMWHs), obtained by different depolymerization methods of UFH, have replaced its use in outpatients due to the improved pharmacokinetic and pharmacodynamic [13]. LMWHs ideally share the same basic chemical structure of UFH but present peculiar terminal end residues which are artifacts of the specific production method (for further reading see [14] (chapter 4)).

Hyaluronic acid (frequently referred as hyaluronan because of its polyanion form) is the only un-sulfated polysaccharide of the class and it has the widest distribution of molecular weight (M_w). In fact, in a completed hyaluronan molecule up to 10,000 repeating units can be found with a molecular mass ranging from 500 to millions of Daltons [15]. HA doesn't show the sequence variability typical of the other GAGs. Indeed, it has a unique basic disaccharide unit consisting of N-acetyl-glucosamine and D-glucuronic acid. However, it presents a complex secondary structure since it can crystallize in several helical forms which symmetry is influenced by pH, humidity and type of counter-ion [7]. HA counts the largest number of applications both in medical and in cosmetic field. It is

used for the treatment of osteoarthritis, for cutaneous wound healing, as biomaterial for bioengineering purposes and filler in dermatologic surgery. Moreover, HA is a well known moisturizing agent and free radical scavenger commonly used in cosmetic formulations [16, 17].

50% of the total amount of HA present in the body is localized in the extracellular matrix of the skin where it plays a key role in maintaining skin homeostasis. Hence, its topical application is useful for the treatment of some skin disorders and HA based products are available on the market for skin care [18, 19]. GAGs in general and in particular HA, resulted also to be able to enhance the delivery of other drugs into the skin and this observation led to the development of a topical formulation (Solaraze®) containing diclofenac in HA gel, approved in many countries for the treatment of actinic keratoses [16].

Transdermal/dermal delivery of such polysaccharides may also represent a non invasive, challenging alternative to the conventional routes for their therapeutic administration since it allows to improve patient compliance, minimize side effects and obtain a sustained release of drug with possibility to reach either a local or a systemic effect [20].

Altogether, GAGs are highly hydrophilic polyanionic macromolecules characterized by large molecular size. In solution, many H-bonds are formed (in addition to those already present between neighboring disaccharide units) and a large hydrodynamic volume is occupied as result of the repulsion between charged groups [6, 16]. Hence, they do not exhibit the suitable properties to cross the outer layer of the skin, the stratum corneum (SC), which, with its brick and mortar structure, represents the rate-limiting barrier to skin permeation.

The study of the diffusion features of GAGs is further complicated by their intrinsic heterogeneity in terms of both chemical structure and conformational behavior. Indeed, in the solid state, GAGs chains fold into helices of different periodicity and in solution the flexibility of some glycosidic linkages produces numerous conformations, which coexist in equilibrium [3].

Nevertheless, polysaccharides have been incorporated in topical formulations for different purposes. The use of topical UFH to treat the symptoms of peripheral vascular disorders is well-established in Europe [21] and, as already stated, creams and gels containing HA are available on the market.

However, the diffusion of these polymers through human skin has been relatively poor investigated and contrasting data are reported in literature.

As far as HA is concerned, Brown and coworkers, after application in vivo of radiolabeled HA, found that it was able to cross the skin barrier reaching the dermis in significant amount and that the permeation of HA was not limited to its small fractions [22]. More recently, in vitro studies carried out by using hairless mice skin evidenced a slow diffusion even of HA tetrasaccharides and confirmed the limiting effect of SC, since the flux resulted to be significantly increased through SC-stripped skin [23].

More extensive and documented research has been focused on heparins (both UFH and LMWHs). Experimental results evidenced a poor passive permeation of these molecules through the skin and the need of an enhancement strategy to improve their flux. Several physical and chemical techniques have been investigated for this purpose [24].

In particular, different methods of perturbation or disruption of SC have been exploited [25-30].

Pacini et al., by using the approved device Transderm®, revealed that iontophoresis have a limited effect on the diffusion of UFH and preferentially enhances the permeation of low molecular weight fractions, suggesting the application of this system for the skin delivery of LMWHs [27]. In contrast, Le and coworkers found an increase of 10-fold of the immediate flux of UFH using iontophoresis and a 13-fold increase of long-term flux after application of ultrasounds [28]. In another study, the pretreatment of the skin with low-frequency ultrasounds improved the in vitro flux of radiolabeled UFH of 21-fold and allowed a sustained delivery of biologically active dalteparin *in vivo* [29]. On the contrary, in *in vitro* studies performing using hairless rat skin, the flux of LMWHs was found to be almost negligible after application of both iontophoresis and ultrasound (0.065 and 0.058 IU/cm^{2}h) [30].

This Ph.D was aimed to clarify which aspects rule the human skin permeability of the different classes of GAGs to assess the real feasibility of transdermal/dermal delivery of these macromolecules. In particular, the research activity was focused on HA and heparins, the two GAGs most employed as both active compounds and drug carriers.

The experimental work was articulated in two main steps:

1) the investigation of the influence of the main structural features (sequence, M_w, polarity, and conformational behavior) on the percutaneous absorption of HA and heparins (UFH and LMWHs), to point out which structural components play a key role in the diffusion through the skin;
2) the fine-tuning of a suitable strategy to improve the permeation of heparins through human skin by using peptides as skin penetration enhancers.

Indeed, although several physical enhancement techniques have been applied (even successfully) to the skin delivery of heparins, any approach resulted to be conclusive and free of concerns. Strategies based on the abrasion or disruption of SC cannot be managed by patients on their own and, altogether, the available data reveal that a combination of methods is preferred to reach a suitable therapeutic effect. To achieve this goal the development of complex devices is required and this may limit the administration to outpatients [24]. On the other hand, the use of chemical enhancers such as Azone® is limited by the toxic and skin irritant potential at certain doses [31].

A novel alternative, which has gained interest in the last years and has not been investigated for this class of macromolecules, is the use of "cell-penetrating peptides (CPPs)" which penetrate, without damaging, the biological membranes at low concentration and with high efficiency. A particular class of these peptides are the so called "skin penetrating peptides" which resulted to be able to enhance the diffusion through the skin of biologic active compounds chemically bound to them (through covalent linkage or electrostatic interaction) [32].

After translocation across the membrane, the drug can be released or directly exerts its action as complex with the peptide. Some of these peptides demonstrated to be also effective without requiring a direct conjugation to the active molecule. As an example, a 23-aminoacid peptide, magainin, by electrostatic interaction with negatively charged lipids of SC, seemed to induce pore formation within lipid bilayers, causing a leakage of the tight barrier and allowing the diffusion of the free drug across it [33]. Phage display is a biotechnological technique which uses phages as expression vectors and which can be exploited to screen skin penetrating peptides for dermal and transdermal delivery. Phages tolerate the fusion of exogenous amino acid sequence to the genes codifying for capside's proteins, without undergoing a loss of functionality. A hybrid fusion protein is formed which is expressed on the outer surface of the phage. Hence, by using a phage

display library, it is possible to screen simultaneously different peptide sequences for the desired function [34]. TD-1 was the first peptide specifically identified by in vivo phage display (on mouse skin) which allowed the systemic absorption of macromolecules applied topically on the skin. To date, TD-1, along with SPACE peptide studied for the delivery of siRNA, is the only skin penetrating peptide found to improve specifically the transdermal delivery of macromolecules [35].

In this work phage display was used to identify a skin penetrating peptide able to deliver heparins into human skin. The Ph.D.-7 Phage Display Peptide Library based on the filamentous phage M13 was used and the experiments were carried out in a vertical Franz diffusion apparatus using human SCE as membrane.

During my Ph.D program I also had the opportunity to spend 8 months as visiting student at the Institut Galien Paris-Sud (Université Paris-Sud 11, Châtenay-Malabry, France) where I gained experience in nano-carriers formulation as well as in cell biology and cell culture. In fact, I was involved in a research project which dealt with the development of liposomes encapsulating a new inhibitor of heat shock protein 90 (Hsp90), 6BrCaQ, for the delivery of the drug to prostate and breast cancer cells. Hsp90 is a molecular chaperone that modulates the biological activity of several oncoproteins, being overexpressed in many types of cancer [36]. Although 6BrCaQ demonstrated a promising cytotoxic effect against different cancer cell lines in vitro, its therapeutic use is limited by its low water solubility that prevents both the full characterization of the biological activity in vivo and the intravenous administration [37]. To overcome this drawback, in this work the drug was encapsulated in liposomes with a dual purpose: to allow the drug solubilization through its distribution in the lipid bilayer and to exploit the ability of liposomal carriers to target cancer. Indeed liposomes, as long as they have certain features (nano-sized dimensions and Stealth® properties), can passively accumulate in solid tumors through the enhanced and retention permeability effect (EPR), improving the bioavailability of the drug at the target site and limiting the exposure of health tissues to the cytotoxic agent [38]. Moreover, they can be internalized into the cells thus potentiating the action of the free drug [39].

Stealth® liposomes were formulated by the conventional thin film hydration method and characterized in terms of size, zeta potential, physical stability and drug leakage. The effect of the encapsulated drug on the tumor growth was evaluated in cell culture in vitro using metastatic prostate and breast cancer cell lines. The results of this experimental work are reported in the Appendix of this thesis.

References

1. Linhardt R. J. and Toshihiko T. Role of Glycosaminoglycans in Cellular Communication. Accounts of Chemical Research 2004, 37, 431-438;
2. Raman R, Sasisekharan V, Sasisekharan R. Structural Insights into Biological Roles of Protein-Glycosaminoglycan Interactions. Chemistry & Biology 2005, 12, 267–277;
3. Imberty A, Lortat-Jacob H, Pérez S, Structural view of glycosaminoglycan-protein interactions, Carbohydrate Research 2007, 342, 430-439;
4. Pomin V.H. Keratan sulfate: An up-to-date review. International Journal of Biological Macromolecules 2015, 72, 282–289;
5. Hayashi M, Kadomatsu K, Kojima T, Ishiguro N. Keratan sulfate and related murine glycosylation can suppress murine cartilage damage in vitro and in vivo. Biochemical and Biophysical Research Communications 2011, 409, 732–737;
6. Gandhi N.S. and Mancera R.L. The Structure of Glycosaminoglycans and their Interactions with ProteinsChemical Biology & Drug Design 2008, 72: 455–482;
7. Ernst S, Langer R, Clooney C.L, Sasisekharan R. Enzymatic Degradation of Glycosaminoglycans. Critical Reviews in Biochemistry and Molecular Biology 1995, 30(5), 387-444;
8. Yamada S. and Sugahara K. Potential therapeutic application of chondroitin sulfate/dermatan sulfate. Current Drug Discovery Technologies 2008, 5(4), 289-301;
9. Volpi N. Therapeutic Applications of Glycosaminoglycans. Current Medicinal Chemistry 2006, 13, 1799-1810;
10. Casu B. 1985. Structure and biological activity of heparin. In: Tipson S. and Horton D, Advances in Carbohydrate Chemistry & Biochemistry, Academic Press Inc, 43, 51-134;
11. Malavaki C.J, Theocharis A.D, Lamari F.N, Kanakis I, Tsegenidis T, Tzanakakis G.N, Karamanos N.K. Heparan sulfate: biological significance, tools for biochemical analysis and structural characterization. Biomedical Chromatography 2011, 25, 11-20;

12. Laremore T.N, Zhang F, Dordick J.S, Liu J, Linhardt R.J. Recent progress and applications in glycosaminoglycans and heparin research. Current Opinion in Chemical Biology 2009, 13, 633-640;
13. Hirsh J. and Raschke R. Heparin and Low-Molecular-Weight Heparin. CHEST 2004, 126 (3), 188S-203S;
14. Minghetti P, Cilurzo F, Franzè S, Musazzi U.M, Itri M. Low molecular weight heparins copies: are they considered to be generics or biosimilars? Drug Discovery Today 2013, 18 (5/6), 305-311;
15. Boeriu C.G, Springer J, Kooy F.K, van den Broek L.A.M, Eggink G. Production Methods for Hyaluronan. International Journal of Carbohydrate Chemistry 2013, 2013, 1-14;
16. Yong-Hong L. Hyaluronan: Pharmaceutical Characterization and Drug Delivery. Drug Delivery 2005, 12, 327–342;
17. Monheit G.D. and Coleman K.M. Hyaluronic acid fillers. Dermatologic Therapy 2006, 19, 141–150;
18. Juhlin L. Hyaluronan in skin. Journal of Internal Medicine 1997, 242, 61–66;
19. Kogan G, Šoltés L, Stern R, Gemeiner P. Hyaluronic acid: a natural biopolymer with a broad range of biomedical and industrial applications. Biotechnology Letters 2007, 29, 17–25;
20. Prausnitz M. R. and Langer R. Transdermal drug delivery. Nature biotechnology 2008, 26 (11), 1261-1268;
21. Vecchio C. and Frisinghelli A. Topically applied Heparins for the Treatment of Vascular Disorders. A Comprehensive Review. Clinical Drug Investigation 2008, 28, 603-614;
22. Brown T.J, Alcorn D, Fraser R.E. Absorption of Hyaluronan Applied to the Surface of Intact Skin. The Journal of Investigative Dermatology 1999, 113 (5), 740-746;
23. Kage M, Tokudome Y, Hashimoto F. Permeation of hyaluronan tetrasaccharides through hairless mouse skin: an in vitro and in vivo study. Archives of Dermatological Research 2013, 305, 69-77;
24. Lanke S.S.S, Strom J.G, Banga A.K. Enhancement of Transdermal Delivery of Heparin by Various Physical and Chemical Enhancement Techniques. Critical Reviews ™ in Therapeutic Drug Carrier Systems 2009, 26 (6), 581-606;

25. Ito Y, Murakami A, Maeda T, Sugioka N, Takada K. Evaluation of self-dissolving needles containing low molecular weight heparin (LMWH) in rats. International Journal of Pharmaceutics 2008, 349, 124-129;
26. Gomaa Y. A, Garland M. J, McInnes F, El-Khordagui L. K, Wilson C, Donnelly R F. Laser-engineered dissolving microneedles for active transdermal delivery of nadroparin calcium. European Journal of Pharmaceutics and Biopharmaceutics 2012, 82, 299–307;
27. Pacini S, Punzi T, Gulisano M, Cecchi F, Vannucchi S, Ruggiero M. Transdermal Delivery of Heparin Using Pulsed Current Iontophoresis. Pharmaceutical Research 2005, 1-7;
28. Le L, Kost J, Mitragoti S. Combined Effect of Low-Frequency Ultrasound and Iontophoresis: Applications for Transdermal Heparin Delivery. Pharmaceutical Research 2000, 17 (9), 1151-1154;
29. Mitragoti S. and Kost J. Transdermal Delivery of Heparin and Low-Molecular Weight Heparin Using Low-Frequency Ultrasound. Pharmaceutical Research 2001, 18 (8), 1151-1156;
30. Lanke S.S.S, Kolli C.S, Strom J.G, Banga A.K. Enhanced transdermal delivery of low molecular weight heparin by barrier perturbation. International Journal of Pharmaceutics 2009, 365 (1–2), 26–33;
31. Bonina F.P. and Montenegro L. Effects of some non-toxic penetration enhancers on in vitro heparin skin permeation from gel vehicles. International Journal of Pharmaceutics 1994, 111, 191-196;
32. Nasrollahi S.A, Taghibiglou C, Azizi E, Farboud E.S. Cell-penetrating Peptides as a Novel Transdermal Drug Delivery System. Chemical Biology & Drug Design 2012, 80, 639–646;
33. Chen Y, Wang M, Fang L. Biomaterials as novel penetration enhancers for transdermal and dermal drug delivery systems. Drug Delivery 2013, 20(5), 199–209;
34. Smith G.P. and Petrenko V.A. Phage display. Chemical Reviews 1997, 97, 391-410;
35. Hsu T. and Mitragotri S. Delivery of siRNA and other macromolecules into skin and cells using a peptide enhancer. PNAS 2011, 108 (38), 15816–15821;
36. Bagatell R. and Whitesell L. Altered Hsp90 function in cancer: A unique therapeutic opportunity. Molecular Cancer Therapeutics 2004, 3(8), 1021-1030;

37. Audisio D, Messaoudi S, Cegielkowski L, Peyrat J, Brion J, Methy-Gonnot I, Radanyi C, Renoir J, Alami M. Discovery and Biological Activity of 6BrCaQ as an Inhibitor of the Hsp90 Protein Folding Machinery. ChemMedChem 2011, 6, 804 – 815;
38. Deshpande P.P, Biswas S, Torchilin V.P. Current trends in the use of liposomes for tumor targeting. Nanomedicine 2013, 8(9), 1-32;
39. Immordino M, Dosio F, Cattel L. Stealth liposomes: review of the basic science, rationale, and clinical applications, existing and potential. International Journal of Nanomedicine. Sep 2006, 1(3), 297–315.

1. The role of the conformational profile of polysaccharides on skin penetration: the case of hyaluronan and its sulfates

Abstract

The data reported in literature suggest the capacity of biomacromolecules to permeate the human skin even though such a transdermal permeation appears to be governed by physicochemical parameters which are significantly different compared to those ruling the skin permeation of small molecules. On these grounds, the present study was undertaken to investigate the in vitro diffusion properties through the human epidermis of hyaluronic acid and their sulfates. Low- and medium-molecular weight hyaluronic acids and the corresponding derivatives at two degrees of sulfation were then tested. In vitro studies evidenced that the sulfated polymers permeate better than the corresponding hyaluronic acid, despite their vastly greater polarity, while the observed permeation markedly decreases when increasing the polymer's molecular weight regardless of the sulfation degree. Using a fluorescent-labeled polysaccharide, it was also evidenced that hyaluronans have a great affinity for corneocytes and likely cross the stratum corneum mainly through a transcellular route. The molecular dynamics study revealed how the observed permeations for the investigated polysaccharides can be rationalized by monitoring their conformational profiles since the permeation was found to be directly related to their capacity to assume extended and flexible conformations

The content of this chapter was published in Chemistry & Biodiversity (Cilurzo et al. Chemistry & Biodiversity 2014, 11 (4), 551-561)

1.1 Introduction

Transdermal administration is a well-established and attractive route of administration. However, the absorption of a drug applied on the skin is limited by the stratum corneum, which presents a multi-layered wall-like structure in which flat keratinized corneocytes are embedded in a lipophilic network of ceramides, cholesterol esters and fatty acids. The barrier properties of this dense layer were investigated in-depth, revealing that lipophilicity and molecular size play key roles in determining the transdermal permeation of small molecules [1; 2].

Conversely, the transdermal permeation of biological drugs was scantly investigated, even though it is commonly accepted that their passive diffusion is limited by both large molecular volume and ability to elicit H-bonds. However, polysaccharides have been successfully and widely applied through the skin, even though very little data on their permeation process has been hitherto reported in literature.

Thus, very few and often contrasting studies are reported for heparin [3], heparinoids [4], chondroitin [3] and hyaluronic acid (also called hyaluronan; HA). As an example, HA was reported to be unable to penetrate the stratum corneum in *in vitro* experiments due to its high hydrophilicity and stiffened random-coil molecular configuration [5; 6]. In another study performed *in vivo* by applying a gel loaded by 3% w/w radiolabelled HA to human forearm, it was able to penetrate into the skin reaching the dermis within 30 min [7].

Aiming to elucidate the penetration mechanism of HA through human epidermis, the present work is focused on the impact of molecular weight, conformation and polarity on the diffusion process of polysaccharides using low- and medium-molecular weight HA and the corresponding derivatives at different degree of sulfation (HAS). Besides their relevant physicochemical profiles, these biomacromolecules were chosen for their significant impact in the biomedical field, since they are widely used as hydration agents, free radical scavengers [8] and skin penetration enhancers [9].

The transdermal penetration of HAs was experimentally determined by the Franz diffusion cell method using human epidermis as a membrane and confirmed by using confocal laser scanner microscopy (CLSM), while the possible relationship between the polymer's conformation and the ability to permeate the human epidermis was studied in

silico by molecular dynamics (MD) simulations. Indeed, despite its relevance in living organisms and artificial biosystems, the conformational properties of the HAs have been scantly investigated at an atomic level [10]. The hitherto reported computational studies have involved only very short oligomers [11], and the effects of sulfonation on the conformation of HA have never been analyzed by MD simulations.

1.2 Experimental Part

1.2.1 Chemicals

All tested Hyaluronic acids (Has) were kindly provided by Fidia Farmaceutici (Italy). As summarized in **Table 1.1**, the study involved six different HAs including both sulfated (HAS) and nonsulfated (HA) polymers differing for the molecular weight (low molecular weight, about 6.5 kDa, and medium molecular weight, about 185 kDa) and for the sulfation degree (1% and 2.5% mol, respectively). The reported polydispersity indices (**Table 1.1**), which encode for the distribution of polymer's molecular mass and tend to unity for homogenous samples, confirm the satisfactory homogeneity of the tested polysaccharide samples. The study also involved a medium molecular weight polymer conjugated with fluorescein isothiocyanate (FITC), an aliquot of 1 mg/ml of which contained 0.2378 μg of fluorescent probe (Fidia Farmaceutici, Italy), hereinafter termed HAF for the sake of brevity. At the end of the depolymerization process, the medium molecular weight HA was dialyzed against water by using a membrane with a 30 kDa molecular weight cut-off (Centricon® Amicon, Millipore, US). The absence of olgomers with molecular weight lower than 30 kDa in the dialyzed fractions was assessed by the carbazole method [12] which allows the quantification of D-glucuronic acid free units produced from the HA hydrolysis. Sodium azide and propidium iodide solution were purchased from Sigma Aldrich (Italy). The water used in the experiments was produced by a MilliQ® system (Millipore, US). All solvents were of analytic grade, unless specified.

Table 1.1 – The main characteristics of hyaluronic acids (HA), the corresponding derivatives at two degrees of sulfation (HAS) and medium molecular weight HA conjugated with fluorescein isothiocyanate (HAF). The relative amounts diffused across human stratum corneum and epidermis after 24 hours (Q_{24}) of treatment are also reported (mean ± standard deviation, n=3).

Name	Substitution degree (% mol)	Mw (kDa)	Polydispersity Index	Q_{24} (nmol/cm^2)
HA	0	6.7	1.352	1.0 ±0.6
		170.2	1.596	0.1 ± 0.0
HAS	1	6.8	1.259	4.9 ± 0.8
		181.3	1.483	0.6 ± 0.2
	2.5	6.4	1.452	2.4 ± 1.0
		200.1	1.390	0.2 ± 0.1
HAF	0	190.3	1.432	0.1 ± 0.0

1.2.2 In vitro permeation studies

The stratum corneum and epidermis used in the permeation studies were obtained from the abdominal skin of donors, who underwent cosmetic surgery (30-50 year old, Eurasian female). The samples were prepared following the internal standard procedure [13]. The full-thickness skin was sealed in evacuated plastic bags and frozen at -20 °C within 24 h after removal. Prior to experiments, the skin was thawed at room temperature, and the excess of fat was carefully removed. The skin sections were cut into squares of about 2.5 cm^2 and, after immersing the skin in water at 60 °C for 1 min, the epidermis was gently separated from the remaining tissue with forceps and carefully inspected by light microscopy for any defects.

Afterwards, the membrane was mounted on the Franz diffusion cell [13], whose receptor compartment (volume: 6.0 ml exactly measured) was filled with degassed water containing 100 µg/ml NaN_3 as preservative. Special care was taken to avoid air bubbles between the buffer and the membrane in the receptor compartment. The upper and lower parts of the Franz cell were sealed with Parafilm® and fastened together by using a clamp,

with the membrane acting as seal between the donor and receptor compartments. The system was kept at 37±1 °C with a circulating water bath so that the membrane surface temperature was at 32±1 °C throughout the experiments. Before starting experiments, the temperature at the surface of each receptor compartment was measured by using a digital thermometer (PCE-T390, PCE Corporation, Italy). The donor compartment was filled by 2% w/w aqueous solution (0.5 ml) and closed. At predetermined times (1, 2, 4, 6, 24 h) 0.2 ml samples were withdrawn from the receiver compartment and immediately replaced with fresh receiver medium. In order to avoid false positive results due to HA eventually present in the human skin, control experiments were carried out in parallel using water as donor phase. The amount of HA eventually present in the receptor phase was subtracted by the sample reading.

A set of experiments was also carried out to determine the penetration mechanism of HAF into the human epidermis. After 0.5, 1, 2, 3, 4 and 24 h, the membranes were dismounted from the Franz cells, immediately washed with water and gently stripped by an adhesive tape strip (Transpore tape, 3M, US) to remove the un-adsorbed permeant. Then, the samples were analyzed by confocal laser scanner microscopy. A permeation experiment using a 5 mg/L aqueous solution of FITC as donor phase was also carried out. Sampling of receiving phase was carried out after 0.25, 0.5, 1, 2, 3, 4 and 24 h of application.

All reported values represent the averages of parallel experiments performed in triplicate.

1.2.3 Confocal laser scanner microscopy

The samples of gently stripped membranes were placed on a glass slide with the stratum corneum side up, stained by a propidium iodide (PI) solution. Acquisition of fluorescent images was performed with a Zeiss LSM 510 confocal microscope (63× objective) with sequential acquisition setting at 1024 × 1024 pixels resolution. Each image was a z series projection, with 1 μm interval between each plane. The absence of any cross-talk between HAF and PI fluorescence was ensured by a multi-track setting. Three to four sites for imaging were randomly selected in each coverslipped section.

1.2.4 Quantitative determination of HA

The amount of HAS was determined in terms of S content by inductively coupled plasma (ICP) MS analysis after depolymerization and mineralisation. The contained Spercentage was used to estimate the amount of permeant. The concentration of HA was measured by using the carbazole method [12]. In both cases, the permeated amounts were calculated by subtracting the amount of S or glucuronic acid determined in the blank.
HAF was determined by a size exclusion chromatography method (HLPC HP 1100 Chemstations) using a BioSuite^{TM} 125 column, 4 μm UHR SEC, 4.6 x 300 mm (Waters, US) eluted with 0.1M PBS at pH adjusted to 8 at a flow rate of 0.35 ml/min and temperature of 25 °C. The eluent was monitored fluorometrically (excitation 494 nm, emission 520 nm; photomultiplier (PMT) gain, 10). Measurements were made with injection volume of 100 μl and the retention time of HA was at about 5.8 min. The end of the run was determined by injecting FITC (retention time: 17 min). The HAF and FTIC contents were determined by using a standard calibration curve ranging from 0.1 to 20 μg/ml and 0.01 to 5 μg/ml, respectively.

1.2.5 In silico construction of the HA oligomers

The oligomers of HA were generated starting from the 3D structure determined by NMR (PDB Id: 2BVK) [14] which is composed by four repeating units (HA_4) of β(1→4)-D-glucuronic acid-β(1→3)-N-acetyl-D-glucosamine (as shown in **Figure 1.1**) and assumes a contracted left-handed four-fold helix geometry. The base HA chain was then obtained by multiplying per five the resolved starting structure to generate a molecule composed by 20 repeating units (HA_{20}). Two chains of different sulfonation degree were built by modifying the base oligomer in the hydroxyl group in 6 of the N-acetyl-D-glucosamine residue. Specifically, the two sulfated polymers were constructed by modifying one D-glucosamine residue every two (HA_{20S10}) and one D-glucosamine residues every four (HA_{20S5}). To investigate the effects of molecular length on HA folding, a non-sulfated chain composed by 10 repeating units (HA_{10}) was also considered.
Overall, four HA polymers were simulated: two non-sulfated oligosaccharides of different length (HA_{10} and HA_{20}) and two sulfated oligosaccharides having the same

length but differing for the sulfonation degree (HA_{20S10} and HA_{20S5}). Even though the differences in the simulated chains cannot exactly match the differences in the tested polysaccharides, and this is clearly due to the fact that short oligomers were here simulated, the four simulated polymers can reveal the conformational effect that a HA experiences when varying molecular weight and sulfation degree. The conformational profile of the generated polymers was analyzed by clustered MonteCarlo procedures (as implemented by VEGA suite of programs) [15] which produce 2,000 conformers by randomly rotating the flexible bonds pertaining the glycosidic linkages. The so obtained lowest energy structures were finally minimized and used in the following MD simulations.

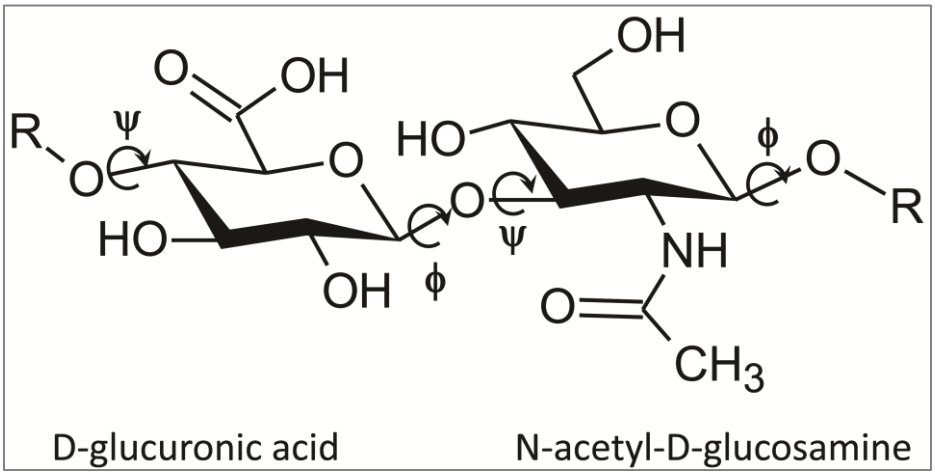

Figure 1.1 – Repeating unit of non-sulfated hyaluronic acid, i.e. (β (1→4)-D-glucuronic acid-β (1→3)-N-acetyl-D-glucosamine). Inter- and intra-repeating unit torsions ψ e ϕ are also indicated.

1.2.6 MD simulations

Firstly, the polymers were neutralized by adding the necessary number of sodium ions whose pose was computed by SODIUM program [16] and then inserted in a 70 Å × 90 Å × 70 Å box of water molecules (apart from HA_{10} which was solvated by a smaller 50 Å × 50 Å × 50 Å water box). It should be noted that, since the initial structure of all simulated oligomers corresponds to a rather extended conformation, the considered simulation space should be large enough to allow a complete flexibility of the oligomers

without biasing constraints. After a preliminary minimization to optimize the relative position of waters and ions, the obtained systems underwent 10 ns MD simulations which had the following characteristics: (a) Newton's equation was integrated using the r-RESPA method (every 4 fs for long-range electrostatic forces, 2 fs for short-range non bonded forces, and 1 fs for bonded forces); (b) the simulation space was stabilized by introducing Periodic Boundary Conditions (75 Å × 100 Å × 75 Å; 55 Å × 55 Å × 55 Å for HA_{10}); (c) the long-range electrostatic potential was treated by the Particle Mesh Ewald summation method (60 × 90 × 60 grid points; 50 × 50 × 50 points for HA_{10}); (d) the temperature was maintained at 300 ± 10 K by means of the Langevin's algorithm; (e) Lennard-Jones (L-J) interactions were calculated with a cut-off of 10 Å and the pair list was updated every 20 iterations; (f) a frame was stored every 20 ps, to yield 500 frames. The simulations were organized in two phases: an initial period of heating from 0 K to 300 K over 30,000 iterations (30 ps, i.e. 10 K/ps) and the monitored phase of 10 ns. All MD runs were carried out using Namd2.7 [17] with the force-field CHARMm v36 and Gasteiger's atomic charges on a 16-core Tyan VX-50 system. All mentioned minimizations were performed using the conjugate gradient algorithm until a r.m.s. equal to 0.01 kcal mol^{-1} $Å^{-1}$.

Similarly, HA_{20} and HA_{20S5} were simulated in a $CHCl_3$ cluster in order to analyze their conformational behavior in an apolar medium which brings to mind the skin's hydrophobic environment. The $CHCl_3$ cluster was built starting from a pair of interacting $CHCl_3$ molecules generated by semi-empirical calculations using MOPAC2010 and adopting the PM6 level of theory. The initial cubic box (135 Å × 135 Å × 135 Å, 14075 molecules) was built by the solvent builder as included in VEGA program and starting from the pair of interacting $CHCl_3$ molecules. The obtained system underwent a preliminary minimization to optimize the relative position of solvent molecules, and then an equilibrating 1 ns MD simulation, which had the above-described characteristics. Such a $CHCl_3$ cluster was then utilized to solvate the HA_{20} and HA_{20S10} oligomers, which underwent 10 ns MD runs applying the same computational protocol above described for the simulations in water.

The conformational profile of the simulated polymers was analyzed by monitoring the two torsion angles, φ and ψ, which describe the glycosidic linkage between two sugar units, while the puckering of furanose rings was not considered. As depicted in **Figure**

1.1, the φ angle pertains to the rotatable bond connecting the anomeric carbon atom of i^{th} saccharide with glycosidic oxygen atom, while the ψ angle refers to the rotatable bond connecting the glycosidic oxygen atom to the carbon atom of $i+1^{th}$ saccharide. Specifically, the φ torsion is the dihedral angle defined by the following atoms $H_{\alpha i}$- $C_{\alpha i}$-O-C_{i+1}, while the ψ torsion is defined by $C_{\alpha i}$-O-C_{i+1}-H_{i+1}. For the sake of simplicity, the angle values were analyzed without discriminating between inter- or intra-repeating unit torsions. To do this, an *ad-hoc* script was written for VEGA software which automatically recognizes the described torsion angles and can also computes average values when analyzing trajectory files.

1.3 Results and Discussion

1.3.1 In vitro penetration studies

Since the sensitivity of the analytic methods permitted to quantify permeants only 24 hours after application (**Table 1.1**), it was possible to determine neither the flux of HAs through the skin nor the lag time.

Table 1.1 reports the amounts of the considered HAs diffused across the human stratum corneum and epidermis as quantified in the receiving phase after 24 hours and shows that molecular weight and sulfation degree strongly influence the permeation of HAs. Thus, an analysis in depth of **Table 1.1** allows two major considerations to be done. Firstly, the comparison of HAs having the same molecular weight but differing for the degrees of substitution reveals that the stratum corneum and epidermis were more permeable to the sulfated derivatives compared to unsubstituted HA. In detail, the reported permeated amounts evidence that the lower substitution degree (i.e. 1% mol) shows favorable skin penetration characteristics providing the highest permeated amounts.

Secondly, the comparison of the three pairs of macromolecules having similar degrees of substitution but differing for the molecular weight indicate that the permeated amounts of low molecular weight compounds are about 10-folds higher than the corresponding medium-molecular weight compounds. Notably, this effect is similarly observed in all compared pairs thus suggesting that the molecular weight effect is not influenced by the degree of sulfation.

1.3.2 Confocal laser scanner microscopy

The penetration pattern of HAs through human stratum corneum and epidermis was then estimated using a medium-molecular weight HA conjugated with fluorescein isothiocyanate (FITC) as a fluorescent probe, hereinafter termed HAF for the sake of brevity.

The confocal images of untreated stratum corneum and epidermis stained by propidium iodide (PI) (red signal) clearly shows corneocytes as well as the nuclei of dead cells of epidermis **(Fig. 1.2 A)**. After 30 min exposure to HAF, a green signal appeared in the stratum corneum (**Fig. 1.2 B)** and reached the equilibrium within 2 hours (**Fig 1.2 C)**.

Fig. 1.3 compares the z-stack projections, namely, the longitudinal views of the epidermis, recorded in skin exposed to the HAF solution (**Fig. 1.3 A**) or a solution containing only FITC (**Fig. 1.3 B**). HAF shows a great affinity for keratins of the stratum corneum, since the overall structure of corneocytes presented a homogeneous green colorimetry, while it is hardly visible in the epidermis (**Fig. 1.3 A**). Conversely, the z-stack projections recorded in the skin samples exposed to the FITC solution evidence only a slightly superficial fluorescence (**Fig. 1.3 B**) remaining constant over time (data not shown).

These results are in agreement with the bio-imaging for the transdermal delivery of FITC after topical administration to the dorsal skin of female hairless mice as provided by Yang and co-workers [18]. Both results imply that FITC alone is unable to bind any components of corneocytes thus indicating that the fluorescent probe diffused through the stratum corneum and epidermis without being retained, unlike HA.

The qualitative results of confocal imaging are consistent with those obtained by gel permeation chromatography. Indeed, FITC was quantified in the receptor phase (0.02 ± 0.01 µg/cm^2) in the first sampling at 15 min, while HAF was detected only after 6 hours and became quantifiable only after 24 hours (**Table 1.1**). No other fluorescent signals were detected in the chromatograms indicating that HAF permeated without being significantly cleaved. This result is also consistent with literature data [7; 18] and allows us to confirm that no significant degradation of HA occurred during the passive diffusion through stratum corneum and epidermis in our experimental conditions.

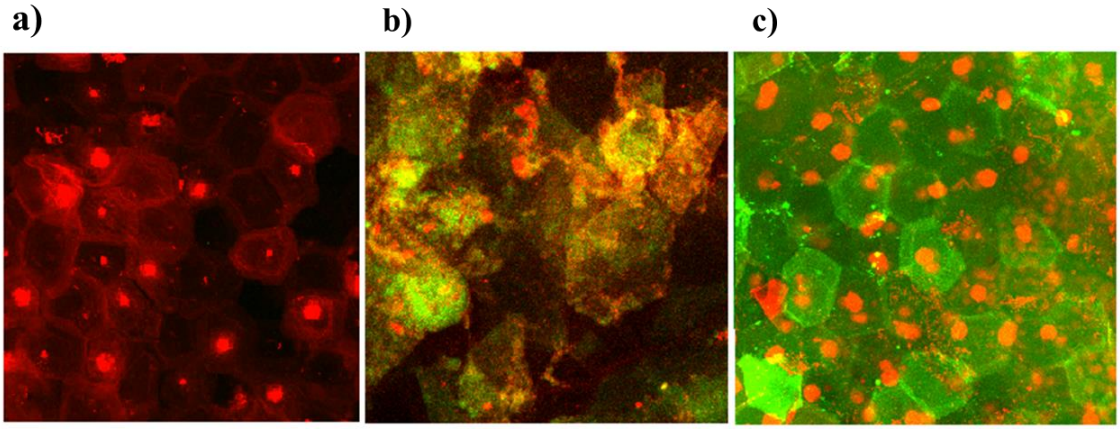

Fig. 1.2 – CLSM images showing distribution of HAF in human stratum corneum and epidermis increasing durations of application: (**B**) 30 min and (**C**) 2 h. Panel **A** depicts the accumulation of free propidium iodide in the inter-corneocyte spaces and the nuclei of dead cells of epidermis. Being lipophilic in nature, the dye is seen to accumulate in intercellular spaces (red stained). HAF appeared in the stratum corneum (green signal) 30 minutes after the application of the solution (**A**) reaching the equilibrium in 2 hours (**B**).

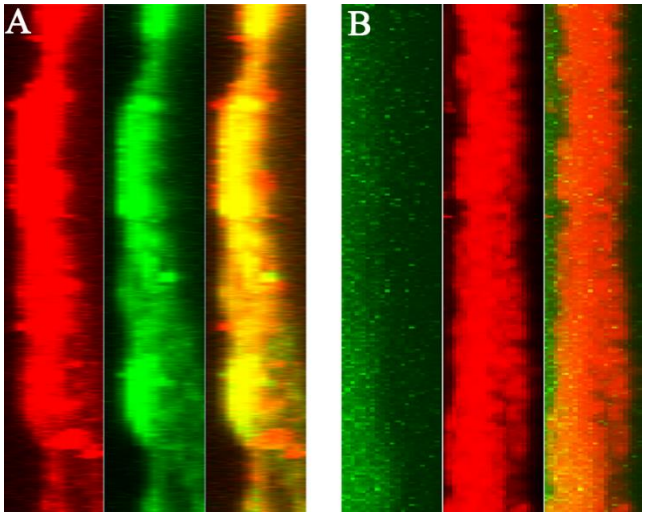

Fig. 1.3 – CLSM images (z-stack projections) showing human stratum corneum and epidermis 30 min after application of (**A**) HAF and (**B**) FTIC in aqueous solution. The green fluorescence corresponds to furrows where HAF and FTIC accumulated. The red color corresponds from the fluorescence emanating from the human stratum corneum and epidermis stained by propidium iodide and the yellow-green from HAF.

1.3.3 In silico studies of hyaluronans

To analyze the conformational profiles of the simulated hyaluronan chains, three descriptors were monitored: (a) the radius of gyration which describes molecular size and shape and is well suited to examining polymer flexibility [19]; (b) the end-to-end distance, namely the distance between one end of the polymer chain and the other end [20], and (c) the percentage of synclinal geometries in the torsions around the anomeric link (φ and ψ, as represented in **Figure 1.1**). The first two descriptors are common indices used in polymer simulations, while the last parameter allows the overall structural properties to be linked to the local conformational changes in the glycosidic linkages.

The first part of the study compares the two non-sulfated polymers of different length (HA_{20} and HA_{10}). The reported values for the aforementioned descriptors (**Table 1.2**) show that the two polymers have a comparable conformational profile as suggested by a similar abundance of synclinal geometries in both torsions but the longer HA_{20} chain shows a more compacted structure (**Fig. 1.4 A**) as evidenced by both end-to-end distance and radius of gyration normalized per the number of the repeating units.

These results confirm that in aqueous solution and at low ionic strength hyaluronic acid assumes a contracted left-handed helix conformation which is stabilized by an extensive H-bond network involving both solute-solvent interactions and inter-residue contacts such those seen between the carboxylate of a glucuronic acid and the acetamide of the adjacent glucosamine [10]. Such a structure is in encouraging agreement with both NMR and X-ray data [14; 21] and emphasizes the conformational versatility of the hyaluronan chains despite the caging effect of water molecules around the glycosidic linkages.

Table 1.2 – Average values (± standard deviation) for the main parameters extracted from MD runs for the non-sulfated HA polymers of different length (HA_{10} and HA_{20}) and the longest sulfated HA polymer at two degrees of sulfation (HA_{20S5} and HA_{20s10}). The conformations are defined as synclinal (in fact including also disfavoured synperiplanar geometries) when comprised in the -90 → +90 ranges. In parenthesis, the average values of radius of gyration and end-to-end distance normalized per the number of HA units are reported.

Oligomers	φ % synclinal geometries	ψ % synclinal geometries	Radius of gyration (Å)	End-to-end distance (Å)
HA_{10}	60.0	100	10.32 ± 1.05 (1.03)	26.91 ± 4.34 (2.69)
HA_{20}	61.5	100	15.67 ± 8.37 (0.78)	25.89 ± 8.57 (1.29)
HA_{20S5}	53.8	97.4	25.92 ± 1.43 (1.29)	59.62 ± 6.07 (2.98)
HA_{20S10}	64.1	97.8	21.51 ± 3.88 (1.08)	46.67 ± 4.15 (2.33)

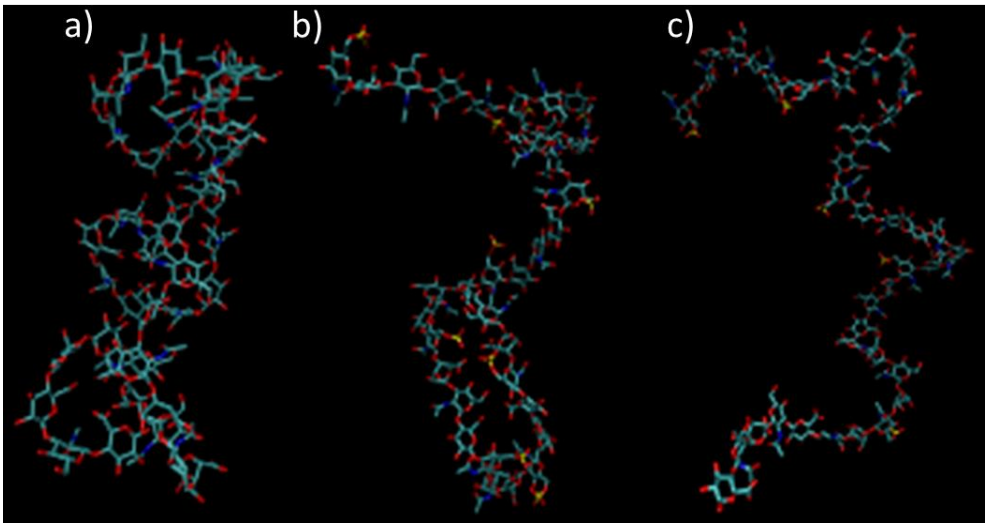

Fig. 1.4 – Representative examples of the hyaluronan conformations as extracted by MD runs. (**A**) Folded structure for non-sulfated HA_{20}: the helical structure is characterized by the axis of about 1.0 nm a loop diameter of about 1.2 nm and 4 disaccharides per turn. (**B**) Intermediate conformation as obtained for HA_{20S10} which loses the helical structure while showing a rather compact conformation in which the polymer ends fold on themselves forming elliptic structures whose shape and width should minimize the electrostatic repulsion between sulfonic groups. (**C**) Extended and flexible structure as observed for HA_{20S5}.

The second part of the study involved the sulfated chains with a view to analyzing how the sulfonation degree can influence their conformational behavior. **Table 1.2** and **Fig. 1.5** compare the longer non-sulfated HA_{20} chain with the two differently sulfated HA_{20S5} and HA_{20S10} chains which can be seen as representative of the tested hyaluronans at medium molecular weight and with a sulfation degree of 1 and 2.5 % mol, respectively. The performed MD simulations suggest that both sulfated polymers undergo large conformational changes and lose the helical architecture seen in the non-sulfated structures.

Although both sulfated chains show a substantial disruption of the helix motifs, **Fig. 1.4** clearly shows the significant differences between them because the less sulfated HA_{20S5} (**Fig. 1.4 C**) chain appears markedly more extended than the other one (**Fig. 1.4 B**). This is also documented by both end-to-end distance and radius of gyration as well as by relative abundance of the synclinal geometries. Concerning the local conformation of the glycosidic linkages. **Table 1.2** confirms that the ψ angle assumes almost exclusively synclinal geometries in all performed simulations regardless of polymer length and sulfonation. In contrast, relevant differences are seen in the conformational profiles of the φ angle since the percentage of synclinal geometries decreases in the HA_{20S5} polymer which appears characterized by more disordered and more extended conformations (vide infra), while the percentage in the HA_{20S10} chain remains comparable with the values observed for the non-sulfated polymers.

A detailed description of the conformational behavior of the simulated chains is provided by the radiuses of gyration (**Fig. 1.5 A**) and the end-to-end distances (**Fig. 1.5 B**).

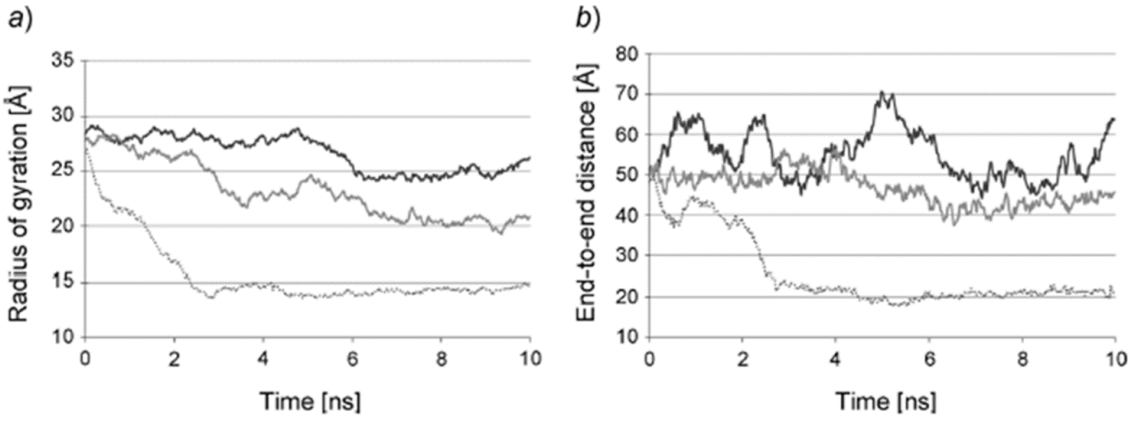

Fig. 1.5 – Dynamic profiles of (**A**) radius of gyration and (**B**) end-to-end distance as computed by MD simulations of non-sulfated HA (HA_{20}, dashed grey line), HA_{20} at low degree of sulfation (HA_{20S5}, black line) and HA_{20} at high degree of sulfation (HA_{20S10}, grey line).

Both these descriptors indicate that the HA_{20S5} polymer assumes significantly extended conformations as confirmed by the highest values in both parameters, while the more sulfated HA_{20S10} chain presents an intermediate behavior characterized by disordered but more folded structures. Moreover, Fig. **1.5 B** shows that the HA_{20S5} polymer has a vastly greater flexibility since it repeatedly changes its whole conformation bouncing between conformations quite similar to those of HA_{20S10} (i.e., d ~ 50 Å) and conformations vastly more extended (i.e., d ~ 70 Å) without reaching an equilibrium phase.

Notably, **Table 1.2** shows that the described differences between sulfated and non-sulfated oligomers are maintained also when simulated in chloroform, which was chosen to simulate an apolar medium roughly comparable to the skin environment. Indeed, HA_{20} assumes a contracted left-handed helix conformation also in chloroform, while HA_{20S5} conserves an elongated and disordered geometry. The differences between simulation in water and chloroform are, on average, marginal even though one may note that the differences between sulfated and non-sulfated oligomers are a little reduced in chloroform and this can be ascribed to the increased solvent weight which slows down the solute movements due to molecular friction as well as to the inability of the solvent to stabilize strong interactions with the simulated oligomers.

Altogether, the performed simulations allow some considerations to be done which can be summarized as follows:

- The non-sulfated chains assume quite ordered left-handed helices and this is in clear agreement with the experimental data. As a trend, the simulations suggest that conformational compactness increases with polymer length.
- The sulfated chains lose the ordered helical motif and assume quite disordered structures, the less sulfated being more flexibly extended than the HA_{20S10} chain. In all simulated polymers conformational rigidity increases with the number of charged groups probably because the repulsion between them plays a dominant role with few charged groups, while an increased number of charged moieties tends to generate an ordered reticulum of ion-pairs which stabilize the polymer conformation [22].
- The observed conformational differences were found to be not markedly influenced by the polarity of the simulated media. At least, they are somewhat affected by solvent friction which however cannot alter the overall conformational profile.

1.4 Conclusions

Although the moisture content of stratum corneum and the aqueous composition of the epidermis permit a significant permeation also for hydrophilic compounds, the skin permeation of small organic molecules strongly decreases when increasing molecular size, polarity and the number of H-bonding groups [1; 23].

The present study clearly evidences that the investigated biopolymers do not obey the aforementioned physicochemical rules. Indeed, the reported experimental results evidenced that hyaluronans have a great affinity for keratin and likely cross human stratum corneum and epidermis mainly through corneocytes rather than intercellular lipidic network. Moreover, the obtained results clearly indicate that sulfated polymers penetrate in a larger extent than the corresponding hyaluronic acids (**Table 1.1**), despite their vastly greater polarity.

The molecular dynamics study can help to rationalize these data, shifting the focus on polymer flexibility and evidencing how the observed penetration behavior can be rationalized by the polymer's conformational profile. In particular, the normalized values of radius of gyration were found to be in line with the extent of diffusion across the

stratum corneum and epidermis over 24 hours, the higher the values of radius of gyration, the higher the diffused amount.

Such a trend can be explained considering that the penetration increases with the capacity to assume extended and flexible structures which can easily adapt themselves to the skin environment, which deeply changes due to the different composition of the viable epidermis, corneocytes and lipophilic network.

Acknowledgment

The Authors would like to thank Fidia Farmaceutici S.p.A. to kindly provide HA and their sulfated derivatives, Dr. Matteo D'Este for the synthesis of FITC labeled HA, and Dr. Fabio Bettella for the quantitative determination of the permeated amount of such compounds.

References

1. Potts R.O, Guy R.H. A predictive algorithm for skin permeability: the effects of molecular size and hydrogen bond activity. Pharmaceutical Research 1995**,** 12 (11), 1628-1633;
2. Geinoz S, Guy R.H, Testa B, Carrupt P.A. Quantitative structure-permeation relationships (QSPeRs) to predict skin permeation: a critical evaluation. Pharmaceutical Research 2004, 21 (1), 83-92;
3. Parisel C, Saffar L, Gattegno L, André A, Abdul-Malak N, Perrier E, Letourneur D. J. Interactions of heparin with human skin cells: binding, location, and transdermal penetration. Journal of Biomedical Materials Research Part A, 2003, 67, 517-523;
4. Lanke S.S.S, Kolli C.S, Strom J.G, Banga A.K. Enhanced transdermal delivery of low molecular weight heparin by barrier perturbation. International Journal of Pharmaceutics 2009, 365 (1-2), 26-33;
5. Brown M.B, Marriott C, Martin G. P. The effect of hyaluronan on the in vitro deposition of diclofenac within the skin. International Journal of Tissue Reaction 1995, 17 (4), 133-140;
6. Laurent T.C, Ryan M, Pietruszkiewicz A. Fractionation of hyaluronic acid. The polydispersity of hyaluronic acid from the bovine vitreous body. Biochimica & Biophysica Acta 1960, 42, 476–485;
7. Brown T.J, Alcorn D, Fraser J.R.E. Absorption of Hyaluronan Applied to the Surface of Intact Skin. The Journal of Investigative Dermatology 1999, 113 (5), 740-746;
8. Brown M.B, Jones S.A, He W, Martin G.P. Hyaluronan: Investigations into the mode of action of hyaluronan in topical drug delivery. ACS Symposium Series 2006, 934, 141-153;
9. Martin G.P, Brown M.B, Bennett F.C, Marriott C. An In Vitro Study of the Diclofenac Delivery Properties of Hyaluronan in Human Skin. Journal of Drug Delivery Science and Technology 1999, 6 (1), 39-43;
10. Furlan S, La Penna G, Perico A, Cesàro A. Hyaluronan chain conformation and dynamics. Carbohydrate Research 2005, 340 (5), 959-970;
11. Gargiulo V, Morando M.A, Silipo A, Nurisso A, Pérez S, Imberty A, Cañada F.J, Parrilli M, Jiménez-Barbero J, De Castro C.. Insights on the conformational properties

of hyaluronic acid by using NMR residual dipolar couplings and MD simulations. Glycobiology 2010, 20 (10), 1208-1216;

12. Bitter T. and Muir H.M. A modified uronic acid carbazole reaction. Analytical Biochemistry 1962, 4, 330-334;
13. Cilurzo F, Minghetti P, Alberti E, Gennari C.G.M, Pallavicini M, Valoti E, Montanari L. An investigation into the influence of counterion on the RS-propranolol and S-propranolol skin permeability. Journal of Pharmaceutic Sciences 2010, 99 (3), 1217-1224;
14. Almond A, Deangelis P. L, Blundell C. D. Hyaluronan: the local solution conformation determined by NMR and computer modeling is close to a contracted left handed 4-fold helix. Journal of Molecular Biology 2006, 258, 1256-1269.
15. Pedretti A, Villa L, Vistoli G. VEGA: a versatile program to convert, handle and visualize molecular structure on Winows-based PCs. Journal of Molecular Graphics 2002, 21, 47-49;
16. Balaeff, A. http://www.ks.uiuc.edu/Development/MDTools/sodium/;
17. Phillips J.C, Braun R, Wang W, Gumbart J, Tajkhorshid E, Villa E, Chipot C, , Skeel R.D, Kalé L, Schulten K. Scalable molecular dynamics with NAMD. Journal of Computational Chemistry 2005, 26 (16), 1781-1802;
18. Yang J, Kim S, Kwon J. H, Kim H, Shin J.H, Yun S.H, Choi K.Y, Hahn S.K. Transdermal delivery of hyaluronic acid -- human growth hormone conjugate Biomaterials, 2012, 33 (25), 5947-5954;
19. Vree C. and Mayr S. G. Dynamics and diffusive–conformational coupling in polymer bulk samples and surfaces: a molecular dynamics study. New Journal of Physics 2010, 12, 023001, 1-10;
20. Mattice W.L. Expansion of the end-to-end distance and radius of gyration in perturbed polymethylene chains. The Journal of Physical Chemistry 1984, 88 (26), 6492.-6494;
21. Donati A, Magnani A, Bonechi C, Barbucci R, Rossi C. Solution structure of hyaluronic acid oligomers by experimental and theoretical NMR, and molecular dynamics simulation. Biopolymers 2001, 59 (6), 434-445;
22. Horkay F, Falus P, Hecht A.M, Geissler E. Length scale dependence of the dynamic properties of hyaluronic acid solutions in the presence of salt. The Journal of Physical Chemistry B 2010, 114 (47), 15445-15450;

23. Minghetti P, Casiraghi A, Cilurzo F, Montanari L, Monzani M.V, Bertolini G, Zaliani A. Solvation enthalpies as descriptors of structure--in vitro percutaneous permeation relationship of benzoxazinones regioisomers. Il Farmaco 2000, 55 (8), 563-568.

2. Influence of chemical and structural features of Low Molecular Weight Heparins (LMWHs) on skin penetration

Abstract

Low molecular weight heparins (LMWHs) are produced from heparin by different depolymerization methods that determine different molecular weights (M_w) and the formation of new structural features on the polysaccharide backbone; moreover, sodium or calcium can be used as counter-ions. This work aimed to elucidate the effect of these factors on the in vitro penetration of LMWHs through human epidermis. LMWHs were assayed determining the ability to inhibit the Factor Xa. The average M_w seemed to play a role in defining the extent of skin penetration of LMWHs. Indeed, Pearson correlation between the log M_W and the amount permeated through the epidermis of sodium LMWHs resulted -0,758. Also the chemical features of LMWHs seemed to have an effect on the permeation process, with bemiparin and enoxaparin, obtained by β-elimination processes, which exhibited the best diffusion properties ($J_{bemiparin}$ = 11.1 ± 0.3 and $J_{enoxaparin}$ = 7.9 ± 1.9 mIU/cm^{2}h). In contrast, parnaparin, which maintained the chemical features of heparin, showed the lowest diffusion and the greatest affinity for the epidermis. Finally, the circular dichroism analyses performed on nadroparin revealed that the use of calcium as counter-ion reduced the chain mobility and consequently significantly decreased the LMWHs permeation through the epidermis.

.

The content of this chapter has been submitted for publication to an international peer-reviewed journal.

2.1 Introduction

Low molecular weight heparins (LMWHs) are anticoagulant and antithrombotic drugs, mainly used in the prevention and treatment of deep vein thrombosis (DVT) after major surgical procedures.

They have almost one third of the molecular mass of unfractionated heparin (UFH) and exhibit a lower affinity for plasma proteins thus providing more predictable effects, better pharmacokinetic parameters and safety profile (e.g. lower risk of bleeding and heparin-induced thrombocytopenia) [1]. Therefore, they are currently administered to outpatients replacing in clinical practice the use of UFH [2].

LMWHs available on the market are obtained by four different depolymerization strategies of UFH, namely deaminative cleavage, chemical or enzymatic β-elimination and oxidative cleavage with radical agents. Depending on the specific reaction and the cleavage points along the UFH chain, LMWHs vary for average molecular weight (M_w) and molecular weight distribution, degree of sulfation, and peculiar terminal end residues, which are artifacts of the production process. As an example, LMWHs obtained by deaminative cleavage with nitrous acid present a 2,5-anhydro mannose residue at the reducing end, whereas β-elimination in alkaline conditions produces 4-enopyranose uronate residues at non reducing ends and N-sulfoglucosamine at the reducing end (**Table 2.1**) [3; 4]. LMWHs obtained by different depolymerization methods are then dissimilar in structure, and exhibit distinct physical, chemical and biological properties [5].

In the last decade, several efforts were made to propose non-invasive alternatives to subcutaneous route of administration [6]. The poor intestinal absorption together with the degradation of heparins both in liver and in gastrointestinal tract make the oral administration not feasible [7]. Transdermal delivery may represent a valid alternative, even if LMWHs diffusivity through the skin is limited by large Mw, hydrophilicity and negative charge [8]. These issues along with the possible strategies to enhance LMWHs permeation through the skin can be easily deduced by literature data [9]. However, since these strategies were mainly applied to a specific LMWH, a systematic evaluation of the impact of the main features of such polysaccharides on their permeation profile is still missing to the best of our knowledge.

With a view to getting an insight on the influence of the production method and the resulting structural features of LMWHs on permeability properties, the current work explored the in vitro passive diffusion through human epidermis of six commercially available LMWHs in comparison with UFH.

Table 2.1- Main features of tested LMWHs

Depolymerization method	LMWH	Substrate	Average M_w (Da)	Major non reducing end	Major reducing end
Deaminative cleavage (nitrous acid)	**Nadroparin**	UFH	4,300	2-O-sulfo-α-l-idopyranosuric acid	6-O-sulfo-2,5-anhydro-d-mannitol
	Dalteparin	UFH	6,000	2-O-sulfo-α-l-idopyranosuric acid	6-O-sulfo-2,5-anhydro-d-mannitol
	Reviparin	UFH	3,900	2-O-sulfo-α-l-idopyranosuric acid	6-O-sulfo-2,5-anhydro-d-mannitol
β-Eliminative cleavage	**Enoxaparin**	Benzyl ester of UFH	4,500	2-O-sulfo-4-enopyranose uronate	2-N,6-O-disulfo-d-glucosamine
	Bemiparin	UFH benzethonium salt	3,800	2-O-sulfo-4-enopyranose uronate	2-N,6-O-disulfo-d-glucosamine
Radical-catalysed depolymerization	**Parnaparin**	UFH	5,000	2-O-sulfo-α-l-idopyranosuric acid	2-N,6-O-disulfo-d-glucosamine

2.2 Experimental section

2.2.1 Materials

Sodium enoxaparin (Clexane®, Sanofi Aventis), sodium parnaparin (Fluxum®, Alfa Wasswemann), calcium nadroparin (Fraxiparina®, GlaxoSmithKline), sodium dalteparin (Fragmin®, Pfizer), sodium reviparin (Clivarina®, Abbott) and sodium bemiparin (Ivor®, Sigma-tau). Sodium UFH (activity 195 IU/mg) was kindly donated by LDO S.p.A. (Milan, Italy). WHO 3rd International Standard for Low Molecular Weight Heparins (NIBSC code: 11/176) was kindly gifted by Italfarmaco S.p.A. (Cinisello Balsamo, Italy). Kit Coatest® Heparin was purchased by Chromogenix Instrumentation Laboratory S.p.A. (Milan, Italy). Ethylenediaminetetracetic acid disodium salt (EDTA) was purchased by Carlo Erba Reagenti (Milan, Italy). Trypsin-EDTA (0.05% trypsin, 0.02% EDTA) solution with phenol red was purchased by EuroClone S.p.A. (Pero, Italy). All other reagents were of analytical grade unless specified.

2.2.2 In vitro human skin permeation studies

In vitro permeation tests were performed by using Franz diffusion cells and human epidermis as membrane. The vertical cells used in the set of experiments have a wider column than the original Franz-type diffusion cell with a diffusion area of 0.636 cm^2 and an average receptor volume of 3.0 mL. Abdominal human skin was obtained by healthy volunteers who underwent cosmetic surgery. Samples were prepared according to an internal standard protocol [10].

The integrity of tissue was preliminary assessed by measuring the electrical impedance of epidermis sheets (voltage: 250 mV, frequency: 100 Hz; Agilent 4263B LCR Meter, Microlease, Italy). Only samples with values above 40 $k\Omega cm^2$ were considered suitable and used for the test.

The human epidermis was mounted on lower half of the Franz cell and the upper and lower parts of the cell were sealed with Parafilm® and fastened together by means of a clamp. The receiver compartment was filled with a 0.05 mol/L Tris-EDTA buffer at pH

7.4 containing 100 µg/mL of sodium azide as preservative, and continuously stirred with a magnetic bar. Donor compartment was loaded with 500 µL of LMWH or UFH solution corresponding to a concentration of 2000 IU/mL.

Particular care was taken to avoid the formation of air bubbles between the membrane and the receptor compartment. The system was kept at 37 ± 1 °C by means of a circulating water bath so that the epidermis surface temperature was at 32 ± 1 °C throughout the experiment.

At predetermined times, 0.2 mL of receiving phase were withdrawn and replaced with fresh medium in order to maintain sink conditions.

Only biologically active permeate was analyzed according to the procedure reported below. At least one control cell loaded with pure saline solution was included in each experiment in order to assess the interference of skin components in the biological assay.

At the end of the in vitro permeation tests, the amount of active substance retained into the epidermis was also determined (R_{24}). Briefly, tested solutions were withdrawn from the donor compartments and the permeation areas were circumscribed. SCE sheets were removed from the cells and cut within the permeation area to obtain sections of 0.2 cm^2 each. These were cleaned with a cotton swab and washed in water to remove any residual trace of LMWHs solution and let to dry.

The extraction of LMWHs from the skin was carried out modifying the method proposed by Song [11]. Epidermis sections were weighted, immersed in 5 mL of 0.05 mol/L Tris-EDTA buffer, vortexed for 2 min exacts and sonicated for 20 min. Then, samples were incubated at 37 ± 0.1 °C for 2 hours under agitation prior to be filtered with 0.45 µm acetate cellulose membrane and analyzed.

The cumulative amount of drug permeated through the skin per unit area was calculated from the concentration of the permeant in the receiving medium and plotted as a function of time. The steady flux (J) was determined as the slope of the linear portion of the plot.

2.2.3 UFH or LMWHs determination

UFH or LMWHs biological activity was measured by using the Coatest® kit (Chromogenix, Instrumentation Laboratory S.p.A.) for the photometric determination of UFH. This relies on the ability of heparins-antitrombin III (AT) complex to react with an

excess of factor Xa (FXa). Unreacted FXa is hydrolyzed by a chromogenic substrate and read spectrophotometrically at 405 nm. The absorbance is inversely proportional to LMWHs concentration. The manufacturer protocol was slightly modified. Test and standard samples were prepared into the stock buffer solution and directly combined with AT without further dilutions. A volume of 100 µL test solution were incubated with AT in the 1:1 ratio for 3 min at 37 ± 1 °C. Subsequently 100 µL of FXa were added and, after vortexing, the mixture was re-incubated at 37 ± 1 °C for 30 s.

The unreacted FXa was hydrolyzed by adding 200 µL of chromogenic substrate S-2222. After incubation for 3 min at 37±1 °C, the reaction was stopped adding 300 µL of 20% acetic acid.

The assay was carried out in parallel for the blank solution.

Calibration curves in the range 0.1-0.003 IU/mL were built up by using the international standard for LMWHs and sodium UFH.

2.2.4 Circular dichroism (CD)

CD spectra were recorded on a J-810 spectropolarimeter, using a quartz cuvette of 0.1 cm path length, between 190 and 260 nm at a scanning rate of 50 nm/min with 0.5 nm resolution. The analysis was carried out on 10 mg/mL samples in water at room temperature. To obtain a solution of sodium nadroparin, the commercial calcium nadroparin was treated with 1.4% w/v disodium EDTA. After overnight incubation, the salts were removed by ultrafiltration and the recovered sample was reconstituted to the original volume.

2.3 Results

All molecules permeated the epidermis to a very low extent **(Table 2.2)**. In the case of calcium nadroparin and UFH, the permeated amounts were quantifiable only at the end of experiments and, therefore, the fluxes were not calculated.

With the exception of parnaparin, all sodium LMWHs showed a Q_{24} almost 10-fold higher than that of UFH, the precursor with the complete polysaccharide chain.

Bemiparin, characterized by the lowest M_w, showed Q_{24} and J values higher than those found for all LMWHs tested ($p<0.03$), with the exception of enoxaparin, which shares the same chemical residues at the terminal ends (**Table 2.1**). In contrast, parnaparin, obtained by radical depolymerization, exhibited the lowest J among sodium LMWHs ($p<0.006$). Within the class of molecules obtained by deaminative cleavage, dalteparin permeated less than reviparin ($p<0.05$) in agreement with its higher M_w (**Table 2.1**).

The pattern of calcium nadroparin appeared anomalous because this molecule permeated the epidermis to a very low extent in spite of the M_w (M_w = 4,300 Da) close to that of enoxaparin (M_w=4,500) and with respect to the compounds obtained by the same synthetic strategy, namely reviparin and dalteparin. This result was in agreement with that of Gooma and co-workers who reported the lack of passive permeation of calcium nadroparin both through animal and human cadaveric skin up to 48 hours [8]. To verify if this feature could be attributed to the influence of the counter-ion (i.e. calcium instead of sodium), the in vitro skin permeation of a solution of calcium nadroparin containing 0.05% of disodium EDTA was assessed. The addition of the chelating agent improved the permeation of nadroparin, which became similar to that of reviparin, but did not affect the amount retained into the human epidermis at the end of the experiments, R_{24} (**Table 2.2**).

The R_{24} values were almost an order of magnitude higher than Q_{24}, in all cases. Furthermore, the R_{24} of all LMWHs resulted 10-fold higher than the value determined for UFH. Finally, this parameter did not appear to be influenced both by the production process and type of counter-ion since any significant difference was determined among the LMWHs (One way ANOVA $p=0.07$, **Table 2.2**).

Table 2.2- Main permeation parameters of the tested compounds (mean value ± SE)

Compound	Q_{24} (IU/cm^2)	R_{24} (IU/cm^2)	J (IU/cm^2 h x 10^{-3})
Calcium nadroparin	0.001 ± 0.000	1.117 ± 0.197	-
Sodium nadroparin*	0.157 ± 0.049	0.992 ± 0.058	5.3 ± 0.9
Sodium dalteparin	0.115 ± 0.000	1.431 ± 0.203	6.2 ± 0.0
Sodium Reviparin	0.147 ± 0.002	1.737 ± 0.172	7.1 ± 0.1
Sodium Enoxaparin	0.179 ± 0.045	0.837 ± 0.221	7.9 ± 1.9
Sodium Bemiparin	0.212 ± 0.020	1.300 ± 0.213	11.1 ± 0.3
Sodium Parnaparin	0.008 ± 0.005	1.571 ± 0.550	0.1 ± 0.1
UFH	0.001 ± 0.000	0.103 ± 0.029	-

**Nadroparin calcium/0.05% Na_2 EDTA solution*

2.4 Discussion

The considered LMWHs globally permeated the epidermis to a low extent after 24 hours of application in agreement with the literature data [8; 11; 12; 13; 14; 15]. The lack of diffusion of these compounds through the skin can be justified considering the large molecular size and hydrophilicity and the repulsive forces between the negatively charges of lipids of stratum corneum and LMWHs [12]. However, some significant difference among the tested compounds was found.

An overview of the obtained data evidenced that the most critical parameter affecting the permeation process through the human epidermis of LMWHs is the nature of the counter-ion. As demonstrated in the case of nadroparin, the substitution of calcium with sodium determined an improvement of the Q_{24} of about two order of magnitude without affecting the R_{24} values. We attributed this behavior to a possible influence of the type of counter-ion on the chain flexibility of the LMWHs. In order to confirm this hypothesis the circular dichroism (CD) spectra of the two compounds were recorded (**Figure 2.1**). The substitution of Ca^{2+} ions with Na^{+} ions determined a significant increase of the intensity and a slight red shift (211.5 nm vs 210 nm) of the negative band centered at about 210 nm, relative to $n \rightarrow \pi^*$ transitions of amide and carboxyl groups across the β 1,4-linkage. These differences in the CD spectra were attributed to the formation of an intramolecular

chelate in which calcium binds two adjacent carboxyl groups within the same chain [16]. The formation of such complex limits the rotation along the glycosidic linkage lowering the flexibility of the molecule [17] and therefore its ability to diffuse through the epidermis. This result is also in agreement with those obtained using hyaluronan and sulfates thereof, which revealed a relationship between the passive permeation through the epidermis of glycosaminoglycans and their ability to assume a flexible structure during the diffusion across the skin environment [18].

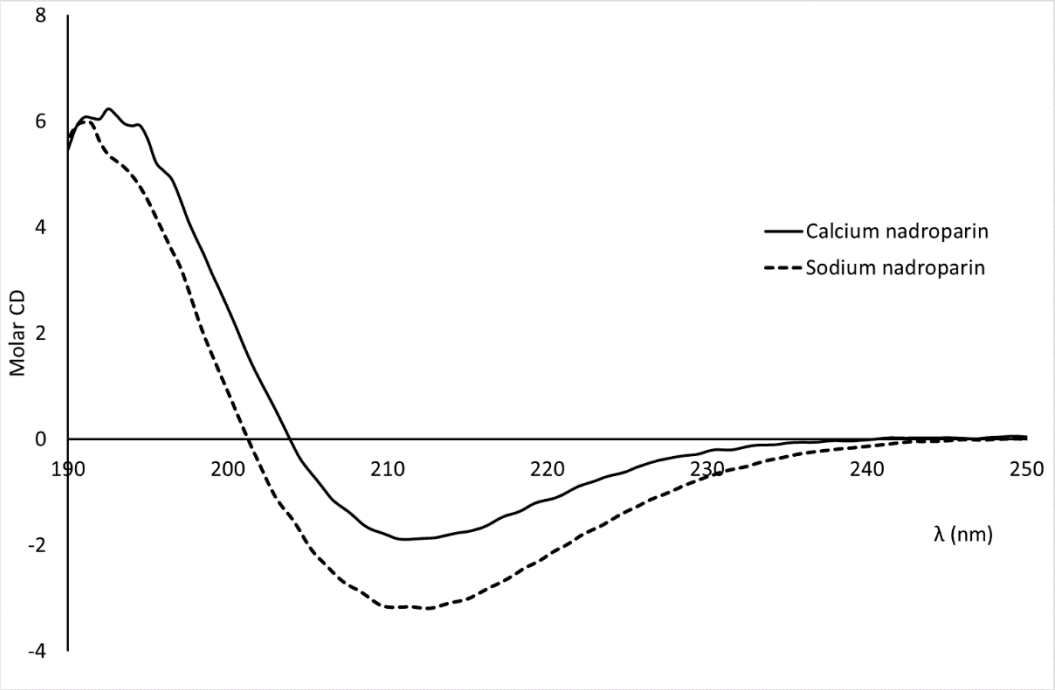

Figure 2.1 – CD spectra of nadroparin: effect of the counter-ion

Among the variables considered in the study, also M_w resulted to play an important role in determining the trend of penetration of such polysaccharides. Indeed, an acceptable Pearson correlation between the Log M_w and Q_{24} values determined for sodium LMWHs was found (R= -0.753). However, the M_w did not completely explain the diffusion pattern of LMWHs. As an example, the J value of parnaparin, having a M_w of 5,000, was about an order of magnitude lower than the J determined for dalteparin (M_w 6,000). Moreover the Q_{24} values found for parnaparin and UFH did not result to be statistically different

($p>0.05$), in spite of the significant larger molecular weight distribution of UFH. Such evidences suggested that the structural features resulting from the different depolymerization processes also exert a fundamental role in determining the extent of permeation of these macromolecules through human epidermis. Indeed, the similar penetration pattern of parnaparin and UFH can be justified by the fact that the oxidative breakage of UFH chain does not involve substantial modifications of the oligosaccharide sequence and, consequently, parnaparin shares almost the same chemical residues of the precursor. Moreover, the oxidative strategy leads to molecules with slightly higher degree of sulfation [4] and, hence, higher polarity, and this negatively impacted on the diffusion through human epidermis.

In contrast, β-elimination method causing the formation of unique chemical features, i.e. unsaturated uronic acid residues at the non-reducing end (**Table 2.1**), seemed to enhance the permeation of LMWHs with respect to the other synthetic strategies (**Table 2.2**). Thus, the highest flux determined for bemiparin can be justified considering both the lowest M_w and the 2-O-sulfo-4-enopyranose uronate residues at the non-reducing ends.

The amount of LMWHs retained into the human epidermis at the end of the experiments was, in all cases, almost an order of magnitude higher than Q_{24}, underling the worst ability of these molecules to diffuse through the human epidermis. Indeed, it was already demonstrated the interaction of UFH/LMWHs with skin cells, mainly keratinocytes, due to their chemical structure and, more specifically, N-acetylglucosamine-6-sulfate moiety [8; 19], consistently with the topical application of LMWHs. Indeed it was suggested that the autocrine activation of epidermal growth factor receptor (EGFR) mediated by interaction of heparins with keratinocytes, may be exploited in cutaneous wound healing and some dermatologic disorders characterized by hyperplasia, such as psoriasis [20; 21; 22]. In this latter case, the design of a cutaneous dosage form should involve a drug which couples the affinity for the epidermal layers with the inability to permeate the skin. In this light, we calculated the R_{24}/Q_{24} ratio for each LMWH as an appropriate descriptor, assuming that the greater the ratio, the greater the affinity for the epidermis layers. **Figure 2.2** evidenced that, among the sodium LMWHs, parnaparin showed the greatest affinity for the epidermis. As stated above, parnaparin is obtained by a radical method which causes such a natural break of the UFH chain and, therefore, the residues and the oligosaccharide sequence of UFH, included the moieties responsible for the binding to

keratinocytes, are well-conserved. Finally, it should be underlined that the use of bivalent cations favors the retention into the epidermis as demonstrated in the case of calcium nadroparin.

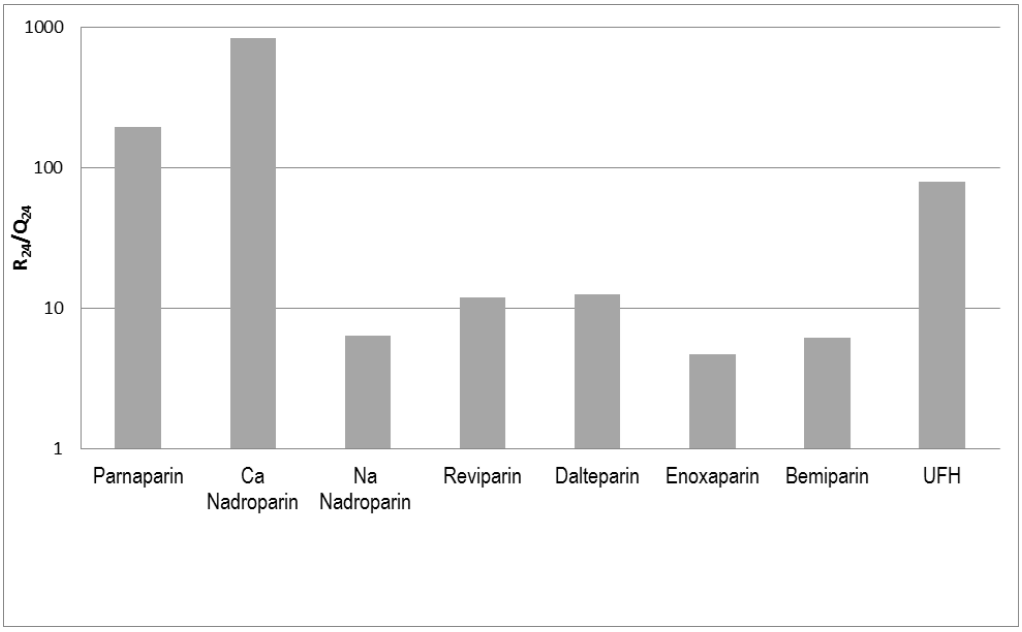

Figure 2.2- R_{24}/Q_{24} ratio of LMWHs and UFH. Greater the value greater the affinity of the tested compound for the human epidermis.

2.5 Conclusions

The influence of the main chemical features of LMWHs (M_w, structural residues and nature of counter-ion) on their ability to diffuse through human epidermis was elucidated. Altogether, the experimental data proved that the chain flexibility is the most evident parameter which influences the penetration pattern of these macromolecules. Indeed, the Ca^{2+}, limiting the rotation along the glycosidic leakage, significantly decreased the skin diffusion of nadroparin with respect to the sodium LMWHs.

As for the other variables in study, M_w, whose relevance in ruling the permeation of small molecules through human skin is well-established, was found to drive to a certain extent also the skin permeability of this class of polysaccharides.

However, in the case of such complex macromolecules, it couldn't completely explain the observed trend of permeation. In fact, the depolymerization method which confers to each LMWH unique properties in terms of residues at the terminal ends, oligosaccharide sequence and distribution of sulfate regions, resulted to play a fundamental role in defining the penetration pattern of LMWHs. In particular, bemiparin and enoxaparin, obtained by β-elimination, showed the best permeability properties (the highest permeation and the lowest R_{24}/Q_{24} ratios) and therefore they appeared as the most suitable candidates for a regional or systemic delivery. Nevertheless, a powerful enhancement strategy should be considered to improve the poor passive flux through human skin to an extent which is compatible with a therapeutic effect. Finally, it should be also underlined that LMWHs with high R_{24}/Q_{24} ratios such as nadroparin calcium and parnaparin, could be further investigated for cutaneous applications.

References

1. Hirsh J. Heparins. Fibrinolysis 1995, 9 (1), 66-68;
2. Hirsh J. and Raschke R. Heparin and Low-Molecular-Weight Heparin. CHEST 2004, 126 (3), 188S-203S;
3. Guerrini M. and Bisio A. Low-Molecular-Weight Heparins: Differential Characterization/Physical Characterization. Handbook of experimental pharmacology. 2012, 207, 127-157;
4. Linhardt R.J and Gunay N.S. Production and Chemical Processing of Low Molecular Weight Heparins. Seminars in Thrombosis and Hemostasis 1999, 25 (3), 5-16;
5. Minghetti P, Cilurzo F, Franzè S, Musazzi U,M, Itri M. Low molecular weight heparins copies: are they considered to be generics or biosimilars? Drug Discovery Today 2013, 18 (5/6), 305-311;
6. Motlekar N. A. and Bi-Botti C. Y. The quest for non-invasive delivery of bioactive macromolecules: A focus on heparins. Journal of Control Release 2006, 113, 91–101;
7. Qi Y, Zhao G, Liu D, Shriver Z, Sundaram M, Sengupta S, Venkataraman G, Langer R, Sasisekharan R. Delivery of therapeutic levels of heparin and low-molecular-weight heparin through a pulmonary route. PNAS 2004, 101 (26), 9867–9872;
8. Gomaa Y. A., Garland M. J, McInnes F., El-Khordagui L. K., Wilson C., Donnelly R. F. Laser-engineered dissolving microneedles for active transdermal delivery of nadroparin calcium. European Journal of Pharmaceutics and Biopharmaceutics 2012, 82, 299–307;
9. Lanke S.S., Strom J.G., Banga A.K. Enhancement of Transdermal Delivery of Heparin by Various Physical and Chemical Enhancement Techniques. Critical Reviews ^{TM} in Therapeutic Drug Carrier Systems 2009, 26 (6), 581-606;
10. Cilurzo F, Vistoli G, Selmin F, Gennari C. G. M, Musazzi U. M, Franzè S, Lo Monte M, and Minghetti P. An Insight into the Skin Penetration Enhancement Mechanism of -Methylpyrrolidone. Molecular Pharmaceutic 2014, 11 (3), 1014–1021;
11. Song Y., Hyun S.Y., Kim H., Kim C., Oh J. Transdermal delivery of low molecular weight heparin loaded in flexible liposomes with bioavailability enhancement: comparison with ethosomes. Journal of Microencapsulation 2011, 28(3), 151–158;

12. Betz G, Nowbakht P, Imboden R, Imanidis G. Heparin penetration into and permeation through human skin from aqueous and liposomal formulations in vitro. International Journal of Pharmaceutics 2001, 228, 147–159;
13. Lanke S.S.S, Kolli C.S, Strom J.G, Banga A.K. Enhanced transdermal delivery of low molecular weight heparin by barrier perturbation. International Journal of Pharmaceutics 2009, 365 (1–2), 26–33;
14. Song Y. and Kim C. Topical delivery of low-molecular-weight heparin with surface-charged flexible liposomes. Biomaterials 2006, 27, 271–280;
15. Mitragoti S. and Kost J. Transdermal Delivery of Heparin and Low-Molecular Weight Heparin Using Low-Frequency Ultrasound. Pharmaceutical Research 2001, 18 (8), 1151-1156;
16. Boyd J, Williamson F, Gettins P. A Physico-chemical Study of Heparin: Evidence for a Calcium-induced Co-operative Conformational Transition. Journal of Molecular Biology 1980, 137, 175-190;
17. Liang J. N. and Chakrabarti B, Ayotte L, Perlin A.S. An essential role for the 2-sulfoamino group in the interaction of calcium ion with heparin. Carbohydrate Research 1982, 106, 101-109;
18. Cilurzo F, Vistoli G, Gennari C.G, Selmin F, Gardoni F, Franzè S, Campisi M, Minghetti P. The role of the conformational profile of polysaccharides on skin penetration: the case of hyaluronan and its sulfates. Chemistry & Biodiversity, 2014, 11(4), 551-61;
19. Parisel C, Saffar L, Gattegno L, Andé V, Abdul-Malak N, Perrier E, Letourneur D. Interaction of heparin with human skin cells: Binding, location, and transdermal penetration. Journal of Biomedical Materials Research Part A. 2003, 67(2), 517-23;
20. Pillai S, Gilliam L, Conrad H.E, Holleran W.M. Heparin and its non-anticoagulant analogues inhibit human keratinocyte growth without inducing differentiation. The Journal of investigative dermatology 1994, 103, 647-650;
21. Shirakata Y, Kimura R, Nanba D, Iwamoto R, Tokumaru S, Morimoto C, Yokota K, Nakamura M, Sayama K, Mekada E, Higashiyama S, Hashimoto K. Heparin-binding EGF-like growth factor accelerates keratinocyte migration and skin wound healing. Journal of Cell Science 2005, 118, 2363-2370;

22. Kratz G, Back M, Arnander C, Larm O. Immobilised heparin accelerates the healing of human wounds in vivo. Scandinavian Journal of Plastic and Reconstructive Surgery and Hand Surgery 1998, 32 (4), 381-386.

3. Skin penetrating peptides as tool to enhance the permeation of heparin through human epidermis

3.1 Introduction

Skin penetration enhancers represent a long-standing approach for improving transdermal delivery of drugs. They are usually small molecules able to perturb the organization of stratum corneum, which represents the main barrier for the penetration of xenobiotics.
In recent years, peptides able to diffuse through the epidermis layers have been also tested to improve the transcutaneous delivery of drugs [1]. As an example, polyarginine has been shown to ferry molecules across the stratum corneum and into the viable epidermis and dermis [2]. Magainin, a naturally occurring pore-forming peptide, was found to increase skin permeability by direct interaction with and disruption of stratum corneum lipids [3; 4].
Among the possible approaches to screen new skin penetrating peptides, the use of phage display peptide libraries is gaining a growing interest [5; 6; 7].
Phage display is a powerful technology for ligand identification, since large libraries expressing peptides or proteins can be screened for target affinity [8].
The first application of phage display aimed to find a peptide which could specifically improve the skin penetration of administered molecules was performed by Chen and coworkers, who identified a peptide that increased the transdermal absorption of insulin in diabetic rats through hair follicles [5]. Using the same approach, Kumar et al. selected a 6-mer peptide which improved the penetration of 5-fluorouracil through porcine and mouse skin [6]. However, the most exhaustive study in this field was carried out by Hsu and Mitragotri. Indeed, the identification of the SPACE peptide provided the first evidence that skin penetrating peptides are able to penetrate the human skin [7]. Furthermore SPACE resulted to be effective in enhancing the skin penetration of nucleic acids and polysaccharides by direct conjugation to the cargo [7] or grafting on the surface of nanocarriers [9].
Altogether, these data revealed that the use of skin penentrating peptides can improve the challenging transdermal delivery of large hydrophilic molecules, overcoming the limits of the conventional chemical enhancers [10].
Heparin (UFH) has been the anticoagulant and antithrombotic drug of choice for several decades even if nowadays its use is restricted to the hospital where it is possible a careful clinical monitoring of the patients. Indeed, the intravenous administration of UFH can be

associated with serious complications such as bleeding risk, thrombocytopenia, effect on bone metabolism, along with pain and poor patient compliance [11]. The delivery of the drug by an alternative, non invasive route of administration may alter the pharmacokinetic/pharmacodynamic profiles and, therefore, potentially minimize the side effects, increasing at the same time patient compliance [12]. In particular, topical application appears as the most attractive alternative to UFH injection since it allows a substained release of the drug with possibility to have either a systemic (transdermal) or local effect [1; 12]. In fact, the cutaneous administration of UFH has also a clinical relevance in the prevention and treatment of the symptoms associated to peripheral vascular disorders, requiring however the application of huge doses of drug to reach the desired antithrombotic effect [13].

The skin penetration of UFH is very poor due to its unfavorable physico-chemical features, namely high M_w, hydrophilicity and ionization [14] and, therefore, a suitable method to improve the UFH diffusion through the skin is desired.

This study aimed to identify a new skin penetrating peptide able to enhance the penetration of UFH through human epidermis. The selection was performed by screening a random 7-mer phage display peptide library.

Furthermore, to clarify the enhancement mechanism of the peptide, its effect on the permeation of small molecules was also studies. Lidocaine and propranolol-HCl were selected as model drugs since they are used for local anesthesia and haemangiomas, respectively [15; 16].

3.2 Materials and Methods

3.2.1 Materials

The Ph.D.-7 Phage Display Peptide Library and escherichia coli K12 strain ER2738 were obtained from New England Biolabs. Luria Broth, agar, NaCl, Blue/white select, polyethylene glycol−8000 (PEG_{8000}), tris-HCl, sodium azide were purchased by Sigma-Aldrich (Italy). Tetracycline was purchased by Fluka Analytical. N-(3-Dimethylaminopropyl)-N′-ethylcarbodiimide hydrochloride (EDC) and N-

Hydroxysulfosuccinimide sodium salt (sulfo-NHS) were purchased by Sigma Aldrich (Italy). Propranolol-HCl and lidocaine were purchased by Sigma-Aldrich (St. Louis, MO). Sodium UFH (activity 195 IU/mg) was kindly provided by LDO S.p.A. (Milan, Italy). Kit Coatest® Heparin was purchased by Chromogenix Instrumentation Laboratory S.p.A. (Milan, Italy).

3.2.2 Preparation of human epidermis samples

The epidermis used in the permeation studies was obtained from the abdominal skin of three donors, who underwent cosmetic surgery (30-50 year old, Eurasian female). Skin samples were prepared following an internal standard procedure [17]. The full-thickness skin was sealed in evacuated plastic bags and frozen at -20 °C within 24 h after removal. Prior to the experiments, the skin was thawed at room temperature and the excess of fat was carefully removed. The skin sections were cut into squares of about 2.5 cm^2 and, after immersing the skin in water at 60 °C for 1 min, the epidermis was gently separated from the remaining tissue with forceps and carefully inspected by light microscopy for any defects. The integrity of the tissue was assessed by measuring the electrical impedance of the epidermis sheets (voltage: 250 mV, frequency: 100 Hz; Agilent 4263B LCR Meter, Microlease, Italy). The human epidermis was hydrated and sandwiched between the donor and the receptor compartments (both filled with physiologic solution), with the stratum corneum facing the donor compartment. The receptor phase was kept at 37 ± 1 °C with continuous stirring (1800 rpm) for 30 min and then the impedance was determined.

3.2.3 Phage Display Library Screening

Physiologic solution was used in the receptor compartment and sodium azide (0.1%) was added as a preservative. The epidermis was equilibrated for 1 h before the experiment. Phage library (2×10^{13} pfu, 50 µL) in 0.45 mL of TBS was placed in the donor compartment. After 24 h, the receiver medium was withdrawn and 1 mL was added to 20 mL of a 1:100 diluted overnight culture of Escherichia coli ER2738 and grown for 4.5 h to amplify the phages. Then, the phages were purified by PEG/NaCl precipitation and

resuspended in TBS. 0.5 mL amplified phages suspension were then used in the second round of screening. The number of phages placed in the donor compartment, 2×10^{13} pfu, was held constant for both rounds of screening. After the second round of selection, phages that permeated the human epidermis consistently were separated on an agar plate. A 10-µL aliquot of the receiver solution was added to 10 µL of Escherichia coli strain ER2738 and plated on IPTG/Xgal plates. 20 plaques were randomly selected and the DNA from each individual plaque, representing a single type of phage, was extracted and sent for DNA sequencing (BMR Genomics, I).

3.2.4 Peptide synthesis and characterization

The peptide selected by phage display was synthetized by microwave assisted solid phase peptide synthesis using the Fmoc-Chemistry (Liberty Microwave Peptide Synthesizer, CEM Corporation) [18]. The peptide was C-terminally amidated and N-terminally acetylated using Rink amide resin with a loading of 0.5 mmol g^{-1} and on a 0.1 mM scale. Single couplings were performed with Fmoc-amino acid (5 eq) activated in situ with HBTU (5 eq), HOBt (5 eq) dissolved in DMF, and DIPEA 1M in NMP (10 eq); each coupling was achieved by using MW irradiation (5 min, 75 °C, 20W). Fmoc cleavage was accomplished by treating the peptidyl-resin with 20% piperidine in DMF (3 min, 75 °C, 40 W). N-acetylation was performed manually using acetic anhydride (10 equiv.) and DIPEA (10 equiv.) in DCM for 30 min at room temperature. The peptide was manually cleaved from the resin with a mixture of TFA/water/TIS (90:5:5 v/v) for 6 h at room temperature. The crude peptide was precipitated from ice-cold diethyl ether and recovered by centrifugation at 4°C for 5 minutes (4500 rpm). The crude peptide was dissolved in DMSO and diluted in ACN/water (50:50 v/v) solution. The purification was performed by preparative RP-HPLC (Jasco BS-997-01 equipment) using a DENALI C-18 column from GRACE VYDAC (10µm, 250 x 22 mm) and a combination of two mobile phases: A = 95% Water, 5 % ACN, 0.1 % TFA; B = 95% ACN, 5% Water, 0.1% TFA. 2 mL of peptide solution were injected at a flow rate of 20 mL/min. The gradient was: 95% A for 5 min, then 95-30% A over 20 min. UV detection was made at 220 nm. The purified peptide was freeze-dried and stored at 0°C.

The conformational profile of the synthetic peptide was investigated by circular dichroism (CD).

Peptide stock solution was prepared in HPLC-quality water (500 µM, 1.5 mL). Spectra were recorded on a J-810 spectropolarimeter, using a quartz cuvette of 0.01 cm path length (Hellma Suprasil), from 195 to 250 nm with a 0.1 nm step and 1 s collection time per step, taking three average. The spectrum of the solvent was subtracted to eliminate interference from cell, solvent, and optical equipment. The CD spectra were plotted as mean residue ellipticity θ (degree x cm^2 x $dmol^{-1}$) versus wavelength λ (nm). Noise-reduction was obtained using a Fourier-transform filter program from Jasco.

3.2.5 Fourier Transform Infrared (FTIR) Spectroscopy

ATR-FTIR spectra were recorded between 4,000 and 650 cm^{-1} using a Bruker Alpha-P spectrometer (128 scans; 4 cm^{-1} resolution), equipped with an attenuated total reflection diamond crystal accessory. The spectrometer was linked to a PC equipped with Bruker OPUS software to allow the automated collection of IR spectra.

Human epidermis was soaked in demineralized water or in a solution of the peptide (0.25 or 0.5 mg/mL) in water for 1 h, then allowed to dry at room temperature for 15 min. The IR spectrum was recorded on epidermis sheets incubated with and without peptide, thus each epidermis sample acted as its own control at each time.

All measurements were performed at room temperature, 25 ± 2°C. The spectra were smoothed and baseline-corrected. The skin lipids absorbance peaks at 2920 cm^{-1} and 2850 cm^{-1} were monitored and variations in the ratio of peak height or area after peptide treatment were determined in comparison to the control.

Fourier self-deconvolution (FSD) of the overlapping amide I band components (1705−1578 cm^{-1}) was performed by using OPUS 7.5 software (Bruker). The amide I bands were resolved by the second-order derivative with respect to the wavelength. Deconvolution was performed using Gaussian line shape.

Since the ATR technique is very sensitive to the contact state during the measurements and the overall intensity of the spectra varied, it was necessary to normalize the spectra. The most intense protein band was the amide I band at 1650 cm^{-1} and therefore it was chosen as internal standard.

3.2.6 In Vitro Skin Permeation Studies

In vitro skin permeation studies were performed using human epidermis in a Franz diffusion cell.

The tested donor solutions were: 0.5 mL peptide (0.5 or 5.0 mg/mL) or 0.5 mL propranolol (0.2 % w/v) or 0.5 mL lidocaine (0.3 % w/v) or 0.3 mL UFH (6.7 mg/mL) saline solutions containing 0.1% sodium azide. All the experiments were repeated preparing the same solutions containing 0.5 mg/mL peptide. Finally, 0.3 mL UFH-peptide conjugate (6.7 mg/mL) was also tested.

The receiver solution (3.0 mL, exactly measured) was saline solution in the case of the peptide and small molecules and tris buffer 0.05 mol/L, pH 7.4 for UFH and UFH-peptide conjugate.

The system was kept at 37 ± 1 °C by means of a circulating water bath so that the epidermis surface temperature was at 32 ± 1 °C throughout the experiment and the receiver medium was continuously maintained under stirring with a magnetic bar.

At predetermined time intervals, samples (0.2 mL) were withdrawn from the receptor chamber and an equivalent volume of fresh medium was added to maintain the sink condition. The tests were always carried out using in parallel pure saline solution in the donor phase as control.

The steady-state flux (Jss, μg/cm2/h) was calculated from the slope of the linear plot of the cumulative amount of the drug permeated per unit area (Q, μg/cm2) as a function of time (h). The lag time (h) was determined from the x-intercept of the slope at steady-state. The enhancement factor (E.F.) was calculated as the ratio of the fluxes at the steady state.

3.2.7 Drug assays

The amounts of propranolol and lidocaine that permeated through human skin were assayed by HPLC, using an Agilent 1100 HPLC system (1100 autosampler, 1100 quaternary pump with degasser, 1100 thermostated column compartment, and 1100 diode array detector) (Agilent, Palo Alto, CA).

Lidocaine determination - The analyses were performed in the following experimental conditions: column: 5 µm C-8, 150 mm x 4.6 mm (Supelco, USA); mobile phase: acetonitrile/water (adjusted to pH 2.5 by 85% ortophosphoric acid) (50/50 v/v); flow rate: 1 ml/min; UV detector: 224 nm; injection volume: 20 µl; temperature: 20°C. The retention time was about 5 min. A calibration curve from 0.2 to 50 µg/ml was calculated on the basis of peak area measurements. It was generated with a correlation coefficient of 0.99990.

Propranolol determination - A reverse-phase column was used as the stationary phase (Bondclone C18, 10 µm, 3.9 x 300 mm, Phenomenex, USA) and a combination of acetonitrile with 0.2% phosphoric acid at the ratio of 40 to 60 at 25 °C was used as the mobile phase. The flow rate was set at 1.2 mL/min. The injection volume was 20 µL. The retention times of propranolol was 8 min. The drug concentration was determined from a standard calibration curve in the range of 0.2-20 µg/mL (correlation coefficient: 0.99996).

UFH determination- UFH concentration was determined by measuring the anti FXa (aXa) activity using the Coatest® kit (Chromogenix, Instrumentation Laboratory S.p.A.). The method relies on the ability of UFH-antitrombin III (AT) complex to react with an excess of factor Xa (FXa). Unreacted FXa is hydrolyzed by a chromogenic substrate and read spectrophotometrically at 405 nm. The absorbance is inversely proportional to UFH concentration. The drug (UFH and UFH-peptide conjugate) concentration was estimated on the basis of calibration curves built in the range 0.03-0.5 µg/mL and 0.15-4.8 µg/mL, respectively.

3.2.8 Synthesis of UFH-peptide conjugate

The conjugation of UFH to the identified peptide was carried out according to Freudenberg et al. [19] with slight modifications. UFH (average M_W 15,000 Da) and a mixture of EDC and sulfo-NHS (2:1 w/w) were dissolved in MilliQ-water on ice. A 5-fold molar excess of activating agent with respect to UFH carboxylic acid (-COOH) groups was used. In parallel, the peptide was dissolved in MilliQ-water (UFH:peptide 1:1 molar ratio) and kept on ice until its use. After vigorous mixing, the UFH and EDC/sulfo-

NHS solution was incubated in ice (approx. 2–4 °C) for 15 min to activate the UFH-COOH. Subsequently the peptide solution was added to the activated UFH. After vortexing and incubation for 10 min at 4 °C, the reaction mixture was maintained at room temperature under continuous stirring for 4-5 h. Afterwards, the reaction product was purified by ultrafiltration (membrane filters Microcon/Amicon, cut-off 3KDa) and the recovered conjugate was freeze-dried.

3.3 Results

3.3.1 Identification of Skin Penetrating Peptide

After the two rounds of screening by in vitro phage display, the 7-mer peptide that consistently diffuses through the human epidermis resulted to be DRTTLTN. Indeed, the DNA sequencing revealed that 66% phages expressed such peptide on their surface.
The identified sequence (skin penetration enhancer heptapeptide, SPEH) was thus chemically synthesized by microwave assisted solid phase peptide synthesis (MW-SPPPS) and acetylated at the N-terminus using protocols previously optimized [18]. The conformational behaviour of SPEH was studied using circular dichroism (CD). The CD spectrum, shown in **Figure 3.1**, is characterized by the presence of a minimum at 198 nm and a negative shoulder around 220 nm, indicating that the peptide in these conditions did not possess a preferred conformation, but that different secondary structures (*i .e.* 3_{10} helix and β) were present. The presence of a β structure was outlined also by ATR-FTIR analysis: in the amide I region of the spectrum a corresponding peak at 1635 cm^{-1} was observed. (**Figure 3.2 b**) A shoulder around 1663 cm^{-1}, indicating a 3_{10} helix contribution was also detected.

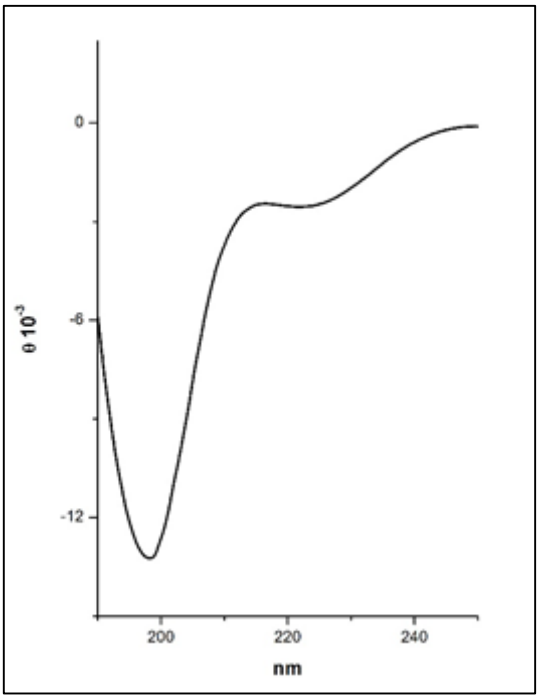

Figura 3.1 – CD Spectra of SPEH

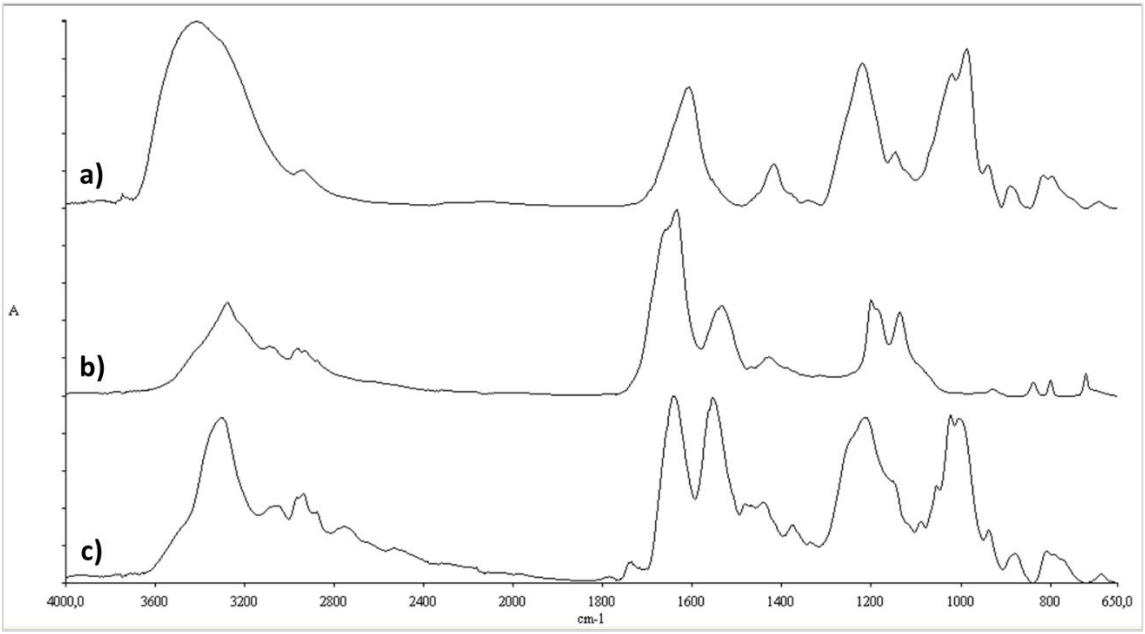

Figure 3.2- ATR-FTIR spectra of **a) UFH, b) SPEH** and **c) UFH-SPEH conjugate**

As depicted in **Figure 3.3,** the SPEH was able to penetrate into the skin in a significant amount even when removed from the phage. Indeed, the 40% of SPEH loaded in the donor compartment of the Franz cell permeated through the epidermis within 30 min, independently of its concentration. Moreover, in both the experiments, the system reached the equilibrium within six hours.

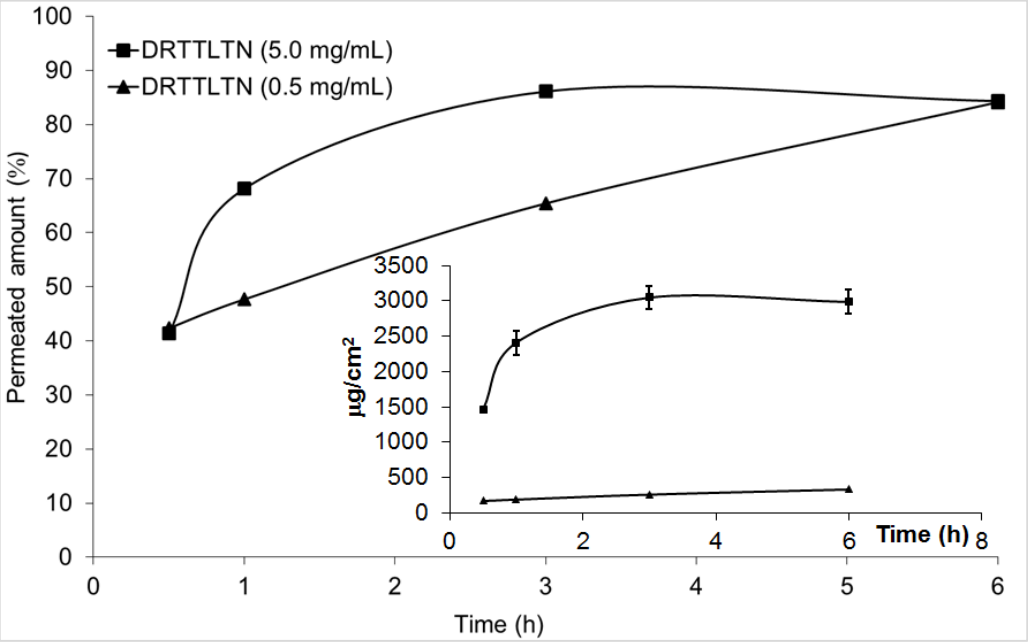

Figure 3.3- Permeation profile of SPEH

A deeper insight on the diffusion through the epidermis and the effects on the organization of the major constituents of the stratum corneum was obtained by the analyses of the ATR-FTIR spectra. To assess the possible effect on molecular conformation of stratum corneum components, the spectrum of human epidermis of each donor exposed to water for 1 h was selected as reference (**Figure 3.4 b**).

The assignments and peak position of the diagnostic bands in the spectra were attributed with reference to the literature [20].

Alteration of the spatial organization of lipidic lamellae of the stratum corneum due to the penetration of a compound can be evidenced by analyzing CH_x stretching regions at about 2950-2850 cm^{-1}. In particular, the change of conformation of the ceramides are detectable by shift of such bands to higher wavenumbers while the increase of the area and/or height of CH_2 stretching (ν -CH_2**)** peaks is associated to a fluidization effect.
The incubation of the epidermis with SPEH did not determine any significant shift of the CH_2 asymmetric (as-CH_2**)** and symmetric (s-CH_2) wavenumbers. However, the height of both these bands increased in the epidermis samples exposed to a 0.5 mg/mL SPEH concentration (**Table 3.1**). At lower level (0.25 mg/mL), the SPEH did not seem completely effective in determining the fluidization of the lipidic network, since the increase of the height of the s-CH_2 band occurred only for one donor (**Table 3.1**).

Table 3.1 – Peak areas of methylene bands arising from the lipids in the SC bilayers and changes in their intensity calculated as ratio between treated and untreated samples deriving from five different donors.

Donor	DRTTLTN (mg/mL)	Epidermis sample	$\nu_{as}(CH_2)$ (height)	Ratio	$\nu_{s}(CH_2)$ (height)	Ratio
a	0.5	Untreated	0.65	1.43	0.335	1.39
		Treated	0.93		0.464	
b	0.5	Untreated	0.736	1.53	0.379	1.66
		Treated	1.124		0.629	
c	0.5	Untreated	0.033	1.12	0.017	1.12
		Treated	0.037		0.019	
d	0.25	Untreated	0.242	1.36	0.117	1.552
		Treated	0.330		0.182	
e	0.25	Untreated	0.380	1.02	0.225	0.843
		Treated	0.388		0.190	

The other interesting band of the stratum corneum is the peak assigned to the C=O stretching of the amide (Amide I) at about 1640 cm^{-1}, which is the result of the contributes of the keratin conformation and presence of ceramides.

Figure 3.5 reports the Gaussian curve fitting of untreated epidermis samples. The bands were assigned, according to our previous work, as follows:

1635 cm^{-1}: intramolecular β-sheet (B);

1694 cm^{-1} and bands in the 1627 cm^{-1} region: intermolecular β-sheets (B);

1668 and 1689 cm^{-1} region: turn structure (T);

1652 cm^{-1}: random coil conformation (R);

1660 cm^{-1}: α-helices (A);

1619 cm^{-1}: ceramides contribute (C);

1612 cm^{-1}: keratin lateral chains vibrations (L).

Furthermore, the band at about 1645 cm^{-1} was attributed to the H-O-H bending vibration (H) of epidermal moisture content.

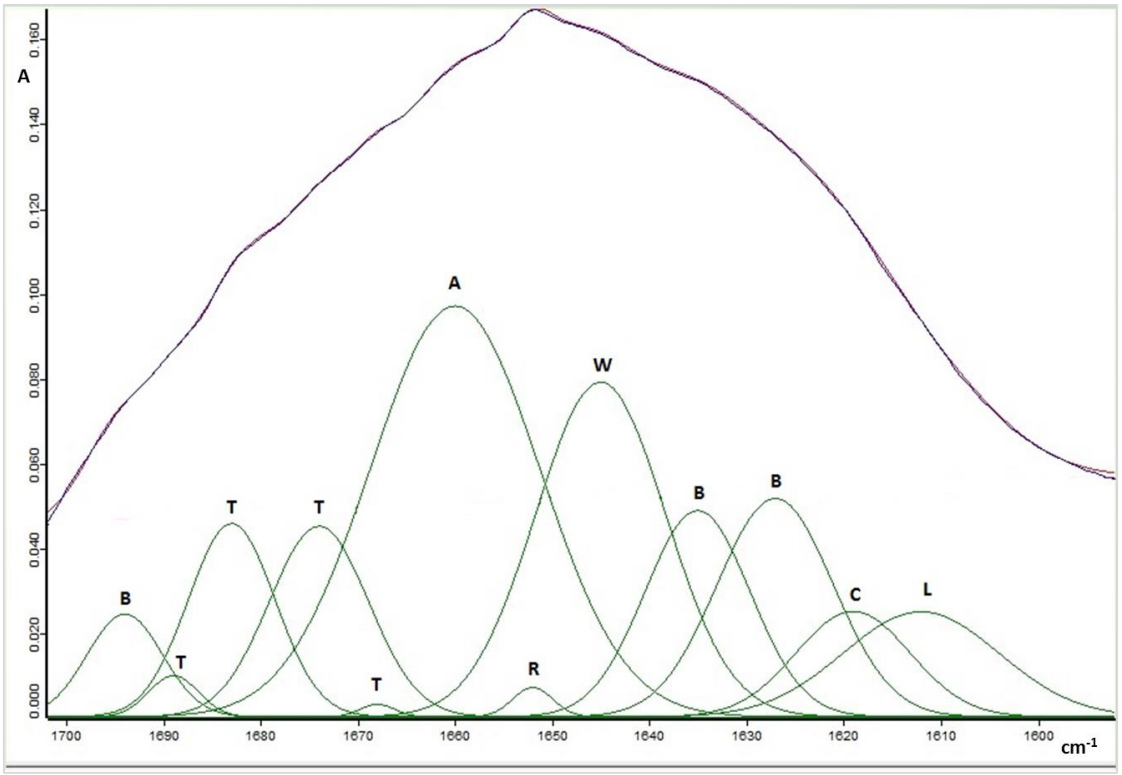

Figure 3.5- Absorbance spectra in the amide I region, deducted after Fourier transform self-deconvolution of human epidermis incubated in physiologic solution for 1 hour. The black and purple curves represent the original and the fitted spectra, respectively. The attributions of each deconvoluted band are marked as **R (random coil)**, **B (β-sheets)**, **A (α-helix)**, **T (turns)**, **L (lateral chains)** and **W (water)**.

The relative abundance (% area) of the deconvoluted bands suggested a possible interaction between SPEH and keratin because the percentages of the secondary structures of keratin changed in the treated samples (**Table 3.2**). In particular, the total areas attributed to random coils and β-turns increased indicating that the keratin assumed a less ordered structure. The unfolding of the keratins due to the interaction with the SPEH was also confirmed by the reduction of the α-helix and β-sheet conformations, suggesting that SPEH has the potentialities to enhance the transdermal permeation of macromolecules by loosening the keratin structure and increasing the degree of freedom for carbon movement [21].

Table 3.2 - Contribution from secondary structures of the deconvoluted amide I band in the ATR-FTIR spectra of human epidermis (stratum corneum side) treated with DRTTLTN compared with the untreated sample.

Attribution	Epidermis sample	Area (%)	P value
L	Untreated	7.37±2.42	0.17
	Treated	5.16±1.32	
C	Untreated	5.64±1.52	0.43
	Treated	4.54±1.82	
B	Untreated	21.92±6.61	0.48
	Treated	18.89±3.92	
W	Untreated	18.96±2.40	0.95
	Treated	18.80±4.67	
R	Untreated	3.90±4.09	0.045*
	Treated	13.89±5.43	
A	Untreated	22.37±0.57	0.019*
	Treated	15.85±3.21	
T	Untreated	19.83±2.39	0.04*
	Treated	23.94±1.61	

* $P<0.05$ by Fisher test

In summary, it could be hypothesized that the SPEH can enhance the permeation of drugs by two different mechanisms: the fluidization of the lipidic network and the decrease of the ordered structure of keratin filaments.

3.3.2 Enhancement effect of SPEH

In order to demonstrate the skin penetration enhancement effect of SPEH on small molecules, the in vitro permeation through human epidermis of lidocaine and propranolol in presence of 0.5 mg/mL SPEH was determined **(Figure 3.6**).

The addition of SPEH increased the fluxes of lidocaine and propranolol of 2.6 and 3.8 fold, respectively. Moreover, the lag time determined for propranolol decreased from about 3 h to about 1 h.

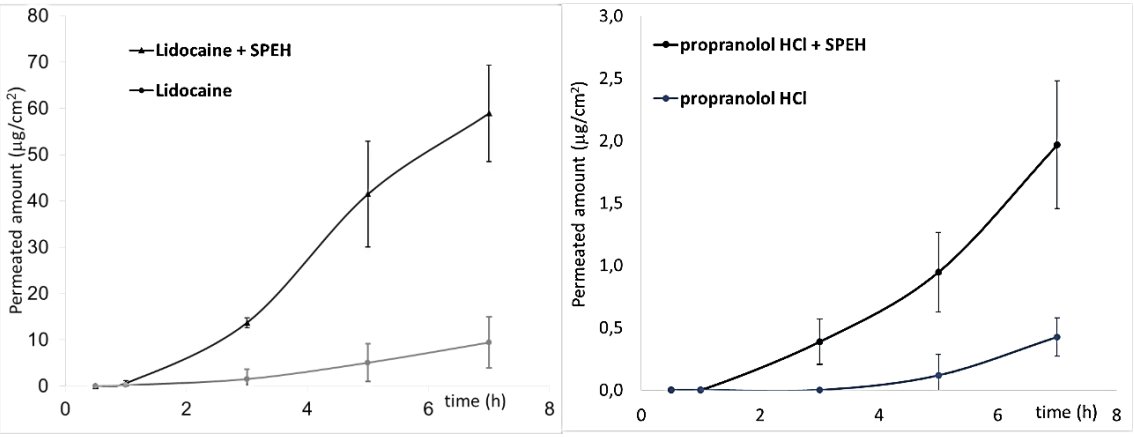

Figure 3.6 - Permeation profiles of lidocaine and propranolol-HCl (sole and in co-administration with SPEH)

On the contrary, the co-administration of SPEH with UFH did not lead to an increase of permeation or retention of the polysaccharide (data not shown). The lack of enhancement can be ascribed to the affinity of UFH for keratin, as revealed by ATR-FTIR spectra of human epidermis. Indeed, after exposure of the epidermis to UFH for 1 h a significant depression of the bands at 1742 cm^{-1} and 1160 cm^{-1} attributed to the C=O stretching of ester groups was observed **(Figure 3.4)**. The reduction of such bands, already described by Lanke et al. [22], suggested the formation of hydrogen bonds between UFH sulfones and hydroxyl moieties and some stratum corneum component [23]. This evidence can

justify the lack of improvement of UFH diffusion after the perturbation of the stratum corneum structures caused by SPEH, when the peptide and the cargo were co-administered.

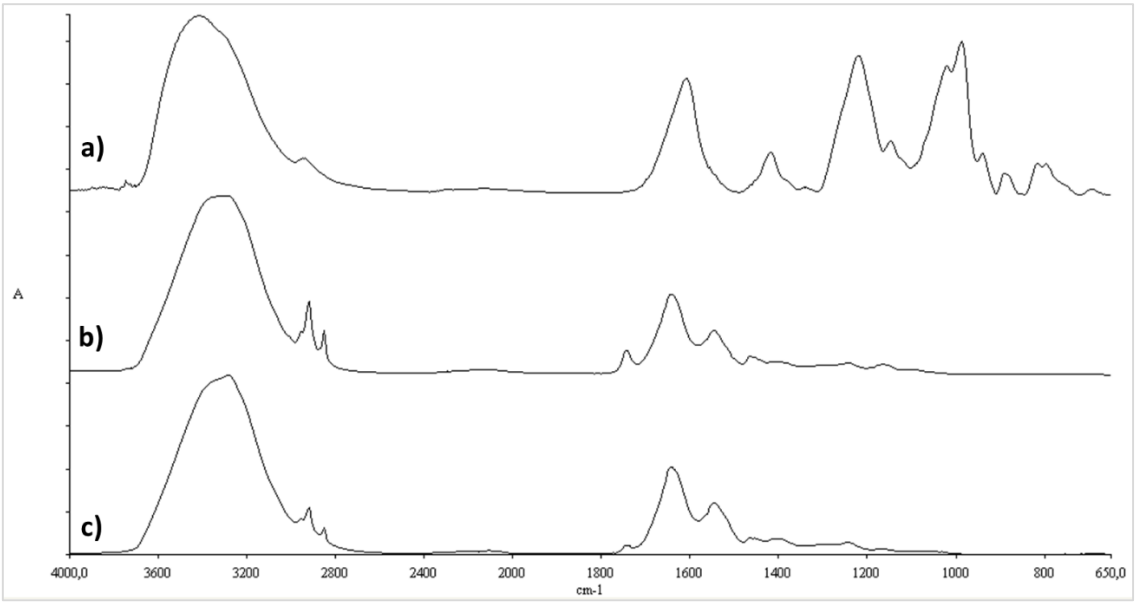

Figure 3.4- ATR-FTIR spectra of **a) UFH**, **b) stratum corneum**, and **c) stratum corneum exposed to UFH for 1 h**

To overcome the resistance related to the affinity of UFH for the stratum corneum, the cargo was conjugated with SPEH by amide bond formation. The biological activity of the UFH-SPEH conjugate was determined after synthesis in comparison to the native UFH. The adopted procedure led to a very significant reduction of the UFH aXa activity, namely about 5-fold (195 UI/mg for UFH vs 36 UI/mg for the conjugate). This reduction was attributed to an alteration of the spatial organization of the UFH due to the presence of the SPEH on the chain and/or to the substitution of the free carboxyl mojeties with succinimide esters formed with NHS during the attivation process. As a matter fact, the conjugation with the peptide was evidenced by ATR-FTIR spectroscopy since the amide I and amide II of the peptide shifted from 1635 cm^{-1} and 1536 cm^{-1} to 1643 cm^{-1} and 1558

cm^{-1}, respectively (**Figure 3.2**). Furthermore the shoulder at 1663 cm^{-1} completely disappeared, indicating a stabilization of the β conformation of the peptide when linked to UFH. The presence of unreacted ester intermediates was also confirmed by ATR-FTIR analysis. A shoulder at about 1730 cm^{-1}, tipical of ester function, was thus detected.
The fluxes determined for the conjugate and free UFH resulted 1.36 $\mu g/cm^2/h$ and 0.04 $\mu g/cm^2/h$ respectively, showing an enhancement factor equal to 34. However, considering the significant reduction of the anticoagulant activity of the conjugate, the true enhancement factor resulted to be about 7.

3.4 Discussion

The peptide identified in this study, SPEH, seems to interact strongly with both lipids and keratin. As it is well known, the stratum corneum is a lamellar structure consisting of approximately 10-15 layers of flattened, α-keratin-containing cells. Within the cells the α-keratin filaments, imbedded in an amorphous matrix of lipids and non fibrous proteins, are arranged roughly parallel to the plane of the membrane. Thus, the diffusion through stratum corneum can follow two different micropathways. The intercellular route is a continuous way through intercellular lipid domains. The diffusion by the transcellular pathway involves the permeation of the corneocytes and, in this case, the permeant has to cross the keratin and then the intercellular lipids [24].
SPEH, penetrating into the intercellular region of stratum corneum, increases the fluidity of the lipid components and consequently the diffusion of drugs through the intercellular route. Secondly, as supported by ATR-FTIR data, the penetration of SPEH in the corneocites, causing the uncoiling and the extension of keratin filaments, can increase the diffusion of molecules through the transcellular route.
The combination of these two mechanisms can justify the increase of the skin penetration of the two tested small molecules, namely lidocaine and propranolol.
In the case of UFH, it is reasonable to think that the large hydrodynamic volume of the molecule prevents the penetration through the intercellular route. On the other hand, the transcellular penetration of sole UFH is precluded by its high affinity for corneocytes,

which causes the retention of the polysaccharide into the membrane, as suggested by other authors [25] and supported by the IR spectra of the epidermis exposed to UFH.

In contrast, the chemical conjugation of the cargo to SPEH may partially reduce the interaction between UFH and stratum corneum due to the steric hindrance of the peptide grafted on the UFH backbone, thus providing the driving force for the permeation. Indeed, the depression of the C=O stretching at 1742 cm^{-1} noticead after the exposure of the human epidermis to UFH (**Figure 3.4**) was not observed when the membrane was treated with the conjugate (data not shown). Thus, the chemical conjugation of the cargo resulted to be essential to improve the skin delivery of such macromolecule which is driven by the diffusion of SPEH.

The enhancement factor (E.F.) due to the conjugation of UFH with SPEH resulted greater than that described for other traditional skin penetration enhancers. Indeed, the pretreatment of the skin with Azone® (E.F.= 3.4) [26] resulted to be an order of magnitude lower than that found in our set of experiments (E.F.=34) and the use of an ethanol/limonene 99/1 blend determined an E.F. of 18 [27]. It should be mentioned that Azone® is not used in commercial drug products due to its skin irritancy and toxicity at certain doses, and the percentage of limonene to be included in topical products is limited by regulatory authorities.

Aiming to improve the skin penetration of UFH, different physical methods were also exploited [28]. Prausnitz and coworkers demonstrated a significant increase of UFH flux after skin electroporation which was accompanied however by a strong reduction of the activity of the transported molecule (one eight of the applied compound) [14]. Similarly, the application of low-frequency ultrasounds seemed to improve consistently the in vitro permeation of radiolabeled UFH (flux 21-fold higher than control) [29]. Nevertheless, also in that case, the biological active samples assayed in the receiver compartement accounted for only 25-40% of all UFH permeated. Using iontophoresis, UFH flux was increased of about 10 fold [30] but the study of the different fraction pools (unfractionated, high-, and low molecular weight heparins) revealed that this technique had a limited effect on the diffusion of high molecular weight polysaccharides, suggesting the application of this system for the skin delivery of LMWHs [31]. Moreover, the application of pulsed current iontophoresis caused a significant decrease in aXa activity (almost 33%) [31].

A successful enhancement strategy should create the driving force for the transdermal delivery in a safe manner. In this regard, the perturbation effects generated by sonophoresis, iontophoresis or electroporation cannot easily confined to the sole stratum corneum, preserving the deeper tissues [1]. Moreover, these enhancement strategies entail the development of specific devices easy to handle.

On the contrary, a biological drug - skin penetrating peptide conjugate can be directly loaded in a topical dosage form which generally meets the good patient compliance. However, the conjugation leads to a new chemical entity that can have different pharmacological and/or toxicological properties with respect to the native drug. To overcome this issue, the design of the conjugate should be tuned to obtain a compound which maintains its features during the diffusion through the stratum corneum and, at the same time, assures the release of the parent drug in the viable epidermis.

References

1. Prausnitz M.R. and Langer R. Transdermal drug delivery. Nature Biotechnology 2008, 26 (11), 1261-1268;
2. Rothbard J.B, Garlington S, Lin Q, Kirschberg T, Kreider E, McGrane P.L, Wender P.A, Khavari P.A. Conjugation of arginine oligomers to cyclosporin A facilitates topical delivery and inhibition of inflammation. Nature Medicine 2000, 6(11), 1253-1257;
3. Kim Y.C, Ludovice P.J, Prausnitz M.R. Transdermal delivery enhanced by magainin pore-forming peptide. Jornal of Control Release 2007, 122(3), 375-383;
4. Kim Y.C, Late S, Banga A.K, Peter J, Ludovice P.J, Prausnitz M.R. Biochemical enhancement of transdermal delivery with magainin peptide: Modification of electrostatic interactions by changing pH. International Journal of Pharmaceutics 2008, 362(1-2), 20–28;
5. Chen Y, Shen Y, Guo X, Zhang C, Yang W, Ma M, Liu S, Zhang M, Wen L-P. Transdermal protein delivery by a coadministered peptide identified via phage display. Nature Biotechnology 2006, 24(4), 455 – 460;
6. Kumar S, Sahdev P, Perumal O, Tummala H. Identification of novel skin penetration enhancement peptide by phage display peptide library screening. Molecular Pharmaceutics 2012, 9, 1320-1330;
7. Hsu T. and Mitragotri S. Delivery of siRNA and other macromolecules into skin and cells using a peptide enhancer. PNAS 2011, 108, 15816-15821;
8. Smith G.P. and Petrenko V.A. Phage display. Chemical Reviews 1997, 97, 391–410;
9. Chen M, Gupta V, Anselmo A.C, Muraski J.A, Mitragotri S. Topical delivery of hyaluronic acid into skin using SPACE-peptide carriers. Journal of Controlled Release 2014, 173, 67–74;
10. Nasrollahi S.A, Taghibiglou C, Azizi E, Farboud E.S. Cell-penetrating Peptides as a Novel Transdermal Drug Delivery System. Chemical Biology & Drug Design 2012, 80, 639–646;
11. Hirsh J. and Raschke R. Heparin and Low-Molecular-Weight Heparin. CHEST 2004, 126 (3), 188S-203S;

12. Motlekar N. A. and Bi-Botti C. Y. The quest for non-invasive delivery of bioactive macromolecules: A focus on heparins. Journal of Control Release 2006, 113, 91–101;
13. Vecchio C. and Frisinghelli A. Topically applied Heparins for the Treatment of Vascular Disorders. A Comprehensive Review. Clinical Drug Investigation 2008, 28, 603-614;
14. Prausnitz M.R, Edelman E.R, Gimm J.A, Langer R, Weaver J.C. Transdermal delivery of heparin by skin electroporation. Biotechnology 1995, 13(11), 1205-1209;.
15. Xu G, Lv R, Zhao Z, Huo R. Topical propranolol for treatment of superficial infantile hemangiomas. Journal of the American Academy of Dermatology 2012, 67 (6), 1211-1213;
16. Buckley M.M. and Benfield P. Eutectic Lidocaine/Prilocaine Cream. Drugs 1993, 46 (1), 126-151;
17. Cilurzo F, Minghetti P, Alberti E, Gennari C. G. M, Pallavicini M, Valoti E, Montanari L. An investigation into the influence of counterion on the RS-propranolol and S-propranolol skin permeability. Journal of Pharmaceutical Sciences 2010, 99(3), 1217-1224;
18. Pellegrino S, Annoni C, Contini A, Clerici F, Gelmi M. L. Expedient chemical synthesis of 75mer DNA binding domain of MafA: an insight on its binding to insulin enhancer. Amino Acids 2012, 43, 1995-2003;
19. Freudenberg U, Hermann A, Welzel P.B, Stirl K, Schwarz S.C, Grimmer M, Zieris A, Panyanuwat W, Zschoche S, Meinhold D, Storch A, Werner C. A star-PEG–heparin hydrogel platform to aid cell replacement therapies for neurodegenerative diseases. Biomaterials 2009, 30, 5049–5060;
20. Cilurzo F, Vistoli G, Selmin F, Gennari C. G. M, Musazzi U. M, Franzè S, Lo Monte M, and Minghetti P. An Insight into the Skin Penetration Enhancement Mechanism of -Methylpyrrolidone. Molecular Pharmaceutic 2014, 11 (3), 1014–1021;
21. Karande P, Jain A, Ergun K, Kispersky V, Mitragotri S. Design principles of chemical penetration enhancers for transdermal drug delivery. PNAS 2005, 102 (13), 4688-4693;
22. Lanke S.S.S., Kolli C.S., Stroma J.G., Banga A.K. Enhanced transdermal delivery of low molecular weight heparin by barrier perturbation. International Journal of Pharmaceutics 2009, 365, 26–33;

23. Cestari M., Muller V., da Silva Rodrigues J.H., Nakamura C.V., Rubira A.F., Muniz E.C. Preparing Silk Fibroin Nanofibers through Electrospinning: Further Heparin Immobilization toward Hemocompatibility Improvement. Biomacromolecules 2014, 15, 1762−1767;
24. Morrow D.I.J., McCarron P.A., Woolfson A.D. and Donnelly R.F. Innovative strategies for enhancing topical and transdermal drug delivery. The Open Drug Delivery Journal 2007, 1, 36-59;
25. Parisel C., Saffar L., Gattegno L., Andé V., Abdul-Malak N., Perrier E., Letourneur D. Interaction of heparin with human skin cells: Binding, location, and transdermal penetration. Journal of Biomedical Materials Research Part A 2003, 67(2), 517-23;
26. Bonina, F. P. and Montenegro L. Penetration enhancer effects on in vitro percutaneous absorption of heparin sodium salt. International Journal of Pharmaceutics 1992, 82, 171-177;
27. Bonina F.P. and Montenegro L. Effects of some non-toxic penetration enhancers on in vitro heparin skin permeation from gel vehicles. International Journal of Pharmaceutics 1994, 111, 191-196;
28. Lanke S.S., Strom J.G., Banga A.K. Enhancement of Transdermal Delivery of Heparin by Various Physical and Chemical Enhancement Techniques. Critical Reviews ™ in Therapeutic Drug Carrier Systems 2009, 26 (6), 581-606;
29. Mitragoti S. and Kost J. Transdermal Delivery of Heparin and Low-Molecular Weight Heparin Using Low-Frequency Ultrasound. Pharmaceutical Research 2001, 18 (8), 1151-1156;
30. Le L., Kost J., Mitragoti S. Combined Effect of Low-Frequency Ultrasound and Iontophoresis: Applications for Transdermal Heparin Delivery. Pharmaceutical Research 2000, 17 (9), 1151-1154;
31. Pacini S., Punzi T., Gulisano M., Cecchi F., Vannucchi S., Ruggiero M. Transdermal Delivery of Heparin Using Pulsed Current Iontophoresis. Pharmaceutical Research 2005, 1-7.

4. Low Molecular Weight Heparins copies: have they to be considered generics or biosimilars?

Abstract

The protection rights of low molecular weight heparins (LMWHs) are expired or are expiring, so the extent and nature of the studies required to obtain a market authorization for LMWHs copies represents a hot topic. FDA classifies LMWHs as semisynthetic drugs and their copies as generics while EMA views them as biological medicines and consequently their copies as biosimilars. Consequently, FDA requires only *in vivo* pharmacodynamic studies, while EMA requires also clinical trials. The current work reviews the chemical composition and therapeutic indications of LMWHs available in the EU and USA markets in order to discuss the two different approaches. Since LMWHs show a high intrinsic variability and a complete characterization is not viable, a conservative approach is desirable.

The content of this chapter was published in Drug Discovery Today (Minghetti et al. Drug Discovery Today 2013, 18 (5/6), 305-311)

4.1 Introduction

Low molecular weight heparins (LMWHs) are a family of glycosoaminoglycans widely used in the treatment of the thromboembolism prophylaxis in patients undergoing to surgical interventions. LMWHs are manufactured by chemical or enzymatic depolymerization of unfractionated heparin (UFH) extracted from animal sources.

Recently, patent rights and supplementary protection certificates of some originator of LMWHs have expired or are about to expire, raising the opportunity to develop copies of the innovator products, thus boosting the competition among pharmaceutical companies. In this scenery, the Marketing Authorisation Application (MAA) can be generally handled as an abridged application, submitting a reduced dossier which contains sufficient data to assure the same level of quality, safety and efficacy of the originator. Nevertheless, the US Food and Drug Administration (FDA) and the European Medicines Agency (EMA) have two distinct viewpoints on the nature of LMWHs which lead to different pathway for granting the MAAs of their copies: LMWHs are classified as semi-synthetic or biological products by the FDA and the EMA, respectively. Therefore, EMA requires appropriately powered clinical trials to establish comparable efficacy and safety between copies and the innovator product. In contrast, the FDA requires only *in vivo* pharmacodynamic studies. The two different approaches have started a thorough debate in the scientific community, as demonstrated by the continuous revision and issue of guidelines.

In the present paper, we review the chemical composition and therapeutic indications of LMWHs available in the EU and US markets in order to provide useful information to discuss the regulatory frameworks of the EMA and the FDA.

4.2 Chemical features and quality requirements of UFH and LMWHs

UFH is a polydisperse mixture consisting of variably sulfated repeating disaccharide units which are composed of a glucosamine 1,4 linked to an uronic acid which is represented by both its epimers, namely the glucuronic (GlcA) and the iduronic acids (IdoA) (**Figure 4.1**). Both monosaccharides can be differently functionalized in the UFH chains: uronic acids can be 2-O-sulfated and glucosamine (GlcN) is N-sulfate ($GlcNSO_3$) or N-acetylate

(GlcNAc). Moreover, $GlcNSO_3$ may be also O-sulfated in the position 3 and/or 6. The GlcNAc residues can be 6-O-sulfated or unsulfated. Hence, the possible presence of four different uronic residues and six different glucosamine derivatives makes UHF's structure very complex and variable [1].

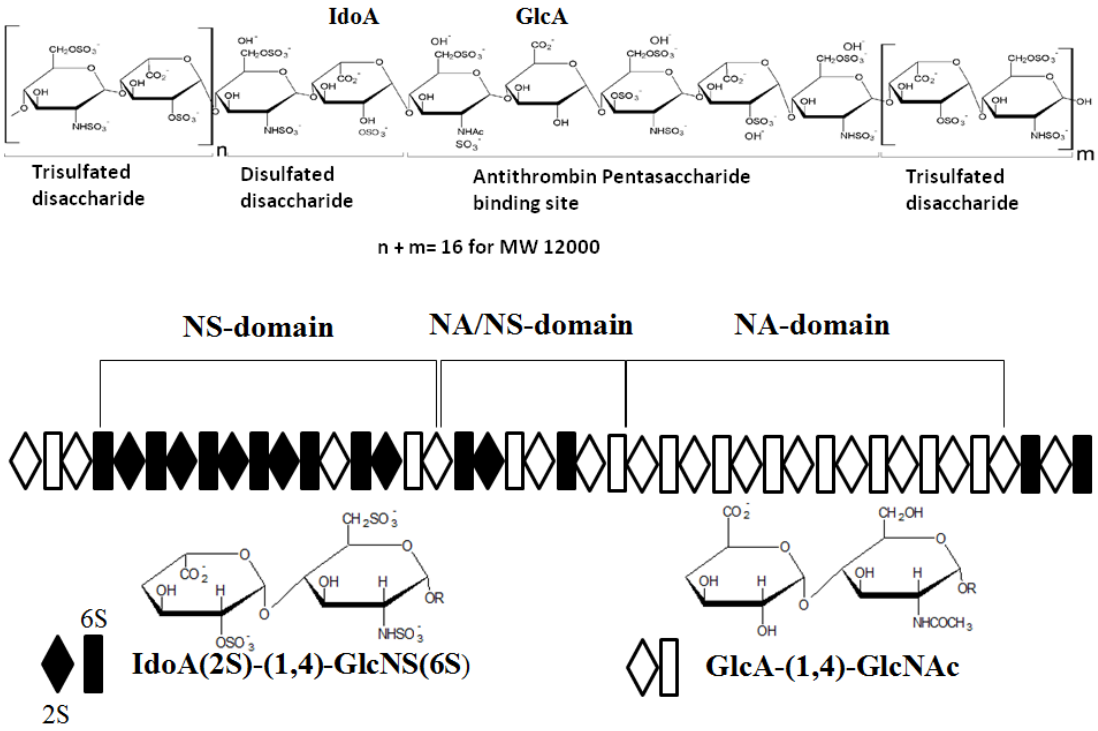

Figure 4.1 - Structure of a representative chain of pharmaceutical heparin (adapted from [9]; Rabenstein, D.L. (2002) Nat. Prod. Rep. 19, 312–331).

In animal organisms, UFH is biosynthetized as a proteoglycan and the primer for the elongation of the polysaccharide is the neutral trisaccharide xylosyl-galactosyl-galactose (Xyl, Gal, Gal). Then, proceeding from reducing to non-reducing end, three different domains can be identified on the basis of the abundance of $GlcNSO_3$ and GlcNAc (**Figure 4.1**). The first domain, namely NA domain, is mainly constituted of the repeating GlcA-GlcNAc disaccharide. The NA/NS domain is characterized by the succession of $GlcNSO_3$ and GlcNAc units. Finally, at the non-reducing end, a region rich in high sulfated

disaccharides is found (NS domain). In particular, sequences of trisulfated disaccharides ($IdoA2SO_3$-$GlcNSO_36SO_3$) seem to be the major constituents [2].

The NS domain contains the specific pentasaccharide unit responsible of the binding with antithrombin III (AT) (**Figure 4.1**). This interaction determines a conformational change in AT resulting in its activation through an increase in the flexibility of its reactive site loop [3]. Once activated, AT inhibits the activity of several proteases involved in blood clotting, namely factor XIIa, XIa, IXa and the most notably factor Xa. This direct effect on AT accounts for most of the increase in inhibitory activity toward factor Xa induced by UFH. Nevertheless, it is of marginal importance in thrombin (Factor IIa) inhibition, which largely depends on a template mechanism, with both thrombin and AT binding adjacently to the same heparin chain (**Figure 4.2**) [4]. For this reason, the minimum chain length required to promote the direct inactivation of thrombin is of about 18 saccharide units ($M_w > 5{,}400$) [5].

UFH can be obtained by domestic mammalians used for food by man [6], namely cattle, sheep and pigs [7], which relate to differences in composition and functional activities, such as AT and thrombin-binding affinities. After the outbreak of the bovine spongiform encephalopathy, UFH is currently extracted only from porcine gut and the process-related impurities include other sulfate polysaccharides, i.e. chondroitin sulfate and dermatan sulfate [8].

LMWHs are obtained by chemical or enzymatic depolymerization of UFH and, depending on the production method, display different chemical structures at the reducing and/or non-reducing end of polysaccharide chains (**Table 4.1**). They are characterized by an average molecular weight less than 8,000 and a polydispersity index ranging 1.1-1.5 range [9] and consequently, partially lose the ability to inactivate factor IIa. Thus, the ratio between anti-factor Xa and anti-factor IIa activities became greater than that of UHF [10].

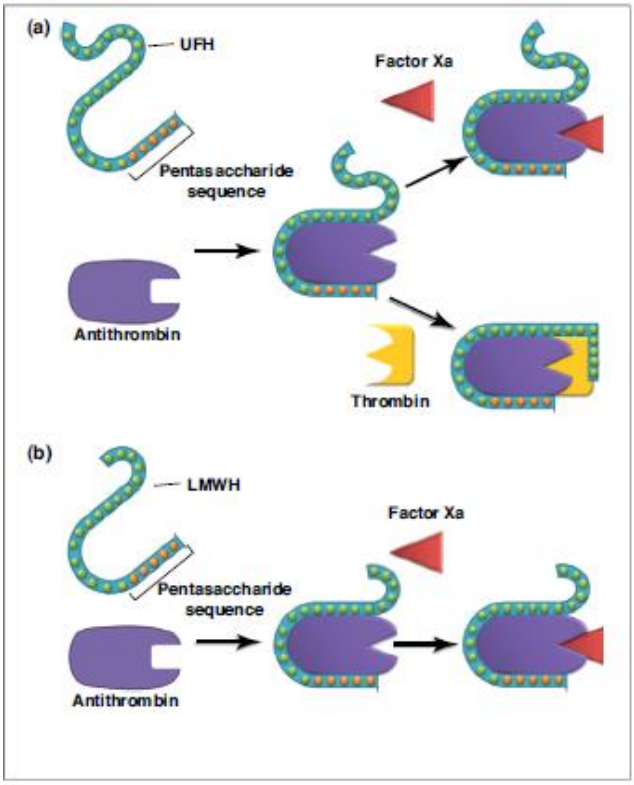

Figure 4.2-Mechanism of action of **UFH (a)** and **LMWHs (b)** (adapted from J. Am. Acad. Orthop. Surg. 2002; 10, 299–302).

.

An ideal LMWH should differ from UHF only in molecular mass. Nevertheless, manufacturing processes alter the structure of the native polysaccharide which can affect the clinical properties of LMWHs. Firstly, the cleavage of the chain can occur within the pentasaccharide sequence determining a reduction of the pharmacological activity [11]. Indeed, in the case of UHF the number of chains containing the pentasaccharide is approximately 30%; this percentage decreases to 15–25% in the LMWH chains [12]. Moreover, the cleavage process leads to variations in the sulfation degree ratio and the formation of unusual end residues which are artifacts of the depolymerization process (**Table 4.1)**. As an example, in the case of enoxaparin, five different residues at the reducing end and two different residues at the non-reducing end are described in literature [13]. Finally, the structural variability of LMWHs with respect to UFH can be further increased by the purification process used to isolate the desired polymeric fractions [9].

The factors governing the quality of LMWHs are also strictly related to the quality of UFH other than to the manufacturing method. After the case of the heparin contamination by oversulfated chondroitin sulfate which caused more than 100 deaths in the USA in 2008 [Information on Adverse Event Reports and Heparin: http://www.fda.gov/Drugs/DrugSafety/PostmarketDrugSafetyInformationforPatientsandProviders/UCM112669], the US and European Pharmacopoeias reviewed their monographs. In particular, H-NMR and anion exchange-HPLC emerged as the two main robust tools to determine impurities and contaminants in heparin [14]. Both Ph. Eur. and USP define the NMR and chromatographic specifications for the identity and purity of UFH and the presence of dermatan sulfate and oversulfated chondroitin sulfate. Nevertheless, despite the attempt of harmonization of UFH and LMWH monographs, several differences still exist. As far as the definition of the UFH potency is concerned, the Ph. Eur. method is based on its ability to delay the clotting time of recalcified citrated plasma of sheep, while USP introduced a chromogenic anti-factor IIa assay for potency assignment. Moreover, USP defined the ratio of anti-factor Xa activity to anti-factor IIa activity and added a limit of galactosamine in total hexosamine which is an indirect measure of dermatan sulfate and other galactosamine containing impurities.

In the EU LMWHs have to comply not only the monograph [15], but also additional requirements reported in the specific substance monograph (**Table 4.1**). The Ph. Eur. tests for LMWHs include identification by ^{13}C-NMR which provides their fingerprints. The structural information is completed with the determination of the molecular weight distribution by means of size-exclusion chromatography (SEC) and the quantification of the anticoagulant activity using a proper in vitro assay. Among LMWHs, USP reports only the monograph of enoxaparin [16] consisting of a complex set of oligosaccharides that have not yet fully characterized because of its high structural variability. The European and US Pharmacopeia requirements for enoxaparin are essentially the same. Nevertheless, the USP monograph describes a specific assay to determine the percentage of materials cyclized in a 1,6-anhydro ring at the reducing end of the chain. This requirement was probably introduced because this bicyclic structure is recognized to play a role in the interaction with AT [17]. This peculiar feature could be also exploited to compare enoxaparin produced by different manufactures.

Despite several sophisticated analytical techniques for the determination of the saccharide sequence of LMWHs as well as specific assays for the evaluation of their pharmacological activity are available, the complexity and the variability of these compounds require a continuous research for the development of new and more sensitive assays. In confirmation of that, a workgroup with the function to collect and harmonize the knowledge of the international experts on this topic has been formed and in UE the general monograph of LMWHs is still under revision as well as the enoxaparin, tinzaparin and nadroparin ones [http://www.edqm.eu/en/european-pharmacopoeia-work-programme-EDQM-607.html].

Table 4.1- Main chemical characteristics of LMWHs currently available in UE and US markets.

Depolimerization method	LMWH (market)	Representative end residues	Average Molecular weight	Anti-Xa/IIa ratio	Degree of sulfation	Pharmacopeia Specific Assays	References
Deaminative cleavage (nitrous acid)	Nadroparin (UE)	Non reducing: 2-O-sulfo-α-L-idopyranosuric acid	4,300 (range 3,600-5,000)	2.5-4	about 2.5	Ethanol; N-NO groups; Free sulfates.	[34]
	Dalteparin (UE and US)	Reducing: 6-O-sulfo-2,5-anhydro-D-mannitol	6,000 (range 5,600-6,400)	2.5-4	1.8 -2.5	Nitrite Boron;	[35]
	Reviparin (UE)		3,900 (range 3,000-4,500)	3.6-6.1	2-2.6		[36, 37]
(isoamyl nitrite)	Certoparin (UE)		3,800	1.5-2.5	2		[36]
β-eliminative cleavage (benzilation and alkaline treatment)	Enoxaparin (UE and US)	Non-reducing: 4-enopyranose uronate Reducing: 1,6-anhydro derivate	4,500 (range 3,800-5,000)	3.3-5.3	2-2.5	Benzyl alcohol content % oligosaccharide chains that are cyclized in 1,6-anhydro ring	[16, 38]
(alkaline treatment with a quaternary ammonium salt)	Bemiparin (UE)	—	3,600-3,800	8.1	--	--	[39, 40]
Enzymatic treatment (heparinase)	Tinzaparin (UE and US)	Non reducing end: 2-O-sulfo-4-enepyranosuric acid Reducing end: 2-N,6-O-disulfo-D-glucosamine	6,500 (range 5,500-7,500)		--	-	[41]
Radical-catalysed depolymerization with hydrogen peroxide and a cupric salt	Parnaparin (UE)	Reducing end: 2-O-sulfo-α-L-idopyranosuric acid Reducing end: 2-N,6-O-disulfo-D-glucosamine	5,000 (range 4,000-6,000)	1.5-3	--	Copper	[42]

4.3 Therapeutic indications of LMWHs

Most of the LMWHs are indicated for the prophylaxis of deep vein thrombosis (DVT) in patients undergoing orthopaedic or general surgery and the treatment of DVT [18-23]. They are the anticoagulant of choice for the prevention of DVT after major orthopaedic surgical procedures.

Dalteparin, enoxaparin and nadroparin in combination with acetylsalicylic acid are also effective for the prophylaxis of ischemic complications in patients with unstable angina and non-Q-wave myocardial infarction [18; 19; 20]. In particular, enoxaparin has consistently been demonstrated to have a superior efficacy than other LMWHs in patients with acute coronary syndrome [24]. Dalteparin, enoxaparin, nadroparin and bemiparin are also indicated for the prevention of clotting in the extra corporeal system during haemodialysis and hemofiltration in patients with acute renal failure or chronic renal insufficiency [18; 19; 20; 23]; Enoxaparin is also used for the prophylaxis of venous thromboembolism (VTE) in non-surgical patients with severely restricted mobility during acute illnesses, such as cardiac insufficiency, respiratory failure, severe infections or rheumatic disease and for the treatment of acute DVT with or without pulmonary embolism [18]. Enoxaparin is the leading LMWH with the widest range of therapeutic indications. Indeed, the administration of enoxaparin to treat acute ST-segment elevation myocardial infarction in patients receiving thrombolysis and being managed medically or with percutaneous coronary intervention was demonstrated to be effective in reducing mortality and ischaemic and bleeding end points [25].

The FDA approved the use of dalteparin for the management of symptomatic VTE (proximal deep vein thrombosis and/or pulmonary embolism) in cancer patients [26].

The design and extent of the clinical studies can have an effect on the indications contained in the Summary of Product Characteristic information. Thus, clinical indications for the same product may differ slightly in the various countries where it has been approved, as exemplified in **Table 4.2**. This incoherence can be observed not only between US and European markets, but also between single countries in the EU, probably due to the fact that LMWHs were marketed in the early ’90s before Regulation 2309/93/CEE coming into effect and MAAs were presented independently in each country.

Table 4.2-Clinical indications of LMWHs approved in USA, Italy and United Kingdom.

	FDA	**IT**	**UK**
Enoxaparin	-Prophylaxis of DVT[a] in patient undergoing orthopaedic or general surgery or medical patients with bedridden due to acute illness -Treatment of acute DVT with or without PE[b]		
	_____	-Prevention of clotting in the extracorporeal system during hemodialysis -Treatment of unstable angina and non-Q wave myocardial infarction, administered concurrently with aspirin	
	-Prophylaxis of ischemic complications of unstable angina and non-Q wave myocardial infarction	_____	-Treatment of STEMI[c] managed medically or with subsequent PCI[d]
Tinzaparin	-Treatment of acute symptomatic DVT with or without PE when administered in conjunction with warfarin sodium	-Not available on the market	-Treatment of DVT and of PE
Dalteparin	-Prophylaxis of DVT in patient undergoing orthopaedic or general surgery		_____
	_____	-Treatment of acute DVT	
	-Prophylaxis of ischemic complications of unstable angina and non-Q wave myocardial infarction -Extended treatment of symptomatic VTE[e] to reduce the recurrence in patients with cancer	-Prevention of clotting in the extracorporeal system during hemodialysis -Treatment of unstable angina and non-Q wave myocardial infarction, administered concurrently with aspirin	-Treatment of PE -Treatment of DVT with PE

Data extrapolated from [18; 19; 25; 26; 43; 44; 45; 46]

[a] DVT: deep vein thrombosis; [b] PE: pulmonary embolism; [c] STEMI: acute ST-segment elevation myocardial infarction; [d] PCI: percutaneous coronary intervention; [e] VTE: venous thromboembolism

4.4 Regulatory aspects of the US-FDA

As mentioned, the FDA considers LMWHs as semisynthetic drugs and, therefore, the generic drug products can be marketed after the approval of an Abbreviated New Drug Application (ANDA), demonstrating bioequivalence, the same active ingredient(s), route of administration, dosage form, strength, conditions of use and labelling as the originator [27].

In July 2010, the FDA approved the first copy of enoxaparin sodium and nowadays two generic versions are available on the market. This decision of the American regulatory agency was not free of blame. Indeed, the Marketing Authorization Holder (Aventis Pharmaceuticals) presented a petition to FDA asking to stop the approval of the generic version of its product, unless the ANDA applicant completely characterized the active substance, even in terms of polysaccharide chains, using the identical production process employed for the synthesis of the originator product or carrying out proper clinical trials. The request was rejected by the FDA on the basis that even the brand product shows a certain level of batch to batch variability and that no regulation requests that the process parameters assessed by the two competitors should be identical. It is sufficient that the applicant uses the same depolymerisation method (β-eliminative cleavage) employed by the Marketing authorization Holder.

The evaluation of the equivalence between the originator and generic products relies on the qualitative and quantitative analysis of the generic product in comparison to different batches of the originator. The same level of variability between the two products is considered as an index of sameness of the active substances. In support of this thesis, FDA also stated that the use of generic versions of UFH has not been associated to any significant increase of side effects despite the less restrictive criteria for the ANDA approval [Generic Enoxaparin Questions and Answers: http://www.fda.gov/Drugs/Drugsafety/PostmarketDrugSafetyInformationforPatientsandProviders/ucm220037.htm]. Following this approach, the FDA scientists established five criteria to assure that the generic product drug contains the same active ingredient as its originator [28].

Criterion 1: equivalence of heparin source material and mode of depolymerization

Porcine intestinal mucosa is the only heparin source authorized by the FDA. It can be expected that UFH obtained from the same source materials contains a similar distribution of the disaccharide building block sequences.

The mode of depolymerization does not perturb the conformation of the "natural" disaccharide building blocks of UFH, but generates a modification of disaccharide units at the terminal ends. Therefore, this criterion is based on the estimation of the same chemical selectivity for UFH of equivalent mode of depolymerization used in the manufacturing process. As a consequence, the modification at the terminal end of the generic and the originator are considered very similar.

Criterion 2: equivalence of physicochemical properties

This criterion is used to ensure that the molecular weight distribution of enoxaparin in the generic drug product is equivalent to that in the originator.

In addition to conventional SEC, complementary analyses termed "chain mapping" by CTA-SAX chromatography, MALDI-MS, GPC-ESI-MS, or RPIP-ESI-MS are required to provide a high resolution fingerprint profile of the oligosaccharide chain lengths and demonstrate the equivalent distribution in the generic drug product and the originator.

Criterion 3: equivalence in disaccharide building blocks, fragment mapping and sequence of oligosaccharide species

This comparison looks at the products' molecular nature: besides confirming the presence of a pharmacologically important 1,6-anhydro ring at the ends of 15–25% of enoxaparin chains, the FDA looks at the spectrum of disaccharide building blocks and the oligosaccharide lengths and sequences-factors affected by the temperature, depolymerization time and other conditions of preparation [29]. Analyses of enoxaparin or partially digested enoxaparin with purified heparinases are carried out by using capillary electrophoresis, RP-HPLC, SAX-HPLC, mass spectroscopy and NMR spectroscopy.

If even this criterion is met, there are substantial supporting evidences that the generic drug product is the same as originator.

Criterion 4: equivalence in biological and biochemical assays

To demonstrate equivalent anticoagulant activity *in vitro* and *in vivo*, the FDA requires the studies of relevant markers, such as activated partial thromboplastin time (aPTT), heptest prolongation time, anti-factor Xa activity, anti-factor IIa activity and anti-factor Xa/anti-factor IIa activity ratio.

Criterion 5: equivalence of in vivo pharmacodynamic profile

The comparison of pharmacodynamic profiles is based upon measurement of anti-factor Xa and anti-factor IIa profiles in human health volunteers. Moreover, the FDA also requests to conduct immunogenicity tests (i.e. Heparin Induced Thrombocytopenia II, HIT II).

Thus, if the five criteria are complied with, the generic enoxaparin will have the same active ingredient as the originator. According to the FDA approach, the first three criteria ensures that the heparin source material, the chemical reaction used in the manufacturing process, and the structure (average molecular weight, polydispersity and chemical composition of the terminal ends) of enoxaparin in the generic drug product is equivalent to that in the originator. The fourth and fifth criteria assure that the generic enoxaparin sodium has the same degree of anticoagulant activity and safety as originator.

4.5 Regulatory aspects of the EMA

The EMA defines LMWHs as biologics regarding their copies as biosimilars. Therefore, in order to obtain the MA, the applicant has to demonstrate the equivalence of biosimilar and originator, in terms of effectiveness and safety, by the "comparability exercise" on the basis of clinical trials [30]. The number and extent of comparability studies required to grant a MA are detailed in the guidelines issued by the Committee for Medicinal Products for Human Use (CHMP). According to the "Guideline on similar biological products containing LMWHs" adopted in 2009 [31], the EMA expects that all LMWHs products meet the physicochemical specifications present in the Ph. Eur. monographs.

Non-clinical requirements

A number of comparative bioassays including evaluations of the anti-factor Xa and anti-factor IIa activity should be carried out to determine relevant pharmacodynamic effects of LMWHs and demonstrate the similar activity between the copies and the originator. The EMA requires also the assessment of the toxicology in a relevant species, e.g. rats, in accordance with the "Note for guidance on repeated dose toxicity" [32] for at least 4 weeks. In contrast, studies on the safety pharmacology, reproduction toxicology, mutagenicity and carcinogenicity are not routine requirements for non-clinical testing of LMWH biosimilars.

Clinical requirements

These studies should be performed to compare the pharmacodynamic and pharmacokinetics parameters of the copy and the originator products. The manufacturer could use pharmacodynamic activities (e.g. anti-factor Xa and anti-factor IIa, tissue factor pathway inhibitor) as surrogate markers for LMWHs circulating concentrations. The study of these parameters should be performed in a randomized two way crossover study in healthy volunteers after the administration of a single subcutaneous dose and other routes of administration, if the originator is authorized.

Since it is assumed that a univocal correlation between pharmacodynamic parameters and clinical effects does not exist, the EMA requires at least one adequately powered, randomised, double-blind, parallel group clinical trial in the setting of prevention of VTE or arterial thromboembolism or treatment of VTE. The clinical trial should be performed in the most sensitive, highest VTE risk population, such as in patients undergoing elective major orthopaedic surgery.

This study is required to demonstrate that the copy exhibits equivalent therapeutic efficacy to the reference product. The most relevant endpoints, namely DVT, pulmonary embolism and VTE-related death, should be analyzed by the most advanced technologies and all data should be evaluated by a central independent and blinded committee of experts, using pre-specified limits.

The EMA also requires a comparative study demonstrating similar safety profile of the biosimilar versus the reference product analyzing the different type, frequency and

severity of the adverse reactions. Finally the applicant has also to perform an analysis for the detection of HIT II [31].

4.6 Concluding remarks

In the clinical practice LMWHs have been demonstrated to be superior to UFH as antithrombotic agents because they have a much longer half-life and exhibit a lower incidence of HIT II. Moreover, unlike to UFH, a frequent monitoring is not needed to adjust the dose. However, LMWHs have different pharmacokinetic and pharmacodynamic profiles due to the specific depolymerization processes and, therefore, they cannot be considered interchangeable. Indeed, the peculiar manufacturing methods lead to a greater structural variability than UFH. At the same time, the high molecular complexity of LMWHs prevents a complete chemical and physical characterization which is essential to predict the biological activity. This intricate background is further complicated by the expiration of protection rights of some LMWHs which raises the opportunity to develop copies. EMA and FDA adopted different approaches to grant MAs. In particular, the EMA considers LMWHs as biosimilar products and recommends phase III clinical trials for the comparability exercise. On the contrary, the FDA, classifying LMWHs as semisynthetic drug products, does not require such trials, but only the determination of pharmacodynamic profiles in healthy human volunteers. The FDA also asserts that the individuated five criteria are more sensitive to evidence differences between two generic LMWHs than the clinical studies recommended in the EMA guideline. In support of FDA's approach, it should be mentioned that the quality requirements are more restrictive in US than UE. As a matter of fact, Ph. Eur. lacks specific assays to determine some relevant structural elements such as the percentage of 1,6-anhydro ring at the reducing end of the enoxaparin chains which, on the contrary, are included in USP. Nevertheless, taking into account the intrinsic variability of LMWHs obtained by the same depolymerization method and the objective current unfeasibility of a complete characterization of these complex semisynthetic compounds of biological origin, a conservative approach is desirable since it guarantees a higher level of safety for the patient's health. Reasonably, the reduction of the number of clinical studies required

by the EMA supported by a more specific chemical and analytical characterization is the direction to be pursued in order to ease the introduction on the market of LMWHs copies with a safety and efficacy profile comparable to that of the originator. In July 2011, the EMA published a concept paper on the revision of its LMWH specific guideline suggesting the possibility to reduce clinical data requirements. The draft guideline should be released for consultation during the course of 2012 [33]. The definition of the extent of clinical studies required for the MA in UE could benefit from the experiences that will be matured in US market, and the availability of pharmacovigilance data.

References

1. Conrad H.E. Structure of heparinoids. In *Heparin binding proteins,* Academic Press 1998, pp 7-60*;*
2. Casu B. Structure and Active Domains of Heparin. In: Garg H.G, Linhardt R.J, Hales C.A, *Chemistry and Biology of Heparin and Heparan sulfate*, Elsevier 2005, pp. 1-28;
3. Chuang Y.J, Swanson R, Raja S.M, Olson S.T. Heparin enhances the specificity of antithrombin for thrombin and factor Xa independent of the reactive center loop sequence. Evidence for an exosite determinant of factor Xa specificity in heparin-activated antithrombin. The Journal of Biological Chemistry 2001, 276 (18), 14961–14971;
4. Casu B. Structure and biological activity of heparin. In: *Advances in Carbohydrate Chemistry and Biochemistry* 1985, 43, 51-134;
5. Casu B.and Lindahl U. Structure and biological interactions of heparin and heparan sulfate. *Advances in Carbohydrate Chemistry and Biochemistry 2001,* 57, 159-206;
6. Heparin sodium in United States Pharmacopeia 35–NF 30, official from May 1, 2012;
7. Heparin sodium. In European Pharmacopeia, 7th Edition Supplement 7.5, 2012 Strasbourg, accessed on line on January 2012;
8. Liverani L, Mascellani G, Spelta F. Heparins: Process-related physico-chemical and compositional characteristics, fingerprints and impurities. Thrombosis and Haemostasis 2009, 102, 846–853;
9. Linhardt R.J and Gunay N.S. Production and Chemical Processing of Low Molecular Weight Heparins. Seminars in Thrombosis and Hemostasis 1999, 25 (3), 5-16;
10. Hirsh J. and Raschke R. Heparin and Low-molecular Weight Heparin. CHEST 2004, 126, 188S-203S;
11. Guerrini M, Guglieri S, Casu B, Torri G, Mourier P, Boudier C, Viskov C. Antithrombin-binding Octasaccharides and Role of Extensions of the Active Pentasaccharide Sequence in the Specificity and Strength of Interaction. The Journal of Biological Chemistry 2008, 283(39), 26662–26675;
12. Rudd T.R, Skidmore M.A, Guimond S.E, Holman J, Turnbull J.E, Lauder R.M, Fernig D.G, Yates E.A.The potential for circular dichroism as an additional facile and

sensitive method of monitoring low-molecular-weight heparins and heparinoids. Thrombosis and Haemostasis 2009, 102 (5), 874-878;

13. Guerrini M, Guglieri S, Naggi A, Sasisekharan R, Torri G. Low Molecular Weight Heparins: Structural Differentiation by Bidimensional Nuclear Magnetic Resonance Spectroscopy. Seminars in Thrombosis and Hemostasis 2007, 33, 478-4875;
14. Keire D.A, Ye H, Trehy M.L, Ye W, Kolinski R.E, Westenberger B.J, Buhse L.F, Nasr M, Al-Hakim A. Characterization of currently marketed heparin products: key tests for quality assurance. Analytical and Bioanalytical Chemistry 2011, 399, 581-591;
15. Heparins, Low-molecular mass. In European Pharmacopeia, 7th Edition Supplement 7.5, 2012 Strasbourg, accessed on line on January 2012;
16. Enoxaparin sodium in United States Pharmacopeia 35–NF 30, official from May 1, 2012;
17. Guerrini M, Elli S., Gaudesi D., Torri G., Casu B., Mourier P., Herman F., Boudier C., Lorenz M., Viskov C. Effects on Molecular Conformation and Anticoagulant Activities of 1,6-Anhydrosugars at the Reducing Terminal of Antithrombin-Binding Octasaccharides Isolated from Low-Molecular-Weight Heparin Enoxaparin. Journal of Medicinal Chemistry 2010, 53, 8030-8040;
18. Summary of Product Characteristics of Clexane (enoxaparin), Sanofi-Aventis revision May, 2011 (IT);
19. Summary of Product Characteristics of Fragmin (dalteparin), Pfizer Italia S.r.l. revision March, 2009 (IT);
20. Summary of Product Characteristics of Fraxiparine(nadroparin) GlaxoSmithKline S.p.A. revision October, 2009 (IT);
21. Summary of Product Characteristics of Fluxum (parnaparin) Alfa Wassermann S.p.A. revision July, 2010 (IT);
22. Summary of Product Characteristics of Clivarina (reviparin) Abbott S.r.l. revision February, 2009 (IT);
23. Summary of Product Characteristics of Ivor 2500 UI (bemiparin) Sigma-Tau Industrie Farmaceutiche Riunite S.p.A. revision March, 2011 (IT);
24. Drouet L. LMWH: how much similarity for how much clinical benefit. Targeted Oncology 2012, 7 Suppl 1, S35-S42;

25. Summary of Product Characteristics of Clexane (enoxaparin), Sanofi-Aventis UK revision December, 2011 (UK);
26. Summary of Product Characteristics of Fragmin (dalteparin), Pfizer Health AB revision October, 2010 (USA);
27. Ofosu F.A. A review of the two major regulatory pathways for non proprietary low-molecular-weight heparins. Thrombosis and Hemostasis 2012, 107, 201-214;
28. FDA response to citizen petition Docket No. FDA-2003-P-0273;
29. Editorial. The identity problem. Nature Biotechnology 2010, 28, 877;
30. Minghetti P, Rocco P, Cilurzo F, Vecchio L.D, Locatelli F. The regulatory framework of biosimilars in the European Union. Drug Discovery Today 2012, 17(1-2), 63-70;
31. European Medicines Agency (2007). *Guideline on non-clinical and clinical development of similar biological products containing low-molecular-weight-heparins.* (EMEA/CHMP/BMWP/118264/2007);
32. European Medicines Agency (2000). *Note for guidance on repeated dose toxicity*. (CPMP/SWP/1042/99);
33. European Medicines Agency (2011). *Revision of the guideline on non-clinical and clinical development of similar biological medicinal products containing low-molecular-weight heparins*. (EMA/CHMP/BMWP/522386/2011);
34. Nadroparin calcium In European Pharmacopeia, 7th Edition Supplement 7.5, 2012 Strasbourg, accessed on line on January 2012;
35. Dalteparin sodium In European Pharmacopeia, 7th Edition Supplement 7.5, 2012 Strasbourg, accessed on line on January 2012;
36. Boneu B. Low Molecular Weight Heparins: Are They Superior to Unfractionated Heparins to Prevent and to Treat Deep Vein Thrombosis? Thrombosis Research 2000, 100, V113–V120;
37. Baumbach A. Low-molecular-weight heparin (reviparin) reduces the incidence of femoropopliteal in-stent stenosis: preliminary results of an ongoing study. Catheterization and Cardiovascular Interventions 1999, 47, 102–106;
38. Enoxaparin sodium In European Pharmacopeia, 7th Edition Supplement 7.5, 2012 Strasbourg, accessed on line on January 2012;

39. Belmonte L. Rovi Lab Farmaceut. Process for the depolymerization of heparin for obtaining heparin with a low molecular weight and having an antithrombotic activity, EP0293539;
40. Falkon L, Sáenz-Campos D, Antonijoan R, Martín S, Barbanoj M, Fontcuberta J. Bioavailability and pharmacokinetics of a new low molecular weight heparin (RO-11)—A three way cross-over study in healthy volunteers. Thrombosis Research 1995, 78(1), 77-86;
41. Tinzaparin sodium In European Pharmacopeia, 7th Edition Supplement 7.5, 2012 Strasbourg, accessed on line on January 2012;
42. Parnaparin sodium In European Pharmacopeia, 7th Edition Supplement 7.5, 2012 Strasbourg, accessed on line on January 2012;
43. Summary of Product Characteristics of Lovenox (enoxaparin), Sanofi-Aventis US revision April, 2011 (USA);
44. Summary of Product Characteristics of Innohep (tinzaparin), LEO Pharma AS revision May, 2010 (USA);
45. Summary of Product Characteristics of Innohep (tinzaparin), LEO Laboratories Limited revision September, 2011 (UK);
46. Summary of Product Characteristics of Fragmin (dalteparin), Pfizer Limited revision June, 2011 (UK).

Final Remarks

This PhD thesis proposed to investigate the physicochemical parameters that rule the permeation through human skin of GAGs, with particular focus on HA and heparins.

The overall experimental data confirmed that M_w represents a fundamental factor in determining the permeability properties also of such polysaccharides. Indeed, in *in vitro* studies performed using human epidermis as membrane, HA at "low M_w" (6.7 KDa) showed a greater penetration than the corresponding polymer at higher M_w (**Chapter 1**). Similarly, LMWHs sodium salts permeated to a larger extent with respect to UFH and a good correlation between Log M_w and Q_{24} was found for LMWHs sodium salts (**Chapter 2**). However, the key parameter that drives the permeation of such macromolecules through the skin resulted to be the polymer flexibility, which allows the compounds to adapt to the different skin environments. In fact, the introduction of sulfate groups on HA chains, causing the disruption of the helical motif, led to less ordered structures, which were able to cross the skin to higher extent compared to unsubstituted HA, despite their increased polarity (**Chapter 1**). Accordingly, the presence of divalent cations in LMWHs solution, causing the reduction of the chain flexibility through the formation of intramolecular chelates, negatively affected the skin permeability properties of calcium nadroparin (**Chapter 2**).

Furthermore, both classes of polysaccharides investigated (HA and heparins) demonstrated to interact with stratum corneum components, in particular keratins, as confirmed by confocal miscroscopy images (HA, **Chapter 1**) and ATR-FTIR spectra (UFH, **Chapter 3**), suggesting that the diffusion through human stratum corneum occurred mainly by transcellular route.

Since the physicochemical features of these polysaccharides (hydrophilicity, negative charge and high M_w) precluded a significant diffusion through the human epidermis, the phage display technique was exploited to screen a skin penetrating peptide which could enhance the skin permeation of such molecules, allowing their transdermal delivery. The in vitro screening allowed to identify a neutral peptide, DRTTLTN, which resulted to be able to increase the permeation of UFH through the skin after chemical conjugation

(**Chapter 3**). These results demonstrated the suitability of skin penetrating peptides to enhance also the transdermal delivery of polysaccharide macromolecules.

The analysis of the scientific literature related to LMWHs evidenced also a critical and debated regulatory topic raised from the expiration of protection rights of brand LMWHs and the incoming introduction on the European market of their medicinal copies. The classification of these copies resulted to be particularly controversial since LMWHs are produced by chemical synthetic strategies involving, however, the depolymerization of a drug obtained from biological sources (UFH). This dual characteristic led EMA and FDA to adopt two different approaches for the classification and, consequently, the regulation of non-proprietary LMWHs. In fact, in the FDA opinion prevailed the synthetic origin of LMWHs and the American agency classified the copies as generics, whereas EMA considered more relevant the biological nature of the precursor thus defining LMWHs copies as biosimilars. The need to deal with this hot regulatory topic boosted the in depth-analysis of the chemistry of LMWHs and the assays provided for their proper characterization and led to the publication of a paper on a peer-reviewed journal (**Chapter 4**).

Appendix

6BrCaQ nano-liposomes as tool to target breast and prostate cancer cells

1. Introduction

Breast and prostate cancers are the two tumors with the major incidence in women and men respectively and are leading causes of mortality in developed countries. Although they develop in organs anatomically and physiologically different, they share many similar biological features, first the hormonal-dependence [1]. Hence, the first line treatment (after surgery) for these types of cancer is the hormonal therapy, which relies on the inhibition of the biosynthesis of steroids or the block of the receptors activity. However, also steroid receptor-positive cancers (two-thirds of breast cancers) develop a hormonal resistance leading to the failure of the therapy based on anti-oestrogen and anti-androgen drugs [2, 3]. Therefore, an intensive research is aimed to select alternative targets along the different pathways involved in the pathogenesis of cancer [4].

Heat shock protein 90 (Hsp90) is a molecular chaperone (90kDa) which modulates the biological action of several client proteins allowing their folding in the active conformation through a cycle regulated by the binding and the hydrolysis of ATP and by other co-chaperons [5]. Inhibitors of Hsp90 lead to the degradation of client proteins by the ubiquitin-proteasome system. At date, at least 200 client proteins of Hsp90 have been identified and, since most of them are oncoproteins, Hsp90 is considered a powerful target in cancer therapy [6]. Although this chaperone is ubiquitously distributed, it represents a selective target, since heat shock proteins are overexpressed in cancer cells in response to different stressful stimuli (such as heat, hypoxia and acidosis) which occur in tumor environment. Moreover, it was demonstrated that Hsp90 from cancer cells shows a higher affinity for the inhibitors with respect to that present in normal tissue [7, 8]. This could limit the risk of side secondary effects for the Hsp90 inhibitors, which constitutes the major concern of the anticancer therapy.

Hsp90 is a homodimer composed of two well conserved N-terminal and C-terminal residues, a middle domain with the binding site of client proteins and a charged region of different length which follows the N-terminal domain [5, 9]. The C-terminal domain is essential for Hsp90 dimerization and contains a secondary site of binding of ATP (recently hypothesized) along with a polypeptide involved in the recognition and binding of co-chaperons. The antibiotic coumarin novobiocin (Nvb) was the first compound identified to weakly bind to this secondary ATP pocket inducing the degradation of Hsp90 client proteins. Once discovered the activity of Nvb, attempts have been made to develop derivatives with greater anti-cancer effect [10]. In fact, the C-terminal inhibitors are supposed not to induce a heat-shock response (induction of "pro-cancer" Hsp70 and Hsp27), which may account for the resistance to the N-terminal inhibitors contributing to the limits of the clinical trials [11].

In this context, Audisio and coworkers, have synthesized a series of quinolein-2-one derivatives of Nvb which exhibited a greater affinity to the C-terminal domain of Hsp90 compared to the natural antibiotic. Among those, the 6-bromo-3-[4-methoxyphenylcarboxamide]-quinolein-2-one, 6BrCaQ (**Figure 1**), resulted to be the most effective as anti-proliferative agent in different cancer cell lines (**Figure 2**). It caused the arrest of MCF-7 breast cancer cells in cell cycle *in vitro* and was able to induce the apoptosis both through the intrinsic and extrinsic pathways [6].

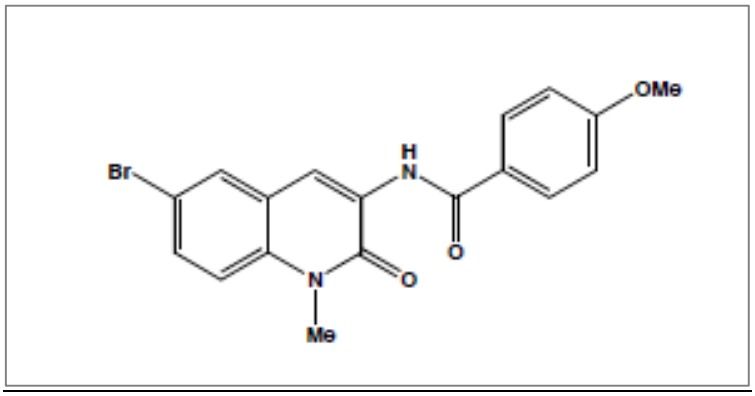

Figure 1- Chemical structure of 6BrCaQ [6]

Antiproliferative effects of selected compounds 2 and 9 in MCF-7 human breast cancer cells.

Compd	GI_{50} [μm] (MCF-7)[a]
2b (6BrCaQ)	7
2c	10
2 f	60
2h	45
9 f	100
9j	8
4TCNA	50
2e	18
2g	27
9e	30
9i	70
DHTCNA	35
Nvb	260

[a]GI_{50}=concentration of compound needed to reduce cell growth by 50% following 72 h cell treatment with the tested drug (average of three experiments). Values are the mean of two independent experiments in which no more than 5.5 variations were measured.

Figure 2- Antiproliferative effect of Nvb and derivatives on MCF-7 breast cancer cells [6]

Despite its promising efficacy as anticancer agent, 6BrCaQ is characterized by a very poor solubility in water (70 mg/L), which prevents its parenteral administration *in vivo*. The encapsulation in liposomes is a well-established expedient to enable the solubilization of hydrophobic drugs [12]. Moreover, liposomes have been extensively and successfully exploited to target cancer since they can passively accumulate in solid tumors through the so-called "enhanced permeability and retention effect (EPR) [13]. Indeed, in spite of slight differences in the various types of cancer, tumors present a leaky vasculature in which endothelial gaps have larger pores compared to a normal endothelium (100-780 nm against 5-10 nm of diameter). Then, colloidal carriers preferentially extravasate into tumor interstitium where they are retained due to the lack of an effective drenage system [14]. This phenomenon, which depends exclusively on the physiologic features of the tumor tissue, is known as "passive targeting" and requires liposomes having size ideally less than 200 nm for a proper extravasation [15]. Along with nano-sized dimensions, stealth® properties represent the other paradigm of cancer targeting. In fact, liposomes could be degraded by the reticuloendothelial system (RES)

through opsonization before reaching the target. The clearance by RES is prevented by grafting hydrophilic moieties, mainly polyethylene glycol (PEG) chains, on the liposome surface (Stealth® liposomes) which obstacle the absorption and binding of opsonins enabling the carriers to persist longer in the bloodstream [16]. Long circulating liposomes, once accumulated in tumor, can deliver the drug directly into the cells (after internalization) or in the extracellular fluid, improving the narrow therapeutic index of the anticancer drugs [16].

This work aimed to encapsulate 6BrCaQ in Stealth® nano-liposomes to overcome the poor solubility of the drug and enable the *in vivo* evaluation and administration. The composition of liposomes (Egg phosphatidylcholine (EPC), 1,2-distearoyl-snglycero-3-phosphoethanol-amine-N-methoxy-[poly-(ethylenglycol)-2000] (DPSE-PEG_{2000}) and cholesterol (Chol)) was selected on the basis of previous promising results obtained with the encapsulation of a hydrophobic anti-oestrogen drug [17]. Liposomes were characterized from a technological point of view, by determining size, zeta potential, encapsulation and purification efficiency, as well as physical stability during both storage and use in culture. The drug leakage in physiological conditions was also evaluated, considering the lipophilic nature of the drug (which can determine a prompt release through the lipid bilayer) and the use of phospholipids with low transition temperature (T_m of EPC= -2 °C). The biological activity of liposomes was evaluated by using metastatic breast and prostate cancer cells in culture, in comparison to that of the non-encapsulated drug. The effect on cell viability and on cell proliferation was investigated by MTS assay and flow cytometry. The possible liposomes-cells interaction was evaluated by using fluorescent lipids and confocal microscopy. Finally, the anti-metastatic potential of the formulation was determined by carrying out *in vitro* migration assays.

2. Materials and Methods

2.1. Materials

6BrCaQ was synthesized in the laboratory BioCIS UMR 8076 (Faculté de Pharmacie, Université Paris-Sud 11). Stock solutions (10 mM) were prepared in chloroform or dimethylsulfoxide (DMSO) depending on the further application (formulation or use in cell culture, respectively). EPC, DPSE-PEG_{2000} and rhodamine-labeled phosphatidylethanolamine (Rho-PE) were purchased by Avanti Polar Lipids Inc., Birmingham, USA. Chol was purchased by Sigma Aldrich (St. Quentin-Fallavier, France). Chemokine CCL2 (Rh-MCP-1) was purchased by Shenandoah Biotechnology Inc. RPMI 1640, Leibovitz's L-15 medium, trypsin/EDTA solution were purchased by Lonza. All other chemicals were reagent grade.

2.2. Preparation of liposomes

Liposomes were prepared by the conventional thin film hydration method, accordingly to a procedure previously described [17].

Briefly, lipids (EPC/Chol/DSPE-PEG_{2000} 64:30:6 molar ratio) were dissolved in chloroform to obtain a final concentration of 50 mM and 6BrCaQ (0.5 mM in chloroform) was added and mixed with lipids. For the preparation of fluorescent liposomes, 1% Rho-PE was added to the lipid mixture. After evaporation of the organic solvent under reduced pressure (BUCHI rotary evaporator, 80mbar, 25°C), the dried film was rehydrated with 3 mL of Hepes buffer (Hepes 10 mM, NaCl 145 mM, pH 7.4). The resulting multilamellar vesicles (MLVs) were extruded (extruder Whitley, Lipex, Vancouver, Canada) sequentially through 0.2 μm (3 passages) and 0.1 μm (5 passages) polycarbonate membranes (Millipore, USA).

Unincorporated 6BrCaQ was removed by ultracentrifugation at 40,000 g for 17 h at 4°C (Rotor 50.4 Ti, Beckman Ultracentrifuge, USA). Liposomes were stored at 4°C under atmosphere of argon until their use.

2.3. Physicochemical characterization of liposomes

Liposomes were characterized in terms of size and zeta potential by dynamic laser scattering (DLS), using a Zetasizer 4 Malvern (Malvern Inst., UK). For size measurement, liposomes samples were diluited 1:10 in Hepes buffer. Each measure was performed in triplicate with an angle of detection of 173°. The zeta potential was measured after proper dilution of the liposomes suspension in deionized water. Also in this case each result corresponds to the mean of three independent determinations.

Lipids content was assayed by using a specific kit for phospholipids dosage Biolabo. This relies on an enzymatic method, which allows the transformation of lipids in colored compounds able to absorb the UV light at 500 nm and it is specific for PC.

Drug encapsulated in liposomes was quantified by spectrofluorimetry (E_x=340 nm, E_m=390 nm) (Hitachi F-2000 spectrofluorimeter) after dilution 1:100 of the samples in DMSO/Hepes buffer (99:1, v/v), to break the lipid vesicles. The concentration of the drug was estimated using a calibration curve built in the range 0.1-10 µM (R^2=0.994). For higher concentrations, the process of fluorescence quenching was observed.

Any interference from lipids or DMSO/Hepes buffer was observed at these wavelengths. The encapsulation efficiency (EE%) was calculated as following:

$$EE\% = \frac{C_L}{C_I}\ x\ 100$$

where C_L is the 6BrCaQ concentration in purified liposomes and C_I is the concentration of 6BrCaQ in the initial suspension. The efficiency of the purification method was assessed by measuring the lipid content before and after ultracentrifugation and according to the equation:

$$\text{Purification efficiency: } \frac{\text{amount of lipids in purified liposomes}}{\text{total amounts of lipids}} \times 100$$

The physical stability of liposomes was evaluated both in storage conditions and in RPMI 1640 medium. In the first case, the size of liposomes was measured immediately after their preparation and after 2 and 3 months of storage in glass vials at 4°C.

To investigate the stability in culture environment, liposomes were suspended in RPMI 1640 and incubated at 37°C under continuous stirring for 72 h, the longest time of

incubation tested during the *in vitro* studies. Then, an aliquot was withdrawn and particle size distribution was measured by DLS (as described earlier) against the culture medium alone, to assess the contribution of proteins. The analysis was performed in triplicate.
Drug-leakage studies at physiological temperature were performed as well, to estimate the ability of the selected formulation to retain the entrapped drug. Briefly, liposomes at concentration of 20 µM were suspended in PBS. 200 µl were withdrawn and assayed by spectrofluorimetry to determine the experimental starting concentration. The suspension was incubated at 37°C under agitation for 72 h and 120 h respectively. At these intervals of time, samples were collected and ultracentrifugated (40,000 g, 17 h, 4°C) to precipitate liposomes from the suspension. Both supernatant and precipitate were assayed for drug quantification. A solution of free drug at the same concentration was prepared and tested in parallel to exclude the precipitation of crystals of the free drug in the pellet during ultracentrifugation.

2.4. Cell culture

In vitro anti-tumor activity of 6BrCaQ encapsulating liposomes was evaluated on two different cancer cell lines: PC3 and MDA-MB-231 (ATCC, Molsheim, France). PC3 is a human prostatic carcinoma cell line derived from bones metastasis. It was cultured in RPMI 1640 medium supplemented with 10% heat-inactivated fetal bovine serum (FBS) and 0.5% antibiotics (penicillin/streptomycin 50 IU/mL and 50µg/mL respectively). Decomplemented FBS was obtained by destroying the complement proteins by heating FBS at 56°C in a water bath.
MDA-MB-231 are mammary/glad cancer cells derived from pleural effusion. They were cultured in Leibovitz's L-15 medium supplemented with 15% decomplemented FBS, 1% glutamine and 0.5% penicillin/streptomycin, in presence of 22 mM sodium bicarbonate allowing the culture of the cells in a CO_2 atmosphere. Cells were maintained at 37 °C and 5% CO_2 in humidified atmosphere.

2.5. Biological activity *in vitro*

Cell viability was assessed using CellTiter 96 Aqueous One Solution® (Promega, Charbonni`eres, France). The method relies on the bioreduction of MTS [3-(4,5-

dimethylthiazol-2-yl)-5-(3-carboxymethoxyphenyl)-2-(4-sulfophenyl)-2H-tetrazolium] by NADPH or NADH produced by dehydrogenase enzymes in metabolically active cells to form a colored formazan product which is soluble in tissue culture medium.
Cells were seeded in a 96 wells plate (2.5 x 10^3 PC3 cells/well and 7.5 x 10^3 MDA-MB 231 cells/well) and let to adhere to the plate for 24 hours. Then they were treated for different times with 6BrCaQ free or liposomes at different concentrations and incubated at 37°C and 5% CO_2. DMSO (the solvent for the free drug) and unloaded liposomes (at the same lipid concentration of loaded ones) were used as controls. At the end of the treatment, 20 µL of reactive were added in each well and the absorbance of the samples at 492 nm was recorded using a 96-well plate reader. The values were corrected by subtracting the absorbance of the control wells containing cell-free medium. The percentage of viability was calculated as the ratio between the absorbance of the treated cells and that of the control (untreated cells).
The cell cycle was analyzed by flow cytometry. PC3 cells were seeded (30,000 cells/cm^2) in a 6 wells plate and let to grow for 24 h, then treated (5 µM drug) for 24 or 72 h. Cells were washed in PBS and detached by adding 1 mL of trypsin at 37°C.
2 x 10^5 cells were precipitated by centrifugation at 500 rpm for 10 min, washed twice in cold PBS and resuspended in 200 µL of PBS, which were added drop by drop to 800 µl of absolute ethanol to permeabilize cells. Cells were stored at -80°C until the day of the analysis. Fixed cells were precipitated by centrifugation (2000 rpm, 10 min) to remove ethanol and suspended in PBS containing 100 µg/ml RNase A and 10 µg/ml propidium iodide. After incubation for 30 min at 37°C, the distribution of cells in the cell cycle was analyzed with a BD Accuri™ C6 flow cytometer (BD Biosciences).

2.6. *In vitro* liposome uptake

The uptake of liposomes into the cells was studied by confocal microscopy. Cells were seeded in a 8 wells system Labteck mounted on a microscope slide (1.6 x 10^4 cells for MDA-MB-231 and 8 x 10^3cells for PC-3). After 24 h of adherence, the culture medium was replaced by a suspension (in culture medium) of fluorescent liposomes containing 6BrCaQ (5µM), for a time of exposure varying from 30 min to 4 h. Cells were washed with cold PBS, fixed with 2% formaldehyde containing 0.5 µg/ml of Hoechst 33342 (for

30 min) and washed again three times with cold water. Samples were covered with a glass slide with the help of Vectashield HardSet Mounting Media to preserve the fluorescence. Confocal imagines were collected using a X63 oil immersion objective at 488 nm from an argon laser using a Zeiss LSM 510 confocal microscope. Untreated cells were analyzed in parallel as control.

2.7. Wound healing assay

The migration of PC3 cells *in vitro*, as index of their metastatic potential, was assessed by wound healing assay. Briefly, cells were seeded in a µ-slide 8 wells (IBIDI) and grown until confluence in complete medium.

As the monolayer was formed, the well was scratched vertically by using a 200 µL pipette tip. The medium containing the cellular debris was removed and replaced by the treatment in 1% FBS RPMI 1640. Culture medium depleted of serum was used in this assay to limit cell proliferation and better observe the effect of the treatment on cell motility. Chemokine CCL2 (40 ng/mL) was added in each well since it is well known its fundamental role in promoting prostate cancer cell chemoattraction, proliferation, and survival [18]. Cells were incubated at 37 °C in atmosphere with 5% CO_2 and their migration in the direction of the wound was followed with a microscope (AxioObserver Z1, Carl Zeiss, German) equipped with a CoolSnap HQ2 CCD camera (Photometrics, Tucson, USA), by taking a picture each h during 24 h.

The test was performed in duplicate by using two distinct batches of liposomes.

Migrating cells were counted by using ImageJ analysis software. A region-of-interest (ROI) within the limits of the wound was selected and the number of cells migrated in this area at each time was measured automatically. The migration profiles were obtained by plotting the number of cells migrated per mm^2 as a function of the time.

3. Results and Discussion

3.1. Physicochemical characterization of liposomes

The main physicochemical parameters of 6BrCaQ encapsulating liposomes are reported in **Table 1**. The negative value found for the zeta potential is in agreement with the results described in literature for the same formulation [17]. Slight differences are congruent with the different ionic strength of the vehicles used for samples dilutions (NaCl 1 mM and water respectively).

Table 1-Main physicochemical characteristics of 6BrCaQ loaded liposomes

Mean Size (nm) (+/-SD)	**pdI**	**Zeta potential (mV) (mean+/-SD)**	**EE %**	**Purification efficiency (%)**
94.27±36.53	0.10	-14.53 ±7.08	63.74±10.61	88.25±14.78

Liposomes resulted to be stable after storage at 4°C for 2 and 3 months since any increment of size was observed by dynamic laser scattering (**Table 2**). Hence, the zeta potential, even if lower than the theoretical minimal value required for stability (30 mV in absolute value), along with the steric interaction between PEG_{2000} chains, caused the repulsion of vesicles, preventing phenomenon of aggregation or fusion of liposomes in the bulk suspension.

Indeed, liposomes also maintained their shape and size after 72 h of incubation in culture medium, suggesting that the presence of PEG_{2000} moieties on the surface of liposomes prevents the absorption of proteins in physiological environment.

Table 2- Stability of liposomes assessed by size measurement after 2 and 3 months of storage at 4°C

Time (months)	Mean Size (nm) (+/-SD)	pdI
0	113.1±37.4	0.08
2	115.5±36.5	0.08
3	111.9±37.0	0.08

To assess whether the liposomes-based formulation of 6BrCaQ was able to retain the drug into the lipid bilayer in physiologic environment, the amount of drug released after 72 and 120 h of incubation in culture medium was determined.

After 72 h of incubation at 37°C, only 9.4% of the drug encapsulated was released from liposomes up to 37.95% after 120 h. These results confirmed that drug leakage is prevented when the bilayer becomes more fluid at physiologic temperature ($T > T_m$ EPC). Therefore, the investigated liposomes resulted to be able to retain the drug for a time sufficient to deliver it into the cells, which occurs in a short time as demonstrated by confocal images (**Figure 7**).

3.2. Biological activity *in vitro*

Preliminary experiments established an IC_{50} (concentration which causes the death of 50% of cells) of 10 µM for free 6BrCaQ for a time of treatment of 72 h for PC-3 cells (and about 5 µM for MDA-MB-231).

The encapsulation of 6BrCaQ in liposomes allowed to reach the IC_{50} still at the concentration of 5 µM after 48 h treatment of MDA-MB 231 cells and any effect on cell viability was exerted by unloaded liposomes containing the same amount of lipids (**Figure 3**).

In contrast, a weak toxicity of empty liposomes was found at the highest lipid concentration tested. This behavior was already observed for the same formulation in another breast cancer cell line [17, 19].

The efficacy of liposomes was greater on prostate cancer cells. Indeed, 56.8 ± 5.8% of the treated cells died after 24 h of exposure at a concentration of 5 µM of drug

encapsulated and at the highest concentration tested (10 µM) the cell viability was almost double for free drug compared to liposomes (p= 5,53086E^{-05}) (**Figure 4**).

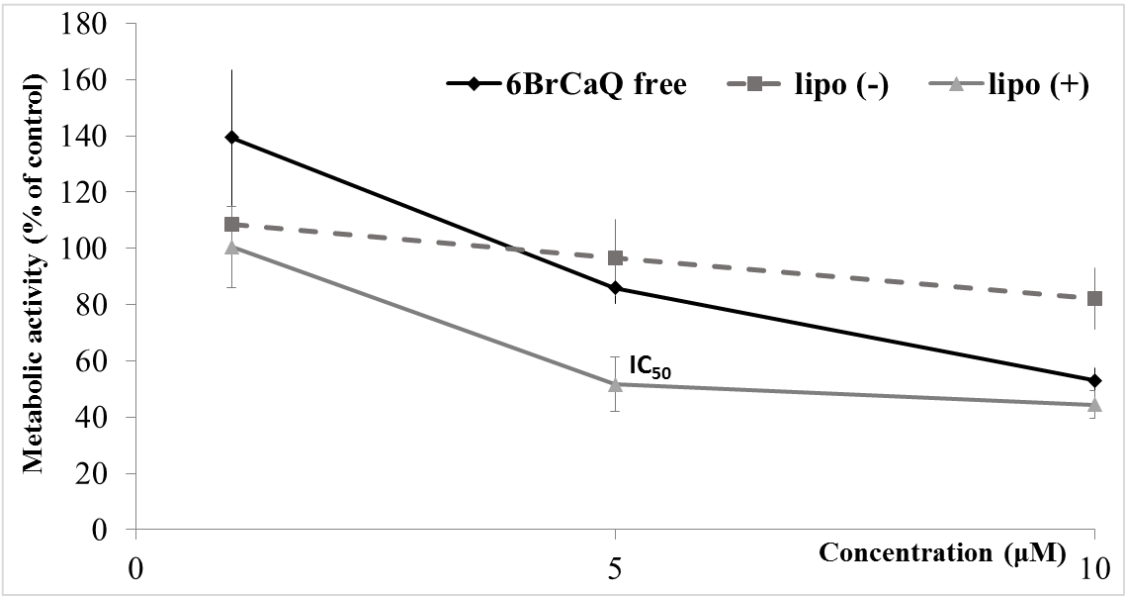

Figure 3-Metabolic activity of MDA-MB-231 cells (MTS assay) after 48 h exposure at 6BrCaQ free or liposomal (lipo (+)) at different concentrations (i.e. 1, 5 and 10 µM). Unloaded liposomes (lipo (-)) were used as controls. The reported data represent the mean of the metabolic activity of three different samples (three wells) for each condition tested.

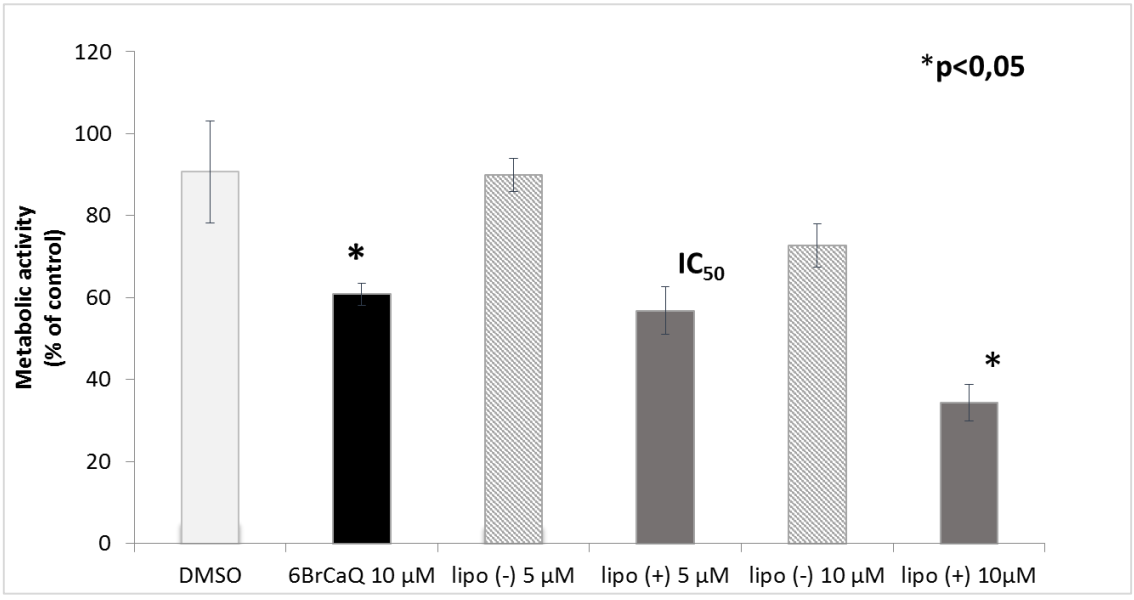

Figure 4- Metabolic activity of PC3 cells (MTS assay) after 24 h treatment with 6BrCaQ free (10µM) and 6BrCaQ liposomes (lipo (+)) (5 µM and 10 µM). Empty liposomes (lipo (-)) were used as controls.

The trend of the biological activity as a function of the time of exposure was evaluated in a kinetic study. For this purpose, cells were seeded in three different plates, exposed at time zero at the same treatment solution and analyzed after 24, 48 and 72 h of incubation. As previously observed, the effect of liposomes was anticipated compared to that of the free drug and also in that case the IC_{50} was found to be 5 µM and to be reached after only 24 h of treatment. In contrast, the free drug resulted to be effective only at 10 µM and after 72 h treatment when loaded liposomes at the same concentration killed the totality of cells present in the well (**Figure 5**). PC3 cells resulted to be more sensitive with respect to MDA-MB 231 cells also to the exposure to empty liposomes for which a certain toxicity was observed (**Figure 5**). However, since the toxic effect didn't increase with the time of treatment, it could be considered as an artifact of the *in vitro* test. This behavior may be explained by the variation of osmotic conditions that occurs in the cell environment as result of the addition of lipids along with a possible slight oxidation of unsaturated lipids, and may be exacerbated *in vitro*. The fact that this effect decreased with the time of exposure may mean that a certain period is required so that cells adapt to the changed surrounding. It should be underlined that also the toxicity of loaded liposomes at a concentration of 5µM resulted to be significantly higher ($p < 0.01$) after 24 h of exposure whereas it remained almost constant for the next times of treatment. In fact, the effect of 5µM liposomes against PC3 cells was not found to be statistically different after 48 and 72 h treatment ($p > 0.05$).

Altogether, the *in vitro* MTS results showed that the encapsulation of 6BrCaQ in liposomes improved the toxicity of the drug on breast and prostate cancer cells, enabling to reach a therapeutic efficacy at lower doses and for shorter time of treatment with respect to the free drug.

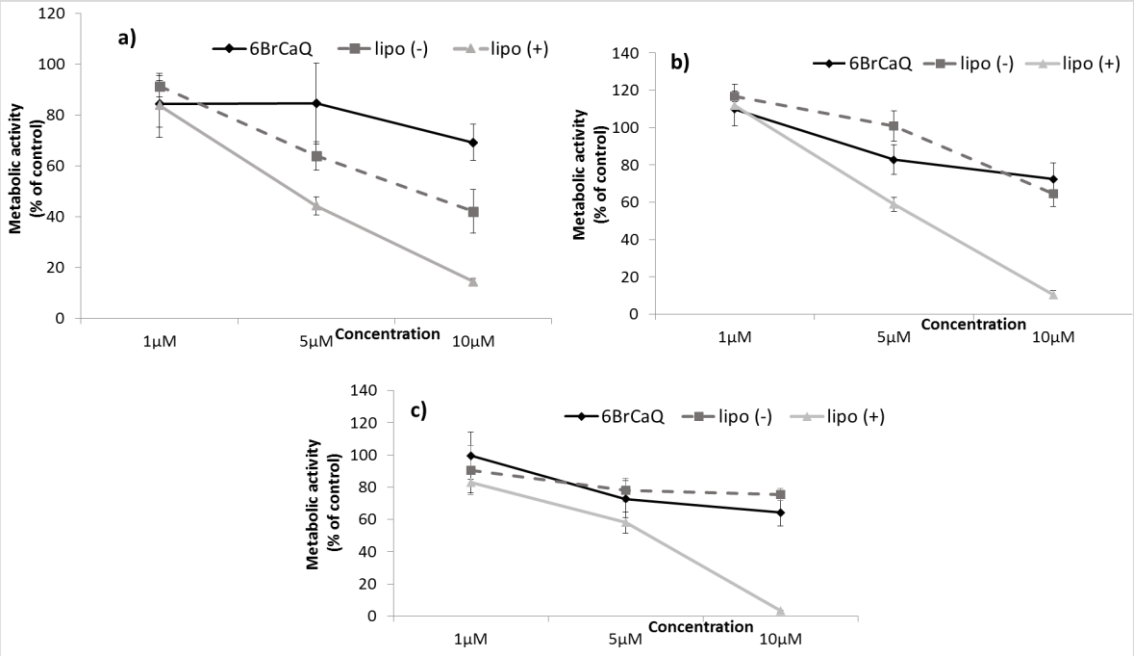

Figure 5- Trend of the metabolic activity of PC3 cells (MTS assay) after **a) 24 h**, **b) 48 h** and **c) 72 h** treatment with 6BrCaQ free, loaded liposomes (lipo (+)) or empty liposomes (lipo (-)) at different concentrations

To investigate whether the mechanism of action of 6BrCaQ remained unvaried after encapsulation in liposomes and to evaluate the effect on the proliferation and survival of prostate cancer cells, the distribution of cells in cell cycle was analyzed. 6BrCaQ, both in solution and encapsulated in liposomes, caused an arrest of cells in phase G2M and S with respect to the controls (**Figure 6**). After 72 h of exposure to the drug (free or encapsulated) an increase of the number of cells in phase S was observed compared to the controls (DMSO and unloaded liposomes), suggesting a potential induction of cell apoptosis through the inhibition of Hsp90 chaperone (**Figure 6 b**). This apoptosis can be induced from the cells blocked in G2/M phase. The internucleosomal degradation of DNA occurs from G2/M cells and then the DNA content is overlaying the DNA synthesis phase (4N DNA). Similar results were obtained in previous experiments on MDA-MB-231 cell line (data not shown).

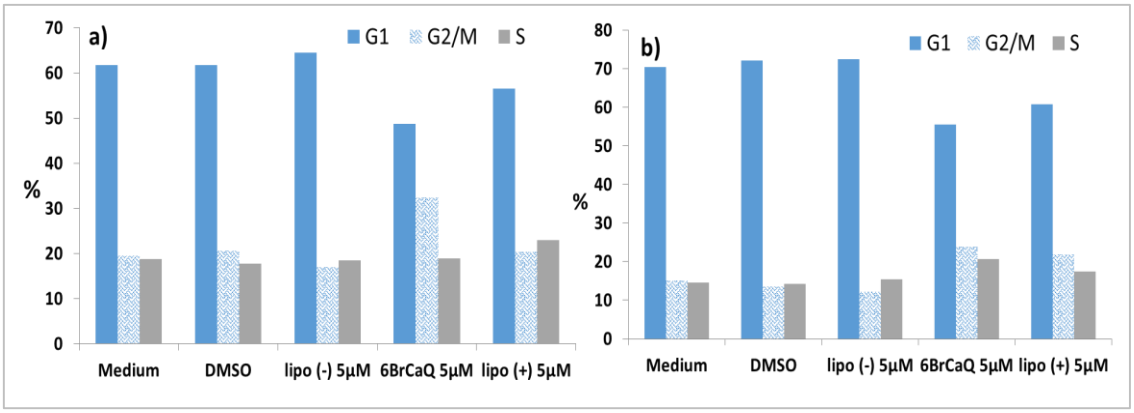

Figure 6-Cell cycle distribution of PC3 cells after: **a) 24 h** and **b) 72 h** of treatment with free or liposomal 6BrCaQ (5µM). DMSO and empty liposomes (lipo (-)) act as controls for free drug and loaded liposomes, respectively.

3.3. *In vitro* liposome uptake

The cellular uptake of liposomes was investigated by exposing MDA-MB-231 and PC-3 cells to fluorescent liposomes (**Figure 7**). Any phenomenon of autofluorescence was observed for control cells. In contrast, when cells were treated with 6BrCaQ liposomes, an intense fluorescence was revealed in the cytoplasm and the signal resulted to be stronger close to the nucleus.

The data confirmed that the improvement of the *in vitro* efficacy of 6BrCaQ encapsulated in liposomes was the result of a quick internalization of colloidal vesicles into the cells. Indeed, the presence of liposomes in the cytoplasm was observed already after 30 min of treatment in both cell lines (**Figure 7**). Hence, investigated liposomes were able to be uptaken into the target cells in short time and this behavior was responsible for the reduction of both effective dose and time of treatment with respect to the free molecule.

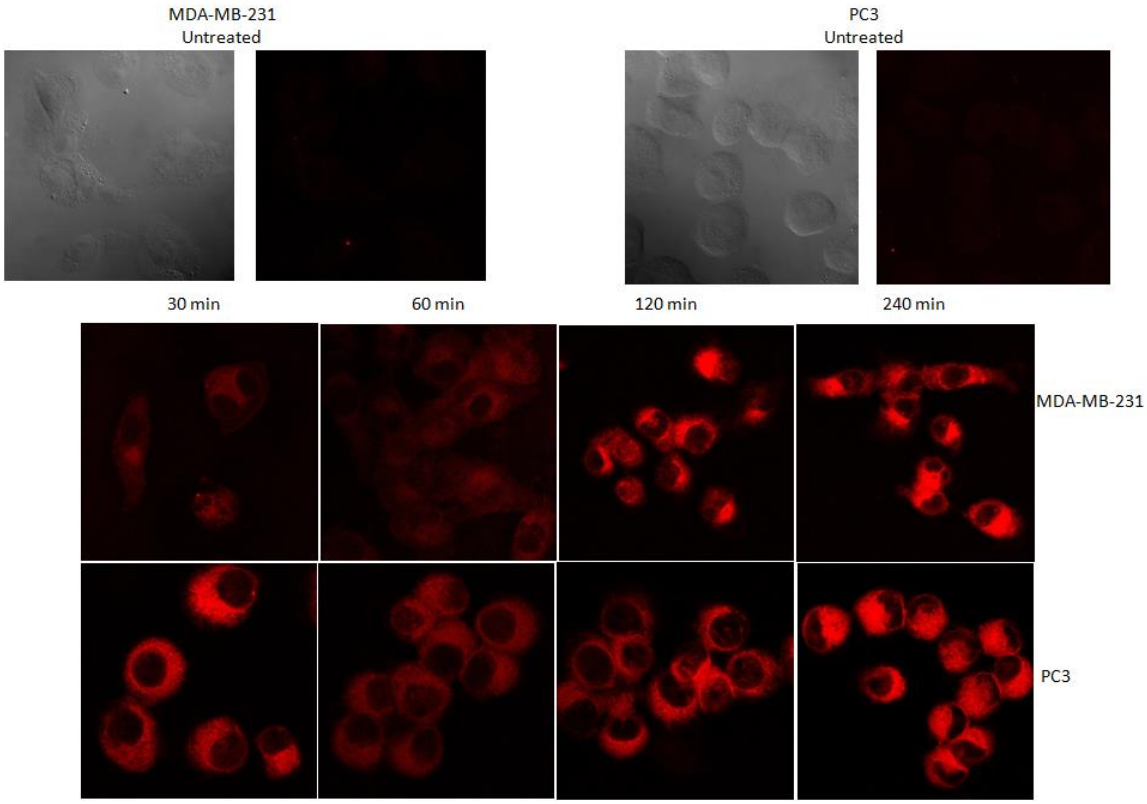

Figure 7-Confocal pictures of PC3 and MDA-MB-231 cells after treatment with fluorescent liposomes (Rho labeled) containing 6BrCaQ (5µM)

3.4. Wound-healing assay

Wound healing assay is a well-established method to study cell migration *in vitro*. When cell monolayers are scratched, the cell-cell contacts are destroyed and cells respond to the damage by increasing the production of growth factors to heal the wound [20].

The migration of the cells during this healing process can be followed *in vitro* by using a video microscope. In our work, the assay was performed in presence of CCL2, also known as monocyte chemoattractant protein-1 (MCP-1), which is overexpressed in malignant prostate cancers [18]. In absence of treatment, prostate cells quickly migrated in the direction of the scratch and the wound resulted to be completely closed after 24 h (**Figures 8 and 9a**). The cell motility instead was strongly inhibited when PC3 cells were treated with 20µM 6BrCaQ free (**Figures 8 and 9b**) or encapsulated in liposomes (**Figures 8 and 9d**), confirming the ability of the drug to arrest the cell migration, contrasting the

chemotactic effect of CCL2. In another preliminary experiment, the efficacy of 6BrCaQ liposomes was compared to that of an inhibitor of CCL2 receptor (CCR2) used at an equal concentration (20µM) and the same degree of neutralization of CCL2 (40 ng/mL) invasion promoting effect was observed for the two drugs (data not shown). In contrast, the rate of migration resulted to be still high in the case of PC3 cells exposed to empty vesicles, as further proof that the efficacy of liposomes relied on the presence of 6BrCaQ (**Figure 8**). Indeed, the number of cells migrated per mm^2 in the well of control (DMSO) and in that of empty liposomes was not found to be statistically different ($p > 0.05$). Recent studies revealed that Hsp90 enhances cell migration binding the CD91 receptor expressed on the cell surface and that the block of Hsp90 activity inhibits the formation of metastasis *in vivo* [21]. In this study it was confirmed that using an inhibitor of the C-terminal domain of Hsp90, it is possible to slow down the migration of prostate cancer cells *in vitro*, thus contrasting their high metastatic potential.

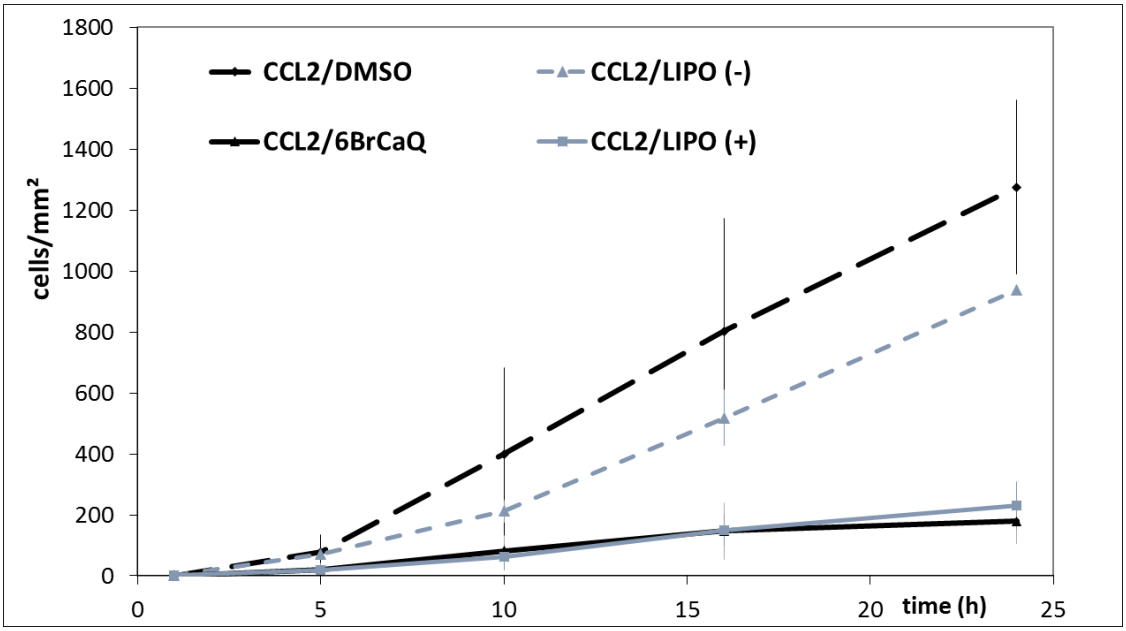

Figure 8- Rate of migration of PC3 cells during wound healing assay. Effect of 6BrCaQ free and liposomal (20 µM) in presence of chemokine CCL2 (40 ng/mL). DMSO and empty liposomes (lipo (-)) were used as controls. The number of cells migrated at each time in a ROI selected within the edges of the scratch is plotted as a function of time.

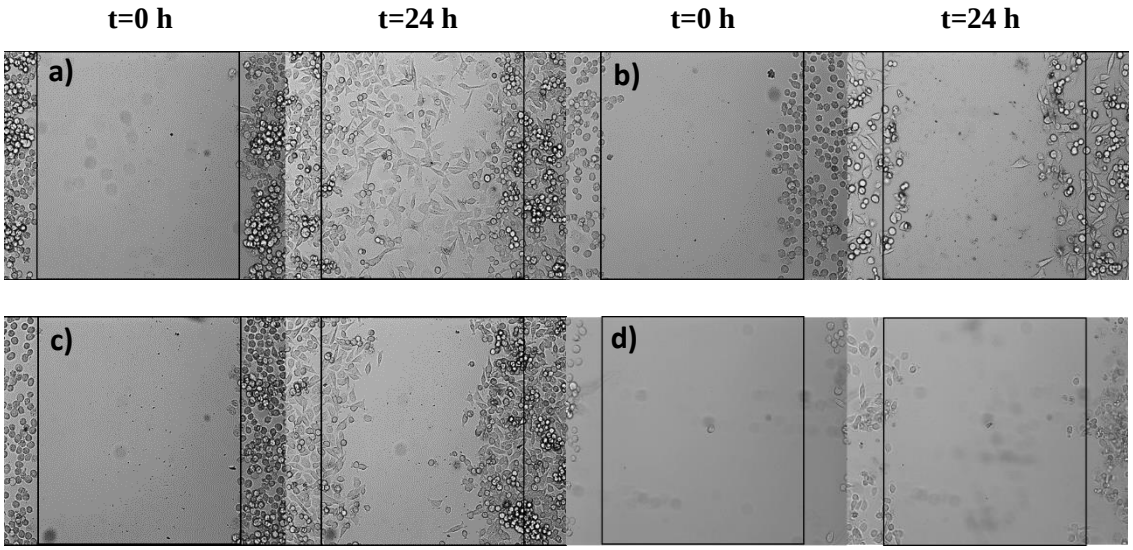

Figure 9- Representative images of PC3 cells migration in the direction of the wound when exposed to: **a) DMSO; b) free drug** (20 µM); **c) empty liposomes** (at the same lipid concentration of loaded ones); **d) 6BrCaQ liposomes** (20 µM). Chemokine CCL2 at a concentration of 40 ng/mL was present in each well. For each treatment condition, representative pictures of the well taken at t=0 h and t= 24 h are shown.

4. Conclusions

In this work Stealth® nanoliposomes have been developed and used as carriers for the administration of an hydrophobic inhibitor of Hsp90 chaperone, 6BrCaQ. The formulated liposomes had the desired nano-sized dimensions and resulted to be stable both in bulk and culture conditions. The quickly intracellular uptake of the nanocarriers (30 minutes) allowed the liposomes to potentiate the effect of the free drug halving the IC_{50} on both prostate and breast cancer cells and decreasing the time of treatment required. It was then confirmed the suitability of Stealth® nanoliposomes as carriers to target cancer.

Moreover, 6BrCaQ encapsulated in liposomes inhibited the proliferation of prostate cancer cells causing an arrest of the cell cycle in G2/M phase. The drug was also able to contrast the chemotactic action of CCL2 slowing down the cell migration *in vitro*. This effect makes 6BrCaQ liposomes a promising tool to be exploited to prevent the formation of metastasis, mainly in bones, which is the major cause of the poor prognosis of this type of cancer.

Altogether, the experimental data confirmed the efficacy of 6BrCaQ to exert anticancer activity through the inhibition of Hsp90 chaperone and the suitability of liposomes as proper vehicles for the administration of this hydrophobic drug *in vivo*.

Acknowledgements

This work was carried out in the laboratory of "Vectorisation et Pharmacologie Cellulaire Appliquées aux anti-infectieux et anti- Cancéreux" (Equipe 8, UMR 8612, Institut Galien Paris-Sud (Director Prof. Elias Fattal) head by Dr. Gillian Barratt, under the supervision of Dr. Juliette Vergnaud-Gauduchon.

References

1. Risbridger G.P., Davis I.D., Birrell S.N. and Tilley W.D. Breast and prostate cancer: more similar than different. Nature Reviews Cancer 2010, 10, 205-212;
2. Ali S. and Coombes R.C. Endocrine-responsive breast cancer and strategies for combating resistance. Nature Reviews Cancer 2002, 2, 101-115;
3. Feldman B. J. and Feldman D. The development of androgen-independent prostate cancer. Nature Reviews Cancer 2001, 1, 35-45;
4. Nwabo Kamdje A. H., Seke Etet P. F., Vecchio L., Muller J. M., Krampera M., Lukong K.E. Signaling pathways in breast cancer: Therapeutic targeting of the microenvironment. Cellular Signalling, 2014, 26 (12), 2843–2856;
5. Li J., Soroka J., Buchner J. The Hsp90 chaperone machinery: Conformational dynamics and regulation by co-chaperones. Biochimica et Biophysica Acta 2012, 1823, 624–635;
6. Audisio D., Messaoudi S., Cegielkowski L., Peyrat J., Brion J., Methy-Gonnot I., Radanyi C., Renoir J., Alami M. Discovery and Biological Activity of 6BrCaQ as an Inhibitor of the Hsp90 Protein Folding Machinery. ChemMedChem 2011, 6, 804 – 815;
7. Bagatell R. and Whitesell L. Altered Hsp90 function in cancer: A unique therapeutic opportunity. Molecular Cancer Therapeutics 2004, 3, 1021-1030;
8. Kamal A., Thao L., Sensintaffar J., Zhang L., Boehm M.F., Fritz L.C., Burrows F.J. A high-affinity conformation of Hsp90 confers tumour selectivity on Hsp90 inhibitors. Nature 2003, 425 (5), 407-410;
9. Pearl L.H. and Prodromou C. Structure and *in vivo* function of Hsp90. Current Opinion in Structural Biology 2000, 10, 46–51;
10. Donnelly A. and Blagg B.S.J. Novobiocin and Additional Inhibitors of the Hsp90 C-Terminal Nucleotide-binding Pocket. Current Medicinal Chemistry 2008, 15(26), 2702–2717;
11. Wang Y. and McAlpine S. R. N-terminal and C-terminal modulation of Hsp90 produce dissimilar phenotypes. Chemical Communications 2014, DOI: 10.1039/C4CC07284G

12. Yang T., Cui F., Choi M., Cho J., Chung S., Shim C., Kim D. Enhanced solubility and stability of PEGylated liposomal paclitaxel: *In vitro* and *in vivo* evaluation. International Journal of Pharmaceutics 2007, 338, 317–326;
13. Maruyama K. Intracellular targeting delivery of liposomal drugs to solid tumors based on EPR effects. Advanced Drug Delivery Reviews 2011, 18;63(3), 161-9;
14. Andresen T. L., Jensen S. S., Jørgensen K. Advanced strategies in liposomal cancer therapy: Problems and prospects of active and tumor specific drug release. Progress in Lipid Research 2005, 44, 68-97;
15. Deshpande P.P., Biswas S., Torchilin V.P. Current trends in the use of liposomes for tumor targeting. Nanomedicine 2013, 8(9), 1-32;
16. Immordino M., Dosio F., Cattel L. Stealth liposomes: review of the basic science, rationale, and clinical applications, existing and potential. International Journal of Nanomedicine. Sep 2006, 1(3), 297–315;
17. Maillard S., Gauduchon J., Marsaud V., Gouilleux F., Connault E., Opolon P., Fattal E., Sola B., Renoir J.-M. Improved antitumoral properties of pure antiestrogen RU 58668-loaded liposomes in multiple myeloma J. Steroid Biochem. Mol. Biol. 2006, 100 (1-3), 67-78;
18. Zhang J., Patel L., Pienta K.J. CC chemokine ligand 2 (CCL2) promotes prostate cancer tumorigenesis and metastasis. Cytokine Growth Factor Review 2010, 21(1), 41–48;
19. Urbinati G., Marsaud V., Plassat V., Fattal E., Lesieur S., Renoir J.M. Liposomes loaded with histone deacetylase inhibitors for breast cancer therapy. International Journal of Pharmaceutics 2010, 397, 184–193;
20. Yarrow J.C., Perlman Z.E., Westwood N.J., Mitchison T.J. A high-throughput cell migration assay using scratch wound healing, a comparison of image-based readout methods. BMC Biotechnology 2004, 4 (21), 1-9;
21. Trepel J., Mollapour M., Giaccone G., Neckers L. Targeting the dynamic Hsp90 complex in cancer. Nature Reviews Cancer 2010, 10 (8), 537-549.

Acknowledgements

First, I would like to thank Prof. Luisa Montanari and Paola Minghetti for having trust me and being good examples and advisors in this professional and personal growth experience.

I would like to thank in particular my tutor, Prof. Francesco Cilurzo, for having always pushed me, for his patience, ideas and teaching and the constant support he gave me over the three years of my Ph.D programm.

Thanks to Dr. Antonella Casiraghi and Dr. Francesca Selmin for their intellectual and personal suggestions and for being always available for each kind of help.

To Dr. Chiara G.M. Gennari for the scientific and, mainly, moral support during this journey as well as for the performance of the in vitro phage display screening. I would like to acknowledge also Dr. Sara Pellegrino for the synthesis of SPEH and to thank both, Dr. Gennari and Dr. Pellegrino, for the collaboration in the redaction of Chapter 3.

I would like to thank Prof. M. Elias Fattal for having given me the opportunity to join his Equipe at the Institut Galien Paris Sud. A special thanks to Dr. Juliette Vergnaud-Gauduchon, who introduced me in the world of biology and cell culture with extraordinary patience, for her guide and support during my experience at the Universitè de Paris Sud XI.
My thanks also to Félix Sauvage for his contribution in some of the experiments reported in the Appendix of this thesis and for the insightful discussions about the research. I would like to acknowledge Dr. Valérie Nicolas, for the help during the performance of the experiments of wound healing with the video microscope, and Dr. Gillian Baratt for her precious advices about liposomes formulation. A great thanks to Rachel for her friendship and to all the members of the research staff of the Equipe 8 and 5 of the Institut Galien, especially all the Ph.D students and post doc fellows for the great moments spent together.

A big thank to all the extraordinary people I met in Paris who made my experience in the "Ville Lumière" wonderful and, of course, to all my friends here in Italy.

I cannot absolutely forget all my past and present colleagues and friends of the Montanari's lab who shared with me this challenging experience, enduring my stressed behavior and lightening the mood with laugh and fun.

Last, but not least, I want to thank my family, who always encouraged and supported me in all my pursuits and choices and without who nothing would have been possible.